AFOSR-TR- 89 1337

Final Technical Report

Laser-Material Interactions

for the period

April 1, 1988 to March 31, 1989

Grant No. AFOSR 86-0120

Principal Investigator:

Professor S. R. J. Brueck
Center for High Technology Materials
University of New Mexico
Albuquerque, NM 87131

DISCLAIMER NOTICE

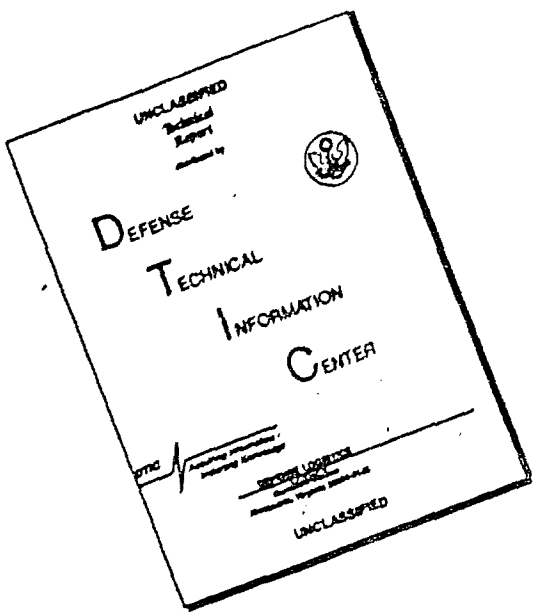

THIS DOCUMENT IS BEST QUALITY AVAILABLE. THE COPY FURNISHED TO DTIC CONTAINED A SIGNIFICANT NUMBER OF PAGES WHICH DO NOT REPRODUCE LEGIBLY.

UNCLASSIFIED
SECURITY CLASSIFICATION OF THIS PAGE

REPORT DOCUMENTATION PAGE

1a. REPORT SECURITY CLASSIFICATION UNCLASSIFIED	1b. RESTRICTIVE MARKINGS
2a. SECURITY CLASSIFICATION AUTHORITY	3. DISTRIBUTION / AVAILABILITY OF REPORT Approved for public release; distribution is unlimited.
2b. DECLASSIFICATION / DOWNGRADING SCHEDULE	
4. PERFORMING ORGANIZATION REPORT NUMBER(S)	5. MONITORING ORGANIZATION REPORT NUMBER(S) AFOSR-TR- 89-1337
6a. NAME OF PERFORMING ORGANIZATION Univ of New Mexico 6b. OFFICE SYMBOL (If applicable)	7a. NAME OF MONITORING ORGANIZATION AFOSR/NP
6c. ADDRESS (City, State, and ZIP Code) Albuquerque, NM 87131	7b. ADDRESS (City, State, and ZIP Code) Building 410, Bolling AFB DC 20332-6448
8a. NAME OF FUNDING / SPONSORING ORGANIZATION AFOSR 8b. OFFICE SYMBOL (If applicable) NP	9. PROCUREMENT INSTRUMENT IDENTIFICATION NUMBER AFOSR-86-0120
8c. ADDRESS (City, State, and ZIP Code) Building 410, Bolling AFB DC 20332-6448	10. SOURCE OF FUNDING NUMBERS PROGRAM ELEMENT NO. 61102F; PROJECT NO. 2301; TASK NO. A1; WORK UNIT ACCESSION NO.

11. TITLE (Include Security Classification)
(U) LASER-SEMICONDUCTOR INTERACTIONS

12. PERSONAL AUTHOR(S)
Professor S. R. J. Brueck

13a. TYPE OF REPORT	13b. TIME COVERED	14. DATE OF REPORT (Year, Month, Day)	15. PAGE COUNT
Final	FROM 1 Apr 86 TO 30 Apr 89	September 1989	136

16. SUPPLEMENTARY NOTATION

17. COSATI CODES			18. SUBJECT TERMS (Continue on reverse if necessary and identify by block number)
FIELD	GROUP	SUB-GROUP	
	20.06		

19. ABSTRACT (Continue on reverse if necessary and identify by block number)

Last year a careful study of the photodegradation of the photoluminescence efficiency for freshly cleaved GaAs 110 surfaces and the first observation of a Raman signature associated with the passivation of the surface with an aqueous Na(2)S solution were presented. This work has continued with additional measurements of the passivation process. Additionally, related measurements of the ultraviolet photodegradation of the GaAs surface were obtained in a prohram on the development of high speed uv-photomixers supported by the Naval Research Laboratory. A very dramatic, irreversible decrease in the detector quantum efficiency was observed under irradiation by the uv-local oscillator at comparable intensities to those used in the photodegradation experiments.

20. DISTRIBUTION / AVAILABILITY OF ABSTRACT X ☐ UNCLASSIFIED/UNLIMITED X ☐ SAME AS RPT. ☐ DTIC USERS	21. ABSTRACT SECURITY CLASSIFICATION UNCLASSIFIED
22a. NAME OF RESPONSIBLE INDIVIDUAL H R Schlossberg	22b. TELEPHONE (Include Area Code) 202 ()-767-4906 AFOSR/NP 22c. OFFICE SYMBOL

DD FORM 1473, 84 MAR 83 APR edition may be used until exhausted. All other editions are obsolete.

SECURITY CLASSIFICATION OF THIS PAGE
UNCLASSIFIED

Introduction:

The Laser-Materials Interaction Laboratory at the Center for High Technology Materials of the University of New Mexico is devoted to the study of a broad range of laser spectroscopic probes of semiconductor and nonlinear-materials, fabrication processes and optoelectronic devices. Much of this work is being carried out in conjunction with the Optoelectronics Research Center Program at CHTM which is also partially funded by the Air Force Office of Scientific Research. Significant progress has been made in this reporting period in a number of areas including: laser-induced photo-degradation of the GaAs surface, studies of grating-coupling into surface-plasma modes at a metal-dielectric interface, electro-optic and nonlinear optical effects in PLZT thin films, and resonant-periodic-gain surface-emitting semiconductor lasers. Brief synopses of this work are presented here. More details are provided in the attached reprints and preprints.

Laser-Induced Degradation of the GaAs Surface

Last year, a careful study of the photodegradation of the photoluminescence efficiency for freshly cleaved GaAs 110 surfaces and the first observation of a Raman signature associated with the passivation of the surface with an aqueous Na_2S solution were presented. This work has continued with additional measurements of the passivation process. Additionally, related measurements of the ultraviolet photodegradation of the GaAs surface were obtained in a program on the development of high-speed uv-photomixers supported by the Naval Research Laboratory. A very dramatic, irreversible decrease in the detector quantum efficiency was observed under irradiation by the uv-local oscillator at comparable intensities to those used in the photodegradation experiments.

Publications:

M. Y. A. Raja, S. R. J. Brueck, M. Osinski, and J. G. McInerney
Degradation of the Photoluminescence Efficiency of GaAs under Low Intensity Laser Irradiation
MRS Proceedings: Advanced Surface Processes for Optoelectronics,
T. Venkatesan, S. Bernasek, G. Stillman, and H. Temkin, eds.
(Materials Research Society 126 265, 1988)

Grating-Coupling into Surface Plasma Waves

Work has continued on experimental and theoretical studies of the coupling of optical waves into waveguides and guided surface plasma waves using submicrometer gratings. Experimentally, grating periods ranging from 330 nm to 800 nm and depths from several Angstroms to approximately one μm have been investigated. This parameter range spans both single and multiple-order coupling into the surface plasma wave mode, coupling efficiencies in excess of 95%, and saturation and eventual decrease in the SPW coupling due to reradiation effects. For deeper gratings, SPW effects are eliminated and polarization and absorption effects become dominant. This work represents the first observation of strong polarization effects for nearly square grating profiles in the visible spectral region.

Theoretical efforts have been devoted to evaluating the scattered, coupled fields within the Rayleigh hypothesis without making any small-signal perturbative approximations. Excellent agreement with the experiments is obtained for grating

depth/grating period ratios as large as 0.4 and qualitative agreement for ratios up to unity. Good agreement has been demonstrated between this relatively simple model and more complex, integral formulations of the vector boundary value problem that involve substantially more complex analytical and numerical evaluations and provide a less satisfactory physical interpretation.

Publications:
Saleem Zaidi, M. Yousaf and S. R. J. Brueck
Grating Coupling to Surface Plasma Waves I - First-Order Coupling
in preparation (draft attached)

Presentations:
S. H. Zaidi and S. R. J. Brueck
Interaction between Surface Plasma Waves and TM-Guided Modes in Metal-Clad Dielectric Waveguides
OSA Annual Meeting, 1988
San Jose, CA

S. H. Zaidi and S. R. J. Brueck
Optical Characteristics of Deeply Modulated Gratings
OSA Annual Meeting, 1988
San Jose, CA

S. H. Zaidi, M. Yousaf, and S. R. J. Brueck
Interactions between First and Second Order Couplings to Surface Plasma Waves
To be presented at LEOS Annual Meeting, 1989
Orlando, FL

S. H. Zaidi, M. Yousaf, and S. R. J. Brueck
First Order Coupling to Surface Plasma Waves
To be presented at LEOS Annual Meeting, 1989
Orlando, FL

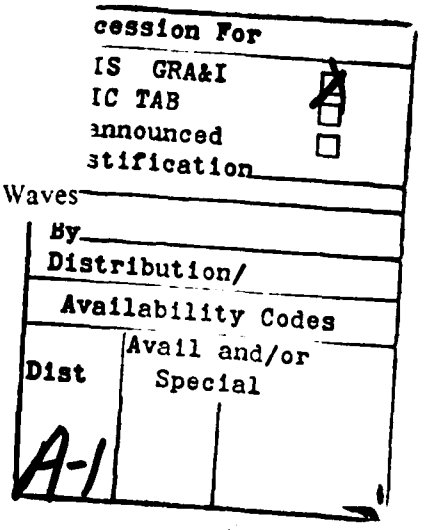

PhD Thesis:
Saleem Hussain Zaidi
An Investigation of Holographic Grating Fabrication and Optical Coupling to Surface Plasma Waves
Department of Physics, University of New Mexico, 1989

Nonlinear Optics of PLZT Thin Films

Investigations of electro-optic and nonlinear optic effects in PLZT thin films have been carried out. Films are deposited on a variety of substrates including SiO_2, SiO_2/Si, Si, GaAs, and Al_2O_3. Highly-oriented films with the 100 direction normal to the film are routinely achieved for PLZT 28/0/100. This composition is on the boundary between cubic and tetragonal ferroelectric phases and exhibits a quadratic electrooptic effect. Measurements have been carried out in a transverse electrode configuration with the optical beams propagating through a 0.5 μm film. Major characteristics include: a measured 40:1 contrast ratio for birefringence transmission; maximum measured Dn of 0.18 at a 200-V bias across a 15-μm gap (this is several times larger than the Dn for $LiNbO_3$ at this same field strength; birefringence switching speed of less than 2 ns, instrumentation-limited measurement; contrast ratio of 900:1 for

electric-field induced second-harmonic generation in the same geometry. Higher-order photorefractive effects have been observed in these films and are exhibited as a long time decay of the second-harmonic signal under continuous irradiation and applied fields. Modeling of this phenomena is underway.

Publications:

A. Mukherjee, S. R. J. Brueck and A. Y. Wu
Electric-Field Induced Second-Harmonic Generation in PLZT
Optics Communications (submitted)

A. Mukherjee, S. R. J. Brueck and A. Y. Wu
Electrooptics of Thin-Film PLZT
Optics Letters (submitted)

Presentations:

A. Mukherjee, S. R. J. Brueck and A. Y. Wu
DC-Field Induced Second Harmonic Generation in PLZT 9/65/35
OSA Topical Meeting on Nonlinear Optical Properties of Materials
Troy, NY (August, 1988)

A. Mukherjee, S. R. J. Brueck and A. Y. Wu
Electrooptics of Thin Film PLZT
CLEO'89
Baltimore, MD (April, 1989)

S. R. J. Brueck
Nonlinear Optics of PLZT Thin Films
Seminar
Sandia National Laboratories
Albuquerque, NM (1989)

Resonant-Periodic Gain Surface-Emitting Semiconductor Lasers

Last year, the first operation of a resonant periodic gain laser media, in which the quantum-well gain regions are spaced by one half the optical wavelength, was reported. Substantial progress has been made in this reporting period. Initial samples were MBE material supplied by Sandia National Laboratories, subsequent samples have been grown by MOCVD at CHTM. A major improvement has been the incorporation of quarter-wavelength resonant multi-layer resonator reflectors as part of the growth process. With estimated reflectivities of over 99%, these mirrors have led to dramatically reduced threshold intensities and continuous operation of these devices. Power conversion efficiencies of over 45% and cw-output powers of over 30 mW have been achieved. Substantial effort has also gone into modeling these resonator structures and the overall device behavior. This work is continuing with efforts on high speed dynamics, electrical pumping, and new materials systems (InGaAs/GaAs).

Publications:

M. Y. A. Raja, S. R. J. Brueck, M. Osinski, C. F. Schaus, J. McInerney, T. M. Brennan and B. E. Hammons
Novel Wavelength Resonant Optoelectronic Structure and its Application to Surface-Emitting Semiconductor Lasers
Electronics Letters 24, 1140 (1988)

M. Y. A. Raja, S. R. J. Brueck, M. Osinski, C. F. Schaus, J. McInerney, T. M. Brennan and B. E. Hammons

Surface-Emitting, Multiple Quantum Well GaAs/AlGaAs Laser with Wavelength Resonant Periodic Gain Medium
Appl. Phys. Lett. 53, 1678 (1988)

C. F. Schaus, H. E. Schaus, S. Sun, M. Y. A. Raja and S. R. J. Brueck
MOCVD Growth of GaAs/AlGaAs Wavelength-Resonant Periodic-Gain Vertical-Cavity Surface-Emitting Laser
Electron. Lett. 25, 538 (1989)

C. F. Schaus, M. Y. A. Raja, J. G. McInerney, H. E. Schaus, S. Sun, M. Mahbobzadeh, and S. R. J. Brueck
High-Efficiency cw Operation of MOCVD-Grown GaAs/AlGaAs Vertical-Cavity Lasers with Resonant Periodic Gain
Electron. Lett. 25, 637 (1989)

M. Y. A. Raja, S. R. J. Brueck, M. Osinski, C. F. Schaus, J. G. McInerney, T. M. Brennan and B. E. Hammons
Resonant-Periodic-Gain Surface-Emitting Semiconductor Lasers
IEEE Jour. of Quantum Electron. QE-25, 1500 (1989)

S. R. J. Brueck, M. Y. A. Raja, M. Osinski, C. F. Schaus, M. Mahbobzadeh, J. G. McInerney and K. J. Dahlhauser
Optical Cavity Design for Wavelength-Resonant Surface-Emitting Semiconductor Lasers
SPIE Proc. 1043, Diode Laser Technology and Applications 111-122 (1989)

Presentations:
M. Y. A. Raja, S. R. J. Brueck, M. Osinski, C. F. Schaus, J. G. McInerney, T. M. Brennan and B. E. Hammons
Wavelength-Resonant, Surface-Emitting Semiconductor Laser: A Novel Quantum Optical Structure
LEOS Annual Meeting
Santa Clara (1988)

S. R. J. Brueck
cw Operation of Surface-Emitting Lasers
IEEE Workshop on Diode Lasers' 1989
Baltimore, MD

M. Y. A. Raja, S. R. J. Brueck, M. Osinski, C. F. Schaus, J. G. McInerney, T. M. Brennan, B. E. Hammons
Surface-Emitting Lasers: A Comparison of Resonant Periodic Gain and Conventional Structures
Conference on Lasers and Electro-Optics, 1989
Baltimore, MD

C. F. Schaus, S. Sun, H. E. Schaus, M. Y. A. Raja, J. G. McInerney, S. R. J. Brueck
300 K cw Operation of MOCVD Grown Optically Pumped GaAs/AlGaAs Resonant Periodic Gain Vertical Cavity Lasers with 45% Efficiency
Conference on Lasers and Electro-Optics, 1989 (postdeadline paper)
Baltimore, MD

S. R. J. Brueck, M. Y. A. Raja, M. Osinski, C. F. Schaus, M. Mahbobzadeh, J. G. McInerney and K. J. Dahlhauser
Optical Cavity Design for Wavelength-Resonant Surface-Emitting Semiconductor Lasers
SPIE Meeting Diode Laser Technology and Applications (1989)
(invited paper)

S. R. J. Brueck
Surface-Emitting Semiconductor Lasers
Seminar
MIT Lincoln Laboratory
United Technologies Research Center
Polaroid Corporation
Bell Communications Research
IBM General Products Division

M. Y. A. Raja
Resonant Periodic Gain Surface-Emitting Semiconductor Lasers
Seminar
Carling Laboratories, Ottawa, Ontario, Canada
Rutgers University, Rutgers, NJ

M. Y. A. Raja, A. Mukherjee, M. A. Mahbobzadeh, C. F. Schaus, and S. R. J. Brueck
Dynamics of Resonant Periodic Gain GaAs/AlGaAs Surface-Emitting Lasers under Picosecond Optical Excitation
To be presented at LEOS Annual Meeting, 1989
Orlando, FL

M. Y. A. Raja, J. G. McInerney, C. F. Schaus, S. R. J. Brueck, H. E. Schaus, and S. Sun
Transverse Mode Structure of Optically Pumped Resonant Periodic Gain Semiconductor Lasers
To be presented at LEOS Annual Meeting, 1989
Orlando, FL

PhD Thesis
Mohammed Yasin Akhtar Raja
Optically Pumped, Wavelength-Resonant Surface-Emitting Semiconductor Laser
Department of Physics, University of New Mexico, 1988

DEGRADATION OF PHOTOLUMINESCENCE EFFICIENCY IN GaAs UNDER LOW INTENSITY LASER IRRADIATION

M. Yasin A. Raja, Steven R. J. Brueck, Marek Osinski, and John G. McInerney
Center for High Technology Materials, University of New Mexico, Albuquerque, NM 87131

ABSTRACT

We report temporal measurements of bandgap photoluminescence (PL) from GaAs surfaces under low-intensity CW laser excitation. We have observed slow PL degradation in n-type, p-type and semi-insulating (Cr-doped and LEC-grown) samples, and have fit the data to a simple power law. Calculations indicate a significant contribution from the bulk material, possibly via recombination-enhanced generation or migration of non-radiative centers. The effectiveness of various methods of surface treatment (photowashing, deposition of epitaxial AlGaAs, spin-coating with organic and inorganic sulfide films) has been assessed. One specific technique, involving coating with sodium sulfide, is effective in enhancing the PL efficiency and suppressing the degradation, but these effects are not permanent.

INTRODUCTION

Recently, excitation photoluminescence (PL) spectroscopy has attracted considerable interest in the context of photowashing [1-4] of GaAs. Interpretation of these experiments, however, is impeded by incomplete understanding of the origin of non-radiative centers, which are believed to cause laser-induced degradation of PL efficiency in GaAs [5-8]. The performance of GaAs optoelectronic devices is adversely affected [8-9] by these non-radiative centers and traps. Better understanding and control of surface PL degradation mechanism in GaAs under low-power excitation could lead to improved device performance and surface passivation techniques [10-11].

Previous studies of PL degradation under laser excitation [5-7] give an incomplete and inconsistent picture. Suzuki and Ogawa [5] attribute PL degradation phenomena in GaAs to surface oxidation. Other authors [6,7] proposed laser-induced defect production at the surface of p-GaAs, while conflicting data are found in the literature on n-GaAs, indicating the presence [5] or absence [6-7] of laser-induced PL degradation. None of the above experiments [5-7] used a large variety of samples i.e. n-GaAs, p-GaAs, doped and undoped semi-insulating GaAs.

We have undertaken a systematic and comprehensive investigation of PL degradation in both treated and untreated GaAs [12]. Careful experimental studies of PL degradation in freshly cleaved n-GaAs (Si-doped), p-GaAs (Zn-doped), Cr-doped semi-insulating (SI) and liquid-encapsulated Czochralski-(LEC-) grown GaAs all revealed qualitatively similar behavior. All samples exhibited PL degradation for excitation intensities ranging from ~ 0.1 to 20 kW/cm^2. No intensity threshold for PL degradation was observed, but all samples showed an intensity-dependent period of relatively constant PL efficiency followed by a

Mat. Res. Soc. Symp. Proc. Vol. 126 ©1988 Materials Research Society

power-law decay. We also observed, for the first time, at least two regimes in rapid PL degradation: a fast decay occurring in 1-2 seconds immediately after a surface was freshly cleaved, and a relatively slower degradation occurring over several minutes at a rate which depended on the excitation intensity.

Here, we report an extension of our earlier investigations [12] to include GaAs surfaces treated by photowashing [1-4] or by application of organic or inorganic sulfide coatings [10]. For completeness, we have also investigated the PL degradation behavior of expitaxially grown $Al_xGa_{1-x}As$/GaAs interfaces and multiple quantum wells (MQWs) [13]. Our results suggest that a common physical mechanism probably related to recombination-enhanced defect generation or migration, is responsible for the PL decay.

EXPERIMENT

All of our experiments were carried out at room temperature in air or N_2-rich ambient. For most experiments the 514.5 nm line of an Ar-ion laser was used, but other lines including 488 and 457.9 nm were also used for comparison. The laser power was varied using neutral density filters. A 10× microscope objective was used both to focus the incident beam (9 - 10 μm diameter) onto the sample and to collect the PL, while another lens was used to match the monochromator f-number.

To probe the (110) surface of GaAs, various samples were cleaved *in-situ* and data collection began within 100 ms after cleaving. The monochromator was set to the peak of the room temperature PL. The detection apparatus included a cooled photomultiplier with photon counting electronics and a computer-controlled data acquisition system.

To investigate spectral changes, if any, during the PL degradation under laser excitation of GaAs, we also took successive spectral scans using an optical multichannel analyzer (OMA).

Photowashing of some GaAs samples was accomplished according to the procedure outlined in [1], though PL measurements could not be done *in-situ*. The photowashed samples were removed from the spinner to the PL measurement setup, the time lapse before PL data collection being ~ 2-3 minutes.

The deposition of sodium sulfide nano-hydrate ($Na_2S.9H_2O$) films [10] involved the spinning (5000 rpm) of a 1M solution in deionized water onto the (100) surface of the GaAs. Before a sulfide film was spun on, the GaAs surface was cleaned using a standard procedure involving organic solvents, rinsing in deionized water and light etching in H_2O_2:NH_4OH:H_2O (1:1:50). As for photowashing, the sample was transferred from the spinner to the PL setup within a few minutes. We also deposited some organic sulfide films using spun-on thiourea.

RESULTS

We have observed, for the first time, two PL degradation regimes for freshly cleaved p-GaAs and n-GaAs (110) surfaces. Fast decay occurring in few seconds was exhibited only by the *in-situ* cleaved p- and n-GaAs in an N_2 atmosphere. All untreated samples showed

an intensity- and doping-dependent slow PL degradation upon irradiation with photons of sufficient energy to excite electron-hole pairs, on a time scale of several minutes. Irradiation with 1.06 μm light for more than 45 minutes had no effect on PL efficiency, and degradation began only when the 514.nm probe beam was applied. The degradation was clearly a consequence of laser irradiation. Once an area had been degraded, photoluminescence efficiency did not recover upon removal of irradiation; PL decay simply resumed with reapplication of the pumping light.

Figure 1 shows PL decay observed from the (110) surface of LEC-GaAs sample at several laser intensities. The points are the experimental data, and the solid line is a fit to a power law of the form:

$$C(t) = \beta (t + t_o)^{-\gamma} + C_\infty \qquad (1)$$

where C(t) is the PL signal at time t, C_∞ its eventual steady state, γ an adjustable intensity-dependent decay rate and t_o and β are fitting parameters. The data from all four untreated sample types do not obey a simple exponential decay, but rather follow the power law (1), with different parameters for each sample type.

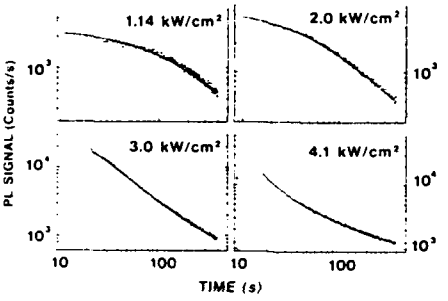

Figure 1 PL degradation in LEC-GaAs

PL degradation is not limited to (110) surfaces, nor does it require fresh surfaces: (100) surfaces also exhibit PL degradation under laser irradiation. All samples showed qualitatively similar degradation behavior, except that the extent of degradation is larger in LEC-GaAs. Most of the data presented here involve the (100) surface of LEC-GaAs.

Successive OMA scans showed a uniform depletion of the PL spectral line during laser-induced degradation. There

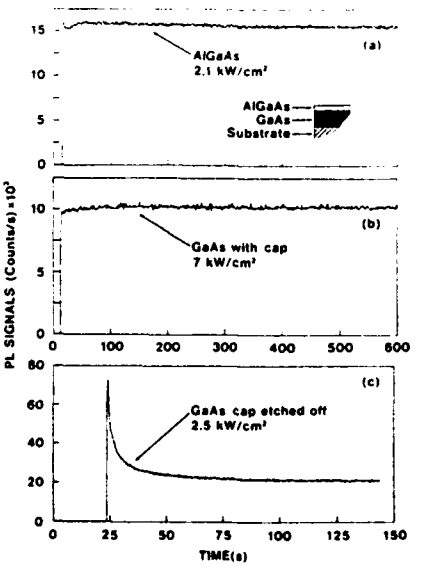

Figure 2 PL from an AlGaAs/GaAs heterostructure

was no noticeable change in any spectral feature, suggesting that the PL degradation is a consequence of production or migration of non-radiative centers.

The temporal behavior of PL from expitaxially grown $Al_xGa_{1-x}As$/GaAs interfaces and MQWs was also investigated. Typical data from LPE-grown $Al_xGa_{1-x}As$/GaAs are shown in Figure 2. Curves (a) and (b) show the time dependence of PL from $Al_{0.25}G_{0.75}As$ (790nm) and GaAs (860nm) in the presence of interface while curve (c) represents the temporal behavior of the GaAs PL when the 2 μm thick AlGaAs cap is etched away. These results are consistent with earlier reports [7,10,13] of PL from AlGaAs/GaAs heterostructures.

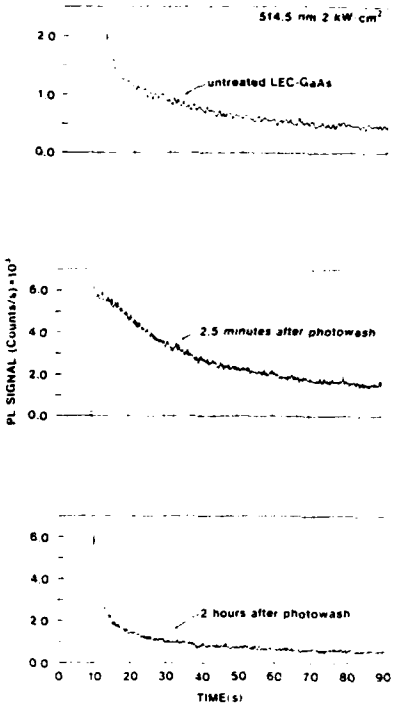

Figure 3 PL from photowashed LEC-GaAs

In Figure 3, we show the time dependence of PL from a photowashed LEC-GaAs (100) surface under low power laser excitation, an untreated sample being included for comparison. The photowashed sample shows a higher PL efficiency and a slower degradation rate, but the effect of photowashing is lost within 2 hours. Obviously, photowashing [1-4] does not prevent PL degradation, but it slows down the decay rate for a short time [10].

In contrast, the results from LEC-GaAs samples coated with $Na_2S{\cdot}9H_2O$ show much more dramatic effects. Figure 4(a) shows the time dependence of PL at three different excitation levels from LEC-GaAs with a freshly deposited film of $Na_2S.9H_2O$. In the inset, PL data are given for a relatively low (1.6kW/cm^2) excitation; after some slight ($\leq$ 10%) initial degradation, the PL remains constant. At somewhat higher intensities, a noticeable trend towards increasing PL efficiency can be seen. At an excitation intensity of 5.5kW/cm^2 the PL signal showed a pronounced improvement before reaching a constant level, and no PL degradation was observed on continued irradiation. However, when the same sample was reexamined 21 hours later, PL degradation was evident at all power levels as shown in Figure 4(b). After 40 hours, the passivating effect of the sodium sulfide film was lost completely. These results were reproducible with every fresh film of $Na_2S.9H_20$.

We also studied the effects of thiourea (NH_2CSNH_2) films on passivation of GaAs. An improvement in initial PL signal level by a factor 3 was observed, but there was no change in the degradation rate.

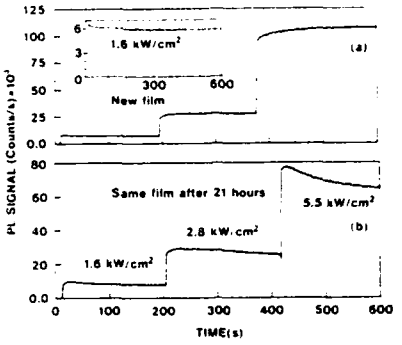

Figure 4 Time dependence of PL from sodium sulfide coated LEC-GaAs

CONCLUSIONS AND DISCUSSION

The observation that all untreated GaAs sample types, showed similar intensity-dependent PL degradation supports the idea that a common physical mechanism is responsible for the degradation. The fact that the phenomenon was also exhibited by GaAs surface exposed to ambient environment for long time and that only above bandgap photons can induce degradation suggests that recombination-enhanced defect production or migration are playing a role [12,14-16].

However, the results from treated surfaces show that the surface clearly plays an important role in the PL degradation process. For example, no PL degradation was seen at all in case of $Al_xGa_{1-x}As$/GaAs interface, but when the $Al_xGa_{1-x}As$ cap layer was etched away selectively the degradation occurred. The interface between GaAs and $Na_2S{\cdot}9H_2O$ film remains apparently fully passivated for 10-15 hours and photochemical oxide [1-4] stays effective up to several minutes only; after that the samples exhibit degradation just like untreated GaAs. From these, one can propose that the defects and non-radiative centers produced at the surface migrate into the bulk under recombination enhanced process. A recent report [8] also provides a direct experimental evidence of defect migration from cladding to the active region of a double hetrostructure light emitting diode. Moreover, our OMA scans furnish evidence that PL degradation is caused by non-radiative centers as there was no spectral change during degradation of room temperature PL.

We discuss our results with reference to recent models [17-19] and proposals [10]. According to Hayashi's model [17], the rapid PL degradation process initiates from the deep levels introduced by the "dangling bond" of an anion vacancy or vacancy complex. These deep levels result in trapping the carriers and ultimate non-radiative recombination. The recombination events provide a mechanism of energy localization that eventually leads to the production of other vacancies; dangling bond energy level associated with "daughter" vacancy becomes another trap [18]. These self reproducing dangling bond levels act as non-radiative

centers and are probably related to recombination-enhanced defect migration [14].

An other model [19] discusses the segregation of As by oxygen uptake of Ga from As_2O_3, resulting in Ga_2O_3 and elemental As which affects the surface recombination velocity in direct proportionality. However oxygen does not diffuse into the bulk [20], only the surface would be affected. Our previous results [12] show that in LEC and SI GaAs even the extreme variation between zero and infinite surface recombination velocity does not account for extent of laser induced PL degradation. The observed data can only be explained by the hypothesis that the non-radiative centers are generated and/or migrate under recombination-enhanced process.

Passivation results with sulfide films and photowashing treatment also are indicative that dangling bonds at the surface need to be completed to stop or slow down PL degradation. Our results confirm that sulfur bonds [10] are relatively more effective and stable than photooxide [1-4].

ACKNOWLEDGMENTS

This work was partially supported by the US Air Force Office of Scientific Research. Special thanks are extended to Dr. L. R. Dawson of Sandia National Laboratories for providing GaAs samples and for valuable comments. We also thank Dr. W. Streifer of Spectra Diode Laboratories and Dr. D. Kendall of CHTM for useful discussions.

REFERENCES

1. S. D. Offsey, J. M. Woodall, A. C. Warren, P. D. Kirchner, T. I. Chappell, and G. D. Pettit, Appl. Phys. Lett. 48, 415 (1986).
2. N. A. Ives, G. S. Stupian, and M. S. Leung, Appl. Phys. Lett. 50, 256 (1987);
3. S. M. Beck and J. E. Wessel, Appl. Phys. Lett., 50, 149 (1987).
4. T. Sawada, H. Hasegawa, and H. Ohno, Jpn. J. Appl. Phys. 26, L1871 (1987).
5. T. Suzuki and M. Ogawa, Appl. Phys. Lett. 34, 473 (1977).
6. N. M. Haegel and A. Winnacker, Appl. Phys. A42, 233 (1987).
7. D. Guidotti, E. Hasan, H-J Hovel, and M. Albert, Appl. Phys. Lett., 50, 912 (1987).
8. J. Ogawa, K. Tamamura, K. Akimoto, and Y. Mori, Appl. Phys. Lett. 51, 1949 (1987).
9. I. Hayashi, Jpn. J. Appl. Phys., 19, Supplement 19-1, 23 (1979).
10. E. Yablonovitch, C. J. Sandroff, R. Bhat, and T. Gmitter, Appl. Phys. Lett., 51, 439 (1987).
11. J. K. Hsu and K. M. Lau, J. Appl. Phys., 63, 962 (1987).
12. M. Y. A. Raja, S. R. J. Brueck, M. Osinski, and J. McInerney, Appl. Phys. Lett., 52, 625 (1988).
13. P. M. Petroff, C. Weisbuch, R. Dingle, A. C. Gossard and W. Wiegmann, J. Vac. Sci. Technol., 19, 57 (1987).
14. D. V. Lang and L. C. Kimerling, Phys. Rev. Lett., 33, 489 (1974).
15. K. Maeda, M. Sato, A. Kubo, and S. Takeuchi, J. Appl. Phys, 54, 161 (1983).
16. A. Sibille, Phys. Rev. B 35, 3929 (1987).
17. I. Hayashi, J. Phys. Soc. Jpn. Suppl. A49, 57 (1980).
18. J. Dow and R. E. Allen, Appl. Phys. Lett. 41, 672 (1982).
19. H. H. Lee and L. Figueroa, J. Electrochem. Soc., 135, 496 (1988).
20. K. Watanabe, M. Hashiba, Y. Hirahota, M. Nishino, and T. Yamashina; Thin Solid Films 56, 63 (1979).

Grating Coupling to Surface Plasma Waves I - First-Order Coupling

Saleem H. Zaidi, M. Yousaf[a,b] and S. R. J. Brueck[c]

Center for High Technology Materials

University of New Mexico, Albuquerque, NM 87131

ABSTRACT

A systematic experimental and theoretical study of first-order grating coupling to surface plasma waves existing at an air-Ag interface is presented. The experiment extends beyond previous work to grating depths comparable to the grating period. Grating profiles range from sinusoidal to rectangular. For TM-polarized incident radiation, this grating depth range includes the entire spectrum of surface plasma wave-radiation coupling from underdamped, to nearly 100% coupling, to overdamped and the disappearance of the resonance from the zero-order reflectance measurements. Strong polarization and absorption effects are observed for the deepest gratings. A simple theoretical model, based on the Rayleigh hypothesis and retaining only resonant diffraction terms without making a small-signal approximation, provides good agreement with the experimental results.

---

[a] Department of Physics

[b] Present address: Electronics Division, PINSTECH, P. O. Box Nilore, Islamabad, Pakistan

[c] Also with the Departments of Electrical Engineering and Physics

1. INTRODUCTION

The study of the interaction of light with periodic structures, gratings, on metals has a long and distinguished history. In 1902, Wood [1] first noticed the anomalous behavior (christened Wood's anomalies) displayed by diffraction gratings of very large and rapid changes in diffraction intensities for small angular and spectral variations. Rayleigh [2-3], in 1907, presented the first theoretical explanation of these anomalies in suggesting that such behavior was due to the cut-off or appearance of a new spectral order. Fano, in 1941, first distinguished between two types of Wood's anomalies: (1) an edge anomaly, with a sharp behavior related to passing off of a diffraction order (i.e. a diffraction order passing over the horizon, 90° to the surface normal); and (2) a resonance anomaly due to excitation of a bound or surface wave at the metal-dielectric interface[4].

Surface plasma waves are TM modes of the electromagnetic field bound to the interface between a metal and a dielectric. The condition for existence of the SPW mode is that $\epsilon_m' < -\epsilon_d$ where ϵ_m' is the real part of the metal dielectric constant and ϵ_d is the dielectric constant of the dielectric. Related modes, first investigated by Sommerfeld [5], exist when one of the media is highly lossy. The SPW phase velocity is less than the light velocity in the dielectric and phasematching between an incident, freely propagating wave and the SPW is accomplished either by prism [6] or grating coupling techniques.

The SPW dispersion relation for a planar metal-air interface is simply given by [7]

$$k_{SPW} = k_0 \sqrt{(\epsilon_m/(\epsilon_m+1))} \qquad (1)$$

where $k_0 = 2\pi/\lambda$ is the free space optical wavevector. The phasematching condition for excitation of SPWs is satisfied whenever $k_0 \sin\theta$, the component of k_0 along the metal-air interface, satisfies the condition

$$k_0 \sin\theta = \pm k_{SPW}' + n\, 2\pi/d \qquad (2)$$

where d is the grating period, θ is the angle of incidence, n=±1,±2,... is the coupling order, and k_{SPW}' is the real part of the SPW wavevector. In Eq. (2), the choice of a negative sign preceding k_{SPW}' corresponds to a SPW moving in the opposite direction to the incident wave. This expression assumes that the grating wavevector is in the plane of incidence, i.e. the grating lines are perpendicular to the incident wavevector.

The SPW dispersion relationship is plotted in Fig. 1 for a lossless, free-electron metal ($\epsilon_m = 1-\omega_p^2/\omega^2$) where the axes are normalized to the plasma frequency, ω_p, and the corresponding optical wavevector ($k_p=\omega_p/c$). Also shown as two vertical dashed lines, corresponding to n=+1 and -1 orders in Eq.(2), are the wavevectors of a surface grating. Finally, the wavevectors accessible in 0 and ±1 orders by varying the angle of incidence are shown as horizontal lines. This figure was drawn for a grating period smaller than the optical wavelength ($\lambda/d > 1$); note that there is only one point that satisfies Eq. (2), for n=-1, and at this incident angle there is no allowed diffraction order.

Y. Y. Teng and E. A. Stern, in 1967, first detected SPWs optically by bombarding 1200 lines/mm (833-nm period) gratings with 10-keV electrons and observing the emitted optical radiation [8]. They observed that the lineshape of the emitted radiation was influenced by the surface condition of the metal, but was independent of the energy of the bombarding electrons. Cowan et. al., carried out a detailed study of the SPW dispersion curves for dielectric-metal layers on concave diffraction gratings, and also developed a quantum-mechanical formalism to describe

their results [9]. Hutley et. al., in 1973, published a detailed experimental study of the anomalies of sinusoidal profile gratings as a function of grating depth [10-12] and characterized the SPW lineshapes for grating depths, h, ranging up to 60 nm for 500-nm period gratings, $h/d \leq 0.12$. The integral formalism developed by Petit et. al. [13] was used to describe these results with good agreement. Pockrand and Raether, in an extensive series of publications [14-18] characterized the SPW coupling as a function of grating period, depth, and profile. The gratings studied were sufficiently deep to realize over 98% coupling into the SPW mode. A perturbation analysis, developed by Kroger and Kretchmann [19] was used in modeling these results with good agreement, although clearly the perturbation approach must breakdown as the coupling efficiency approaches 100%. A very complete theoretical treatment of grating coupling to SPWs has been provided by Mills, Maraduddin and co-workers[20-21]. Their approach uses an integral-formulation of the boundary-value problem at the grating interface and an extinction theorem mechanism following from Green's theorem. This work does not give simple analytic results, but relies on extensive computational and numerical evaluation. Yamashita and Tsuji [22] developed a much simpler differential formulation which treats the resonantly generated fields on a par with the incident fields and allows for saturation and decreases in coupling with increasing grating depths. This work employed a power series expansion in $k_o h$ and was restricted to small grating amplitudes; simple analytic expressions were obtained for the coupling strength as a function of h.

In this work, a comprehensive experimental and theoretical study of first-order grating coupling to SPWs for a wide range of grating parameters is presented. The experimental work establishes, for the first time, a relationship between grating depth and period for SPW coupling, and extends to grating depths which no longer support SPWs but rather show polarization and absorption effects. The theoretical approach is an extension of the Rayleigh hypothesis including only resonant terms in the Rayleigh expansion. This results in considerable simplification; reasonable agreement between

theory and experiment is found out to depth/period ratios of ~0.5. A similar approach has been used by Gupta et al.[23] in describing grating coupling to long-range SPW modes on thin, symmetrically bounded, metal films.

2. GRATING FABRICATION

Gratings were fabricated holographically in positive photoresist layers spun onto Si substrates using the 488-nm line from a single-mode Ar-ion laser. Details of the grating fabrication have been presented elsewhere [24]. The grating profiles were approximately sinusoidal for shallow depths, evolving towards rectangular profiles as the depth was increased (cf. Fig 4). After development, these gratings were coated with ~ 100-nm thick e-beam evaporated Ag films. Films were deposited at room temperature and background pressures of low 10^{-6} Torr.

3. OPTICAL ARRANGEMENT

All of the measurements reported here are of the angular dependance of the zero-order reflectance for a fixed-frequency TM-polarized HeNe laser beam at 633 nm. The samples were mounted as one surface in a 90° corner reflector attached to a computer-controlled rotation stage. This arrangement insured that the reflected beam was always returned in the same direction and eliminated the necessity of a second rotation stage for the detector. The incident laser beam was focused with a long focal length lens (0.5 m) to a spot of ~ 2 mm. This provided an angular limitation of 0.05°, much smaller than the observed reflectance variations. Care was taken with the alignment to insure that the axis of the rotation stage was in the plane of the grating so that the laser spot sampled the same area of the grating throughout a scan. Grating depths were measured in cross section with a scanning electron microscope (SEM). This introduces some errors, estimated at ±5 nm, due to uncertainties in the SEM calibration

and variations in the grating depth for the different areas sampled in the optical and SEM measurements.

4. EXPERIMENTAL RESULTS

Zero-order reflectance measurements for a series of 510-nm gratings with increasing depth are shown on the left-hand side of Fig. 2. The theoretical modeling shown on the right-hand side will be discussed below. The major features to note in these measurements include:

1. the excitation of SPWs at $\theta \sim 11.6°$ corresponding to the sharp dip in the reflectivity; (Note that there is no diffracted order at this angle so that this decrease corresponds directly to energy coupled into the SPW mode.)
2. the rapid increase in coupling efficiency with increasing grating depth to a maximum observed coupling of 94% at a grating depth of 35 nm; and
3. the horizon for the -1 diffracted order at $\theta \sim 13.8°$; (This is apparent as the cusp in the reflectivity as energy is transferred from the specularly reflected beam to the diffracted beam.)

Similar results for deeper gratings are presented on the left-hand side of Figure 3. Note the larger angular scale in this figure. Specific features to note include:

1. the relatively gradual decrease in the coupling efficiency to SPWs;
2. the clear broadening of the SPW resonance with increasing depth;
3. the shift in the SPW resonance to smaller angles with increasing depth;
4. the residual SPW coupling even at very large grating depth/period ratios; and
5. the increasing coupling to the -1 diffraction order. (The sharp spike at ~ 38° corresponds to the collection of the -1 diffraction order in the optical

system and is not part of the zero-order reflectance. It does provide a useful monitor of the energy in the diffracted order.)

Scanning electron micrograph (SEM) images of the gratings used for the measurements of Fig. 3, taken in cross-section, are shown in Fig. 4. Note that the grating shapes are sinusoidal at very low depths but gradually show increasing harmonic components and trend towards rectangular profiles for the deepest gratings investigated. This profile modification results from the grating fabrication technique.[24]

Similar experiments were performed for gratings with periods of 392 nm and 440 nm, in order to investigate the dependance of the coupling efficiency on grating depth and grating period. All experiments were carried out at a wavelength of 633 nm to avoid variations in the metal optical properties. Qualitatively similar behavior was observed with comparable coupling efficiencies occuring at shallower grating depths for finer gratings. Experimentally determined coupling efficiencies, resonance angles, and resonance linewidths for all three sets of gratings are presented in Figs 5-7. The solid curves are theoretical and will be discussed subsequently. With increasing grating depth, each of the data sets displays an initial rapid increase in coupling efficiency, peaking at over 90%, and a slower decrease in efficiency; an approximately quadratic decrease in the resonant coupling angle, and an approximately quadratic increase in the resonance width.

These results are summarized in Fig 8, which shows all three sets of data plotted against the dimensionless parameter h/d, i.e. grating depth/grating period. Within experimental uncertainties, these results appear to follow a common behavior. Some of the variability may well arise from differing grating profiles, especially for the deeper gratings.

Further increases in grating depth, accompanied by a change in profile to rectangular, lead to an elimination of SPW effects. For approximately square gratings,

very strong polarization effects demonstrate the possibility of fabricating reflective polarizers for visible radiation. This is shown in Fig. 9 where reflectance scans for the three grating periods are shown for depths of 200 nm (392-nm period), 170 nm (440-nm period) and 190 nm (510-nm period) which resulted in maximum polarization effects. Note that for TM polarization, almost 100% of the incident energy (~96% for the 510-nm period grating) is coupled into the first-order diffraction peak for angles beyond the horizon for this order. In contrast, only about 20% of the energy polarized in the TE direction is coupled out of the zero-order reflected beam. Careful variations of grating depth and profile must be investigated to optimize the polarization of the reflected beam. Such polarization behavior for square gratings has been predicted [25-26] and demonstrated in the infrared [27], to our knowledge, this is the first observation of these effects in the visible spectral region. SEM pictures of the gratings are shown in Fig. 10.

Further increases in grating depth result in rectangular profiles with decreasing line space ratios. Angular reflectance scans for deep rectangular gratings are shown in Fig. 11. (top 320-nm deep, 392-nm period; middle 330-nm deep, 440-nm period; bottom 300-nm deep, 510-nm period) There is a broad absorption of TM-polarized radiation while very large diffraction efficiency, increasing with increasing periods, is observed for TE polarization. Figure 12 shows SEMs of these gratings.

5. THEORY

During the past thirty years, many grating theories based on the vector character of the electromagnetic field have been developed. An excellent summary can be found in references [6,13,20]. Integral methods, developed by Petit et. al. evaluate the field at any point in terms of an integral over the grating surface A, cf. Fig. 13. A variation of these integral techniques based on a Green's function formalism specifically directed to the evaluation of the SPW dispersion relation on a periodic surface has been extensively developed by Mills, Maraduddin [20,21] and Otagawa [28]. In addition, a differential

formalism, developed by Nevierre et. al. [13] has been applied to SPWs on periodic surface by Numata [29]. All of these approaches are fully rigorous, hold for arbitrary profiles, and require extensive computation, typically involving matrices of order 40 or higher.

A number of differential analyses, usually based on a perturbation expansion in k_oh where h is the grating depth, and relying on a Rayleigh or plane wave approach have also been presented[19,30,31]. In these treatments, the scattered field amplitudes are also treated as small quantities, of the order of k_oh times the incident and reflected/transmitted field amplitudes. These models have the virtue of relatively simple analytical results and ready physical interpretation. These perturbational approaches clearly breakdown as the coupling efficiencies into SPW modes and diffraction orders approach unity since they do not self-consistently describe the necessary decrease in the zero-order reflected and transmitted beams. Yamashita et al. [22] treated the coupling problem within the Rayleigh hypothesis without making the small-signal approximation for the resonant scattered fields; however, their treatment retained the expansion in k_oh which limits its applicability to larger grating amplitudes. Nevertheless, their model provided a very elegant analytic result which included the quadratic, $\propto(k_oh)^2$, increase in the SPW intensity with grating depth for shallow gratings, saturation of the SPW intensity at a coupling efficiency near 100%, and a gradual decrease of the coupling, $\propto(k_oh)^{-2}$, for deeper gratings as the energy is coupled back into the radiating fields, in qualitative agreement with the experimental results presented above.

These models begin with a time harmonic, plane wave expansion of the electromagnetic field in the regions outside of the grating kerf ($z<0$ and $z>h$, Fig. 13) the magnetic field of the TM-polarized fields are given by

$$B^v = B^v e_x=(\exp(ik_y y+ik_z z) + \Sigma B^v{}_n \exp[i(k_n y-\alpha_n z)])e_x \quad z<0 \qquad (3a)$$

and

$$B^m = B^m e_x = \Sigma B^m{}_n \exp[i(k_n y+\beta_n z)]\, e_x \qquad z>h \qquad (3b)$$

where $k_y=k_o\sin\theta$, $k_z=k_o\cos\theta$, $k_n=k_y+ng$, $n=0,\pm1,\pm2,...$, $g=2\pi/d$ is the grating wavevector with d the grating period, $\alpha_n=\iota\sqrt{(k_n^2-k_o^2)}$, $\beta_n=\iota\sqrt{(k_n^2-\epsilon_m k_o^2)}$ and ϵ_m is the metal dielectric constant. Within the grating kerf, $(0<z<h)$, the validity of this expansion is not well-established. Rayleigh made the assumption, known as the Rayleigh hypothesis, that for sufficiently shallow gratings, this expansion is valid everywhere. This hypothesis was investigated by Van den Berg et al. [32] and shown to be analytically correct; Petit et al. [33] showed that for TE polarization, the Rayleigh expansion is convergent for $h/d<0.14$ and pointed out that reliable results could still be obtained even for h/d as much as twice this limit.

The approach used in this comparison with experiment is to apply the Rayleigh hypothesis for TM-polarized input radiation. For the gratings used in these experiments, h/d extends to 0.8 although detailed comparisons are only attempted to ~0.3. The calculation does not make a small signal approximation for either the grating depth or the diffracted field amplitudes. The plane wave expansion, Eq. 3, is truncated by keeping resonant terms, e.g. n=0, -1. In addition, the next terms, n=-2 and +1 are retained in the numerical evaluations and are determined to be small relative to the resonant terms. Energy conservation, i.e. a constant total of the energies in the diffracted beams and absorbed in the metal is used as a further check on the calculation.

Thus, Eq. 3 is assumed to hold up to the grating surface defined by

$$f(y) = u \sin(gy) \qquad (4)$$

where $u=h/2$ is the grating amplitude. Using the generating function for Bessel functions, we can write

$$e^{i\gamma f(y)} = e^{i\gamma u \sin(gy)} = \Sigma e^{ipgy} J_p(\gamma u) \tag{5}$$

The boundary conditions satisfied by these fields are

$$\{B^v(y,z) = B^m(y,z)\}|_{z=f(y)} \tag{6}$$

and

$$\left\{ \frac{\partial B^v(y,z)}{\partial n} = \frac{1}{\epsilon_m} \frac{\partial B^m(y,z)}{\partial n} \right\} \Bigg|_{z=f(y)} \tag{7}$$

where

$$\frac{\partial}{\partial n} = \left(1 + \left(\frac{\partial f}{\partial y}\right)^2\right)^{-1/2} \left(\frac{\partial}{\partial z} - \frac{\partial f}{\partial y}\frac{\partial}{\partial y}\right)$$

Applying these boundary conditions leads to a set of coupled linear equations:

$$J_p(k_z u) + \Sigma B^v_n (-1)^{p-n} J_{p-n}(\alpha_n u) - \Sigma B^m_n J_{p-n}(\beta_n u) = 0 \tag{8}$$

and

$$(k_z - pgk_o/k_z) J_p(k_z u) - \Sigma(\alpha_n - (p-n)gk_n/\alpha_n) B^v_n (-1)^{p-n} J_{p-n}(\alpha_n u)$$

$$- 1/\epsilon_m \Sigma(\beta_n - (p-n)gk_n/\beta_n) B^m_n J_{p-n}(\beta_n u) = 0. \tag{9}$$

where p,n are integers extending from $-\infty$ to $+\infty$. Note that no small signal approximation has been made in deriving these equations. These equations are now truncated by keeping only the fields for n=0 and n=-1, the reflected/transmitted and resonant diffracted terms which are expected to be large based on phasematching arguments (cf. Eq. 2 and Fig. 1). In addition the fields for n=+1,-2 were also retained

as a check on the convergence. The relative field intensities for these two orders for a 510-nm period grating at a depth of 22 nm were 0.017 and 0.0018, respectively, lending support to this truncation procedure. This leads to an 8x8 matrix inversion to solve for the field intensities.

Using the Green's function approach developed by Mills et al.[20], Garcia evaluated the SPW fields and lineshape for sinusoidal gratings [34]. Results, obtained by including 60 terms in the numerical analysis, are shown in Fig. 14a for parameters appropriate to an 800-nm period Au grating of various depths, $h_1=h/2d$. For this grating period and wavelength, 633 nm, $\lambda/d<1$ and there are two possible propagating diffraction orders. The resonance shown in Fig 14 corresponds to the n=+1 SPW coupling; there is also a propagating n=-1 diffraction order throughout this angular range. The numbers labeling the SPW curves in the figure represent the relative intensity of the mode. The results from the present treatment for the same parameters are shown in Fig. 14b-d. Note the overall similarity of the calculated intensities and lineshapes. Interestingly, the largest discrepancy is for the shallowest grating, $h_1=0.01$, where the present calculation yields a SPW intensity 24% larger than the more rigorous calculation of Garcia[34]. For deeper gratings, the agreement is generally within 10%. This comparison indicates that, despite the relative simplicity of the formulation, the present model provides substantial insight into SPW coupling.

6. Comparison of Theory and Experiment

The initial step in comparing this model with the experimental results is in establishing the dielectric properties of the Ag films. Johnson and Christy [35] have measured a complex dielectric constant of (-16.4,0.54) for Ag at 633 nm. However, this was measured for very carefully prepared bulk material; in general, the dielectric properties of thin-films will differ from this value as a result of deposition and substrate dependent columnar structure, granularity, sub-ideal density and incorporated impurities.

The effective dielectric constant for such films can be described using the Maxwell-Garnet model [30]. This model provides an effective ϵ for a composite material composed of spherical dielectric grains, with spatial dimensions much less than a wavelength, interspersed throughout a metal matrix with the mole fraction, X, of the dielectric as the only adjustable parameter. The effective dielectric properties are given by

$$\epsilon = \epsilon_m \frac{(2\epsilon_m(1-X) + (1+2X))}{(\epsilon_m(2+X) + (1-X))} \qquad (10)$$

where the dielectric has been assumed to have $\epsilon_d=1$. In Fig. 15, the experimental result for a depth of 22 nm is shown along with the calculated results for X=0 and X=0.11. This value was chosen to match the experimental and calculated resonance angles. The experimental trace is somewhat broader than the theoretical indicating that there may be an additional loss mechanism, possibly due to scattering or to the effects of a non-sinusoidal grating profile. For X=0.11, the composite dielectric constant is ϵ=(-13.5,0.46); this value of ϵ was used in all of the comparisons with experiment without any further adjustment.

Comparisons with the experimental results are shown on the right-hand side of Figs. 2 and 3. In each case, the grating depth for the calculation is adjusted to give coupling efficiencies that match the experimental results. While the experimental depths and linewidths are systematically larger than the model calculations, the overall behavior is well described. For the deepest grating shown experimentally, h = 145 nm, there is a substantial difference with the model that is probably associated with the significant deviation from a simple sinusoidal profile at this depth (cf. Fig. 4). Figures 5-7 present the model results along with the experimental data for the coupling efficiency, resonance angle and resonance linewidth for all three grating periods investigated. The theory systematically overstates the coupling strength and understates the linewidth for all three

grating sets. There is reasonably good agreement with the resonance angle, which was the parameter used to adjust the metal-film dielectric properties. There is an excellent qualitative match between theory and experiment. The coupling efficiencies first increase rapidly as the grating depth is increased, saturate near 100% coupling and then decrease as the resonance becomes over-coupled due to radiative damping back into the zero-order radiation fields. This coupling change is accompanied by approximately quadratic changes in the resonance angle and linewidth with increasing grating depth.

The model results are summarized in Fig. 16 which shows the calculated resonance angle, linewidth, and coupling strength plotted against the dimensionless parameter h/d for the three grating periods investigated. For evaluation of the coupling efficiency, this parameter is reasonably invariant, there are more significant deviations in the evaluation of the resonance lineshape parameters.

Overall, this simple model provides a good picture of the experimentally observed resonance variations. Disagreements between theory and experiment increase for deeper gratings and larger periods. A significant phenomenon not included in the theoretical model is the deviation from sinusoidal grating profiles which increases as the grating depth is increased and also is more significant for larger grating periods. The films also exhibit significant surface roughness, see Fig. 4, which has not been included in the model and may impact the observed lineshapes.

Calculated zero-order, TM-polarization reflectivity curves for deeper gratings, up to h/d~1, are shown in Fig. 17. Again, there is very good qualitative agreement with the large coupling into the diffraction order for deep gratings, h/d~0.5, although detailed comparisons are not possible because of the strong deviation from a simple sinusoidal profile of the experimental gratings. The model does not show the absorption of TM-polarized radiation seen experimentally. Detailed comparison with experiment requires very deep sinusoidal gratings that are inherently difficult to fabricate because of the strong nonlinearities of existing photoresists [24]. More nearly sinusoidal gratings

can be fabricated on a transparent substrate, work is in progress to allow a better experimental test of the model for deep gratings. The theoretical model looses much of its simplicity for rectangular gratings where many Fourier components of the grating profile are comparable in intensity.

7. Summary

A systematic experimental and theoretical study of first-order grating coupling to SPWs existing at an air-Ag interface has been reported. The experiment extends the range of grating depths that have been investigated to h/d~1. For TM-polarized incident radiation, this includes the entire range of SPW-radiation coupling from underdamped to nearly 100% coupling to overdamped and the ultimate disappearance of the SPW resonance from the observed zero-order reflectance. Strong polarization and absorption effects are observed for the deepest gratings. A simple theoretical model, based on the Rayleigh hypothesis and retaining only resonant diffraction terms without making a small-signal approximation, provides good agreement with the experimental results.

Several extensions of this work are immediately apparent. For larger grating periods, there are more diffraction orders and SPW coupling resonances. Interesting coupling effects occur when two of these resonances occur at approximately the same angle. These effects have been investigated experimentally and theoretically and will be reported in a subsequent publication. In addition, the SPW resonance can be used to characterize metal optical constants under a variety of deposition conditions. Work is underway to compare this technique with more conventional techniques such as ellipsometry.

Acknowledgement: This work was partially supported by the Air Force Office of Scientific Research.

References:

1. R. W. Wood, Philos. Mag. 4, 396 (1902).

2. Lord Rayleigh, Philos. Mag. 14, 60 (1907)

3. Lord Rayleigh, Proc. R. Soc. London Ser. A79, 399 (1907).

4. U. Fano, J. Opt. Soc. Am. 31, 213 (1941).

5. A. Sommerfeld, Ann. Physik 28, 665 (1909).

6. *Electromagnetic Surface Modes*, edited by A. D. Boardman, John Wiley and Sons, 1982.

7. E. A. Stern, as quoted in R. A. Ferrel, Phys. Rev. 111, 1214 (1958).

8. Y. Y. Teng and E. A. Stern, Phys. Rev. Lett. 19, 511 (1967).

9. J. J. Cowan and E. T. Arakawa, Z. Physik 235, 97 (1970).

10. M. C. Hutley, Optica Acta 20, 607 (1973).

11. M. C. Hutley and V. M. Bird, Optica Acta 20, 771 (1973).

12. M. C. Hutley and D. Maystre, Opt. Comm. 19, 431 (1976).

13. *Electromagnetic Theory of Gratings*, Edited by R. Petit, Springer-Verlag, 1980.

14. I. Pockrand, Phys. Lett. 49A, 259 (1974).

15. I. Pockrand and H. Raether, Opt. Comm. 18, 395 (1976).

16. I. Pockrand, J. Phys. D9, 2423 (1976).

17. I. Pockrand and H. Raether, Appl. Opt. 16, 1784 (1977).

18. H. Raether, Opt. Comm. 42, 217 (1982).

19. E. Kroger and E. Kretschmann, Phys. Stat. Sol. B76, 515 (1976).

20. *Surface Polaritons*, Edited by V. M. Agranovich and D. L. Mills, North-Holland, 1982.

21. M. Weber and D. L. Mills, Phys. Rev. B27, 2698 (1983)

22. M. Yamashita and M. Tsuji, J. Phys. Soc. Jpn. 52, 2462 (1983).

23. S. D. Gupta, G. V. Varada, and G. S. Agarwal, Phys. Rev. B36, 6331 (1987).

24. Saleem H. Zaidi and S. R. J. Brueck, Appl. Opt. 27, 2999 (1988).

25. J. L. Roumiguieres, D. Maystre, and R. Petit, J. Opt. Soc. Am. 67, 557 (1977).

26. J. L. Roumiguieres, Opt. Comm. 19, 76 (1976)

27. K. Knop, Opt. Comm. 26, 28 (1978).

28. Kenji Utagawa, J. Opt. Soc. Am. 69, 333 (1979).

29. H. Numata, J. Phys. Soc. Jpn. 51, 2575 (1982).

30. S. S. Jha, J. R. Kirtley, and J. C. Tsang, Phys. Rev. B22, 3973 (1980).

31. F. Toigo, A. Marvin, V. Celli, and N. R. Hill, Phys. Rev. B15, 5618 (1977).

32. P. M. Van den Berg and J. T. Fokkema, J. Opt. Soc. Am. 69, 27 (1979)

33. R. Petit and M. Cadilhac, C. R. Acad. Sci. 262, 468 (1966).

34. N. Garcia, Opt. Comm. 45, 307 (1983); ibid. 45, 301 (1983).

35. P. B. Johnson and R. W. Christy, Phys. Rev. B6, 4370 (1972).

36. J. P. Marton and J. R. Lemon, Phys. Rev. B4, 271 (1971).

Figure Captions:

Fig. 1: Dispersion relation of SPWs for a lossless, free-electron metal ($\epsilon=1-\omega_p^2/\omega^2$). The axes are normalized to ω_p and $k_p=\omega_p/c$. The grating wavevectors corresponding to n=±1 order of a grating of period d are shown as vertical dashed lines. The range of wavevectors accessible by varying the input angle from normal to grazing incidence for n=0,±1 are shown as horizontal lines. Note that for this choice of parameters, ($\lambda/d<1$), there is only one SPW coupling resonance and at this resonance angle, there is no propagating diffraction order.

Fig. 2: Zero-order reflectance at 633 nm for 510-nm period gratings with varying grating depths. The left side, (a-d), presents experimental results; the right side, (e-h), presents theoretical modeling. See text for details.

Fig. 3: Continuation of Fig.2 for deeper gratings. Note the expanded angular scale. Again, the left side (a-d) presents experimental results, the right side (e-h) theoretical modeling. The sharp spikes on the experimental data at ~38° correspond to the n=-1 diffraction order entering the collection optics and are not a part of the zero-order reflectivity.

Fig. 4: Cross section SEMs of the gratings used for the experiments. The measured depths are: a- 43 nm, b- 57 nm, c- 88 nm, and d- 145 nm.

Fig. 5: Coupling efficiency into the SPW mode for gratings with periods of (a) 392 nm, (b) 440 nm, and (c) 510 nm and varying depths. The solid curves are the result of theoretical modeling, see text for details.

Fig. 6: SPW resonance angle for gratings with periods of (a) 392 nm, (b) 440 nm, and (c) 510 nm and varying depths. The solid curves are the result of theoretical modeling, see text for details.

Fig. 7: SPW resonance linewidth (FWHM) for gratings with periods of (a) 392 nm, (b) 440 nm, and (c) 510 nm and varying depths. The solid curves are the result of theoretical modeling, see text for details.

Fig. 8: Data of Figs. 5-7 for the SPW resonance angle, resonance width, and coupling efficiency replotted against the dimensionless parameter h/d. Note that this parameter is approximately invariant for these three grating periods.

Fig. 9: Sequence of zero-order reflectance scans for approximately square gratings (h/d~0.5) showing strong polarizing effects: (a) h=200 nm, d=392 nm; (b) h=170 nm, d=440 nm; and (c) h=190 nm, d=510 nm.

Fig 10: SEMs of the gratings used for the measurements of Fig. 9.

Fig. 11: Sequence of zero-order reflectance scans for deeper rectangular gratings (h/d~1) showing strong absorption effects: (a) h=320 nm, d=392 nm; (b) h=330 nm, d=440 nm; and (c) h=300 nm, d=510 nm.

Fig 12: SEMs of the gratings used for the measurements of Fig. 11.

Fig. 13: Geometry used in the analysis.

Fig. 14: Comparison of calculations of Garcia[34] (a) with present calculations (b-e) for 800-nm period Au gratings at 633 nm. (h_1=h/2d)

Fig. 15: Calculated zero-order reflectivity SPW resonance lineshapes for X=0 and X=0.11 where X is the mole fraction of voids in the Ag film. (h= 15 nm, d=510 nm) A Maxwell-Garnet model is used to adjust the composite dielectric constant. The experimental result (h= 22 nm) is shown as the dotted line.

Fig. 16: Calculated SPW resonance parameters plotted against the dimensionless parameter h/d.

Fig. 17: Calculated zero-order reflectivity for deep (h/d~1) sinusoidal gratings in TM polarization (d=510 nm).

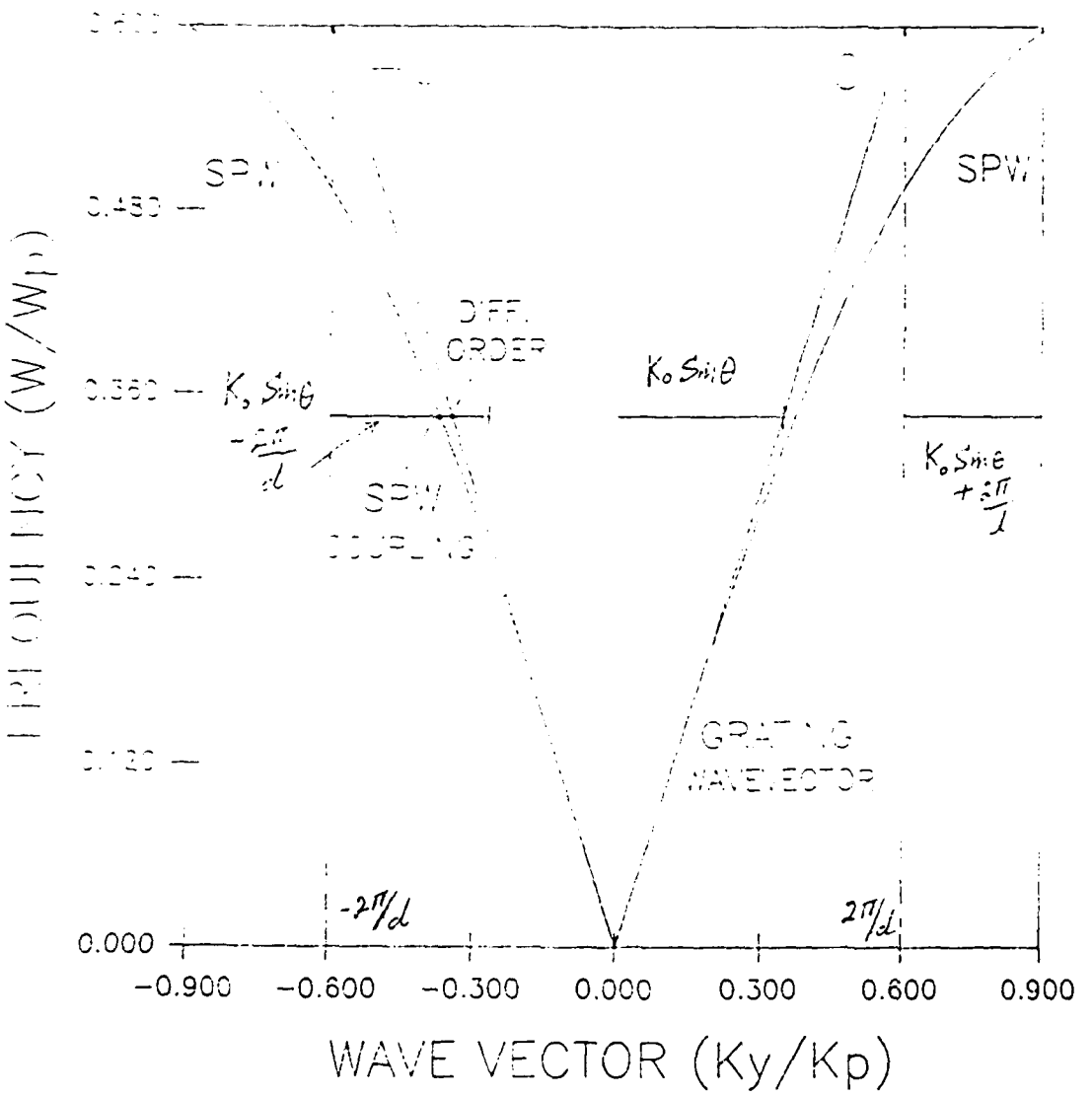
SPW
SPW
DIFF. ORDER
$K_o \sin\theta$
$K_o \sin\theta - \frac{2\pi}{d}$
$K_o \sin\theta + \frac{2\pi}{\lambda}$
SPW COUPLING
GRATING WAVEVECTOR
$-2\pi/d$
$2\pi/d$
0.480
0.360
0.240
0.120
0.000
−0.900
−0.600
−0.300
0.000
0.300
0.600
0.900
FREQUENCY (W/Wp)
WAVE VECTOR (Ky/Kp)

Fig. ①

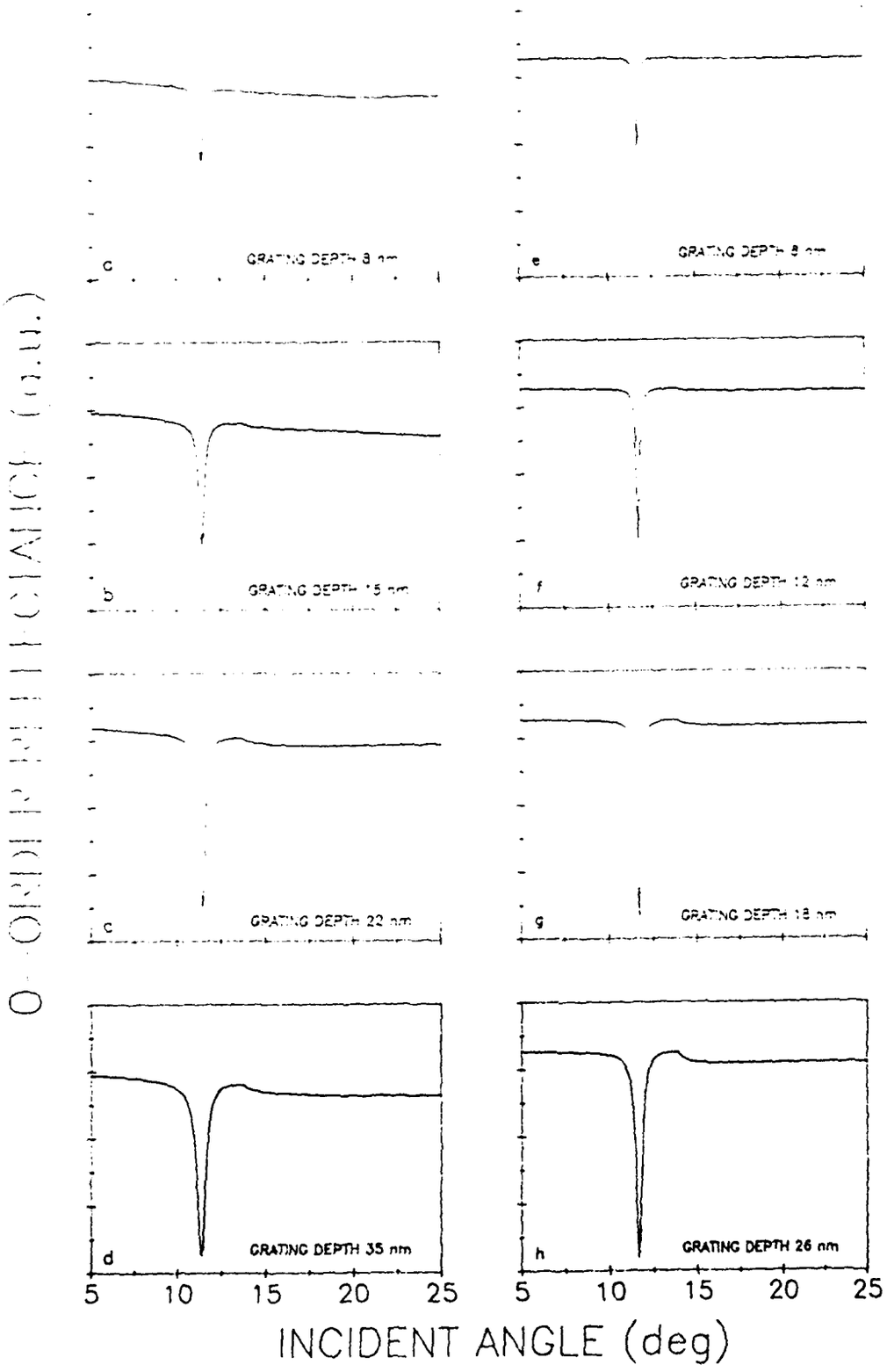
0-ORDER REFLECTANCE (a.u.)
c
GRATING DEPTH 8 nm
e
GRATING DEPTH 8 nm
b
GRATING DEPTH 15 nm
f
GRATING DEPTH 12 nm
a
GRATING DEPTH 22 nm
g
GRATING DEPTH 18 nm
d
GRATING DEPTH 35 nm
h
GRATING DEPTH 26 nm
5
10
15
20
25
INCIDENT ANGLE (deg)

Fig 3

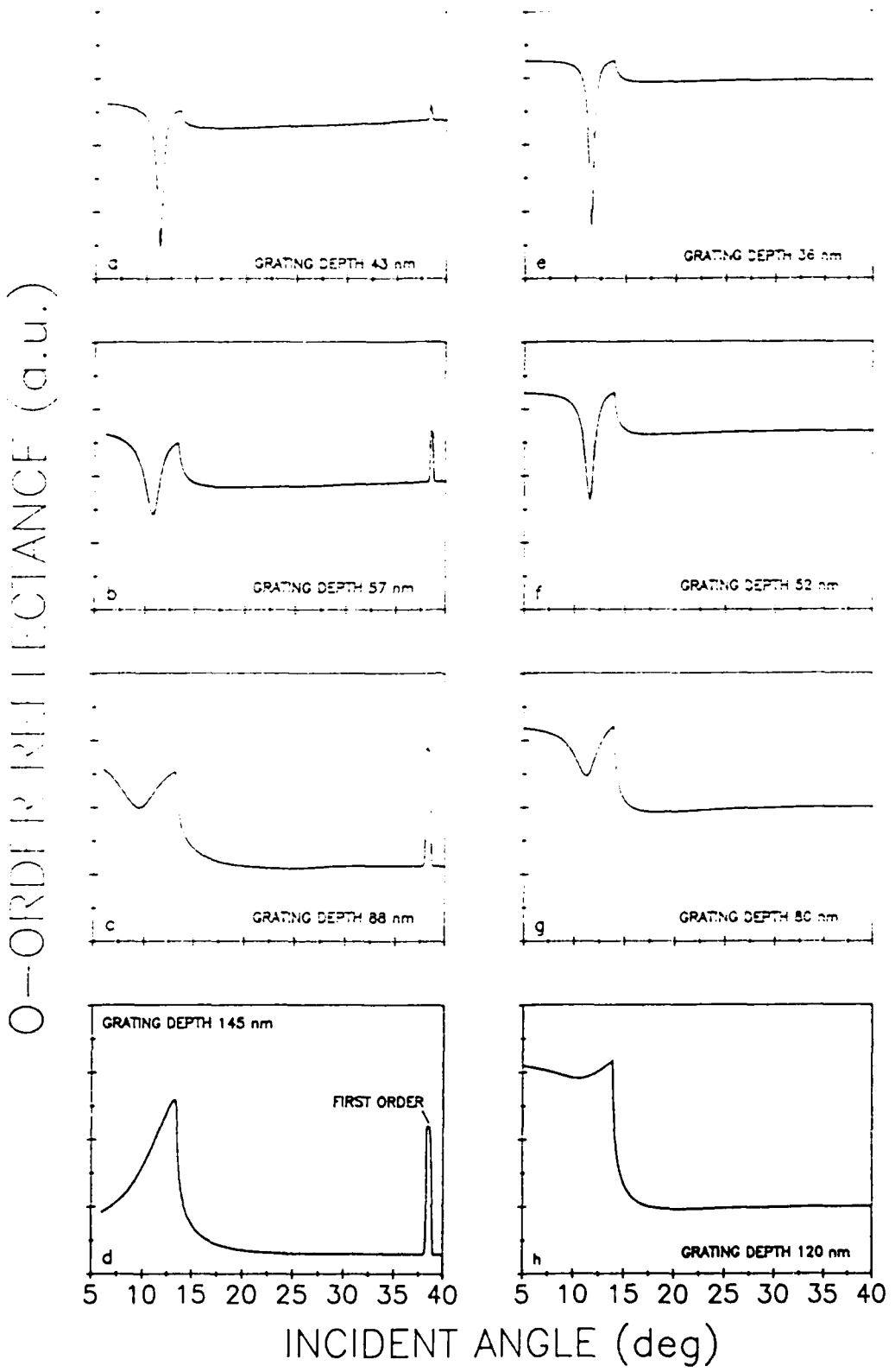
0-ORDER REFLECTANCE (a.u.)
a
GRATING DEPTH 43 nm
e
GRATING DEPTH 36 nm
b
GRATING DEPTH 57 nm
f
GRATING DEPTH 52 nm
c
GRATING DEPTH 88 nm
g
GRATING DEPTH 80 nm
GRATING DEPTH 145 nm
FIRST ORDER
d
h
GRATING DEPTH 120 nm
5 10 15 20 25 30 35 40
5 10 15 20 25 30 35 40
INCIDENT ANGLE (deg)

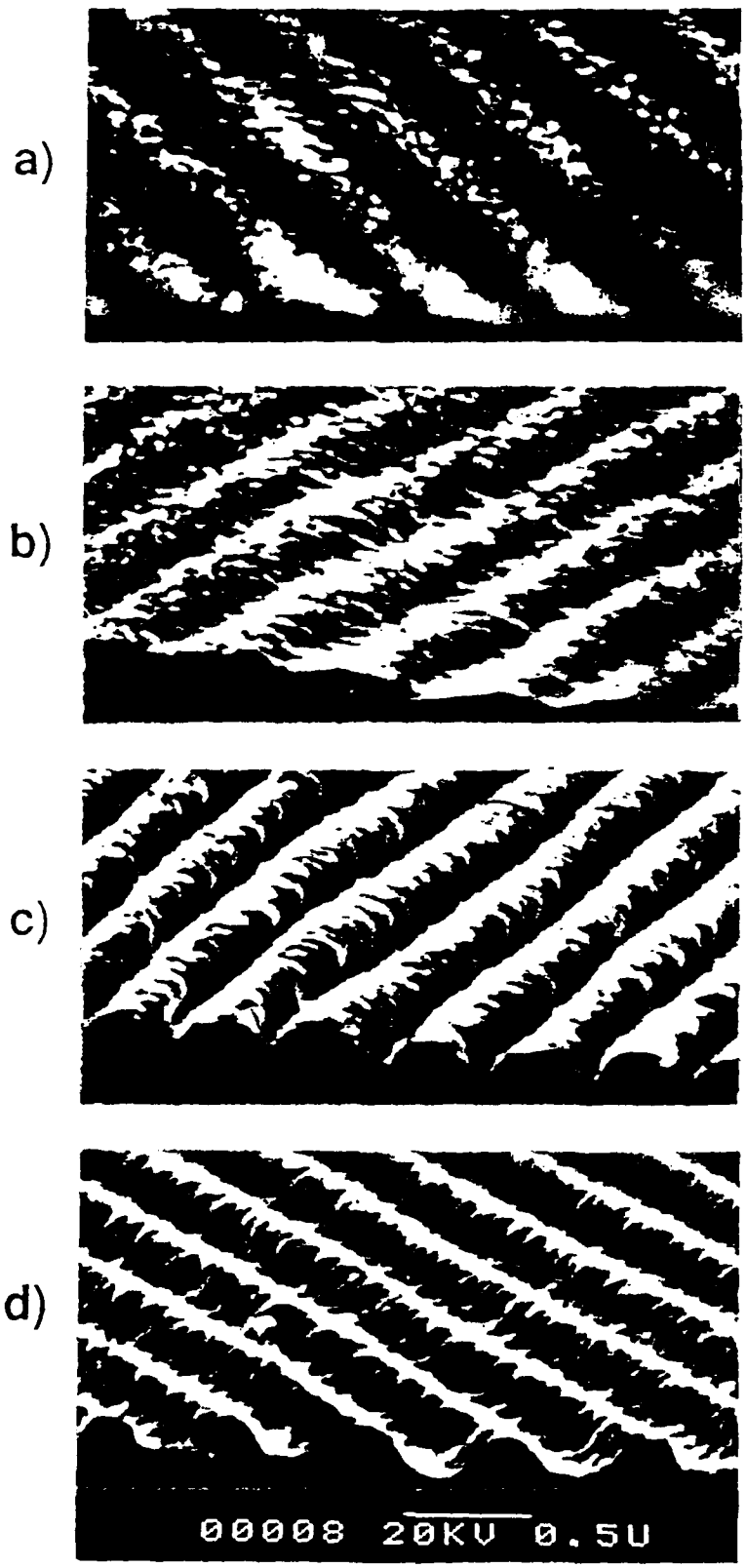

Fig 4

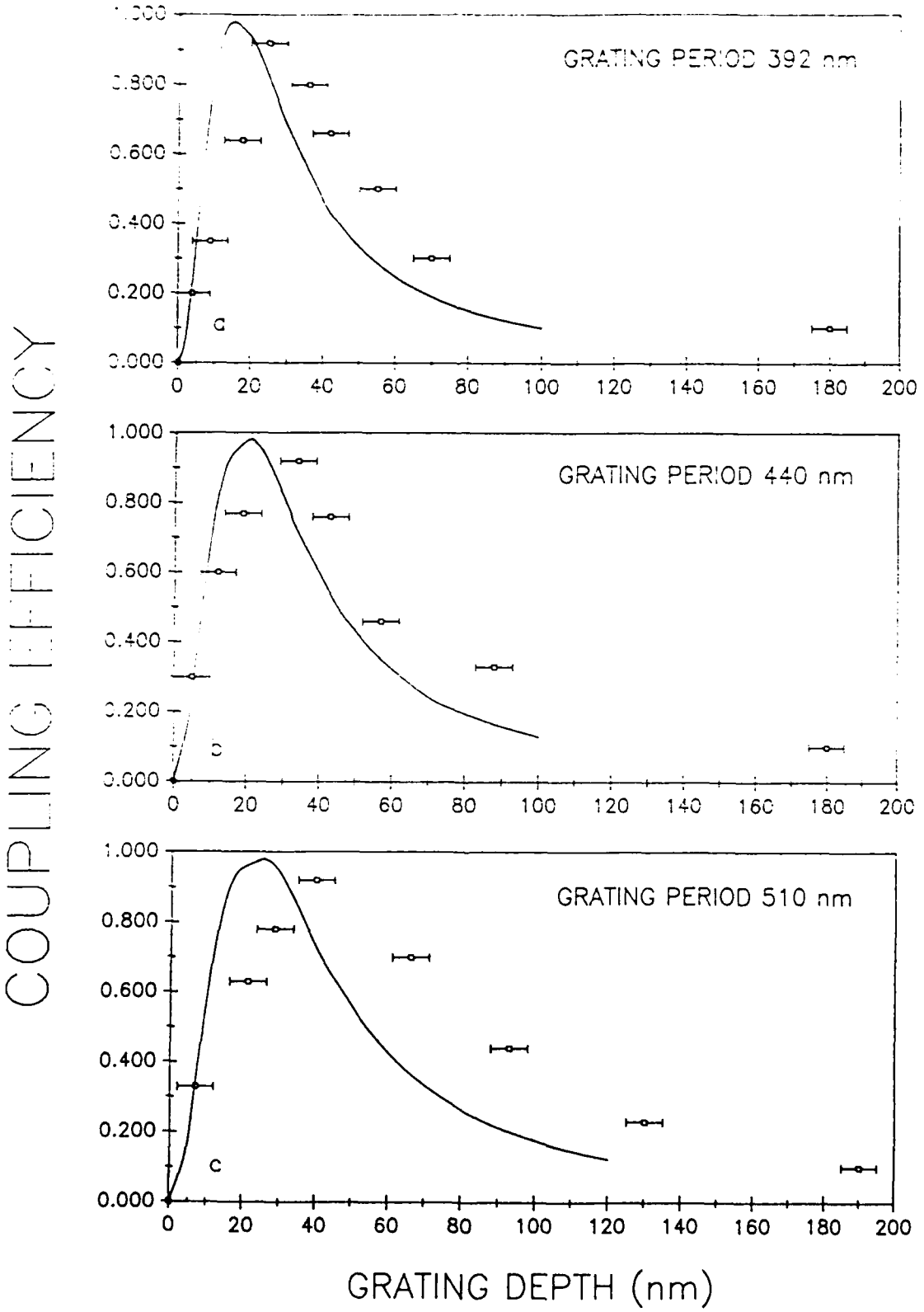
COUPLING EFFICIENCY
GRATING PERIOD 392 nm
GRATING PERIOD 440 nm
GRATING PERIOD 510 nm
1.000
0.800
0.600
0.400
0.200
0.000
0
20
40
60
80
100
120
140
160
180
200
GRATING DEPTH (nm)

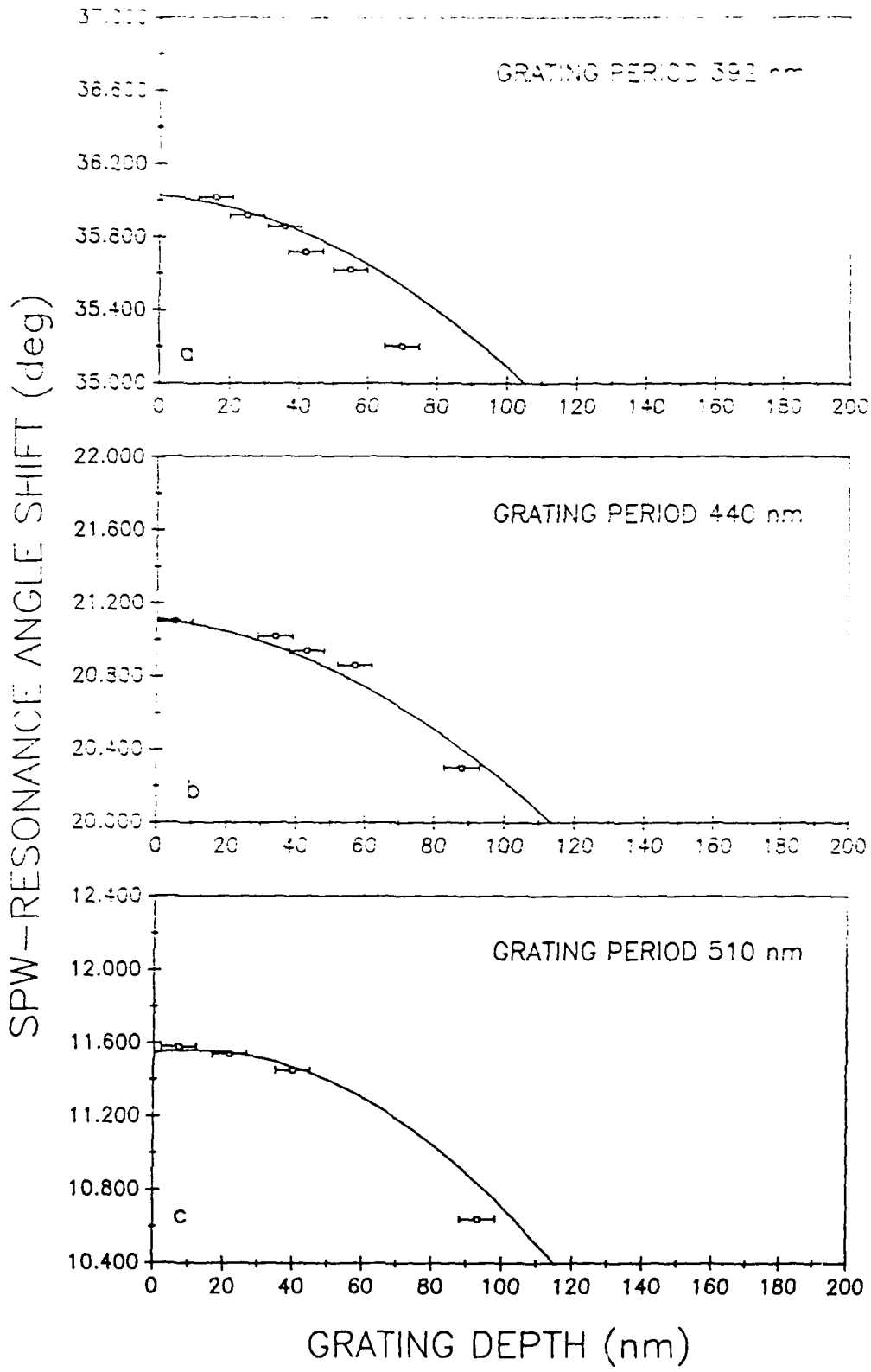
GRATING PERIOD 391 nm
36.800
36.200
35.800
35.400
35.000
a
0 20 40 60 80 100 120 140 160 180 200
22.000
21.600
21.200
20.800
20.400
20.000
GRATING PERIOD 440 nm
b
0 20 40 60 80 100 120 140 160 180 200
12.400
12.000
11.600
11.200
10.800
10.400
GRATING PERIOD 510 nm
c
0 20 40 60 80 100 120 140 160 180 200
SPW–RESONANCE ANGLE SHIFT (deg)
GRATING DEPTH (nm)

Fig 10.

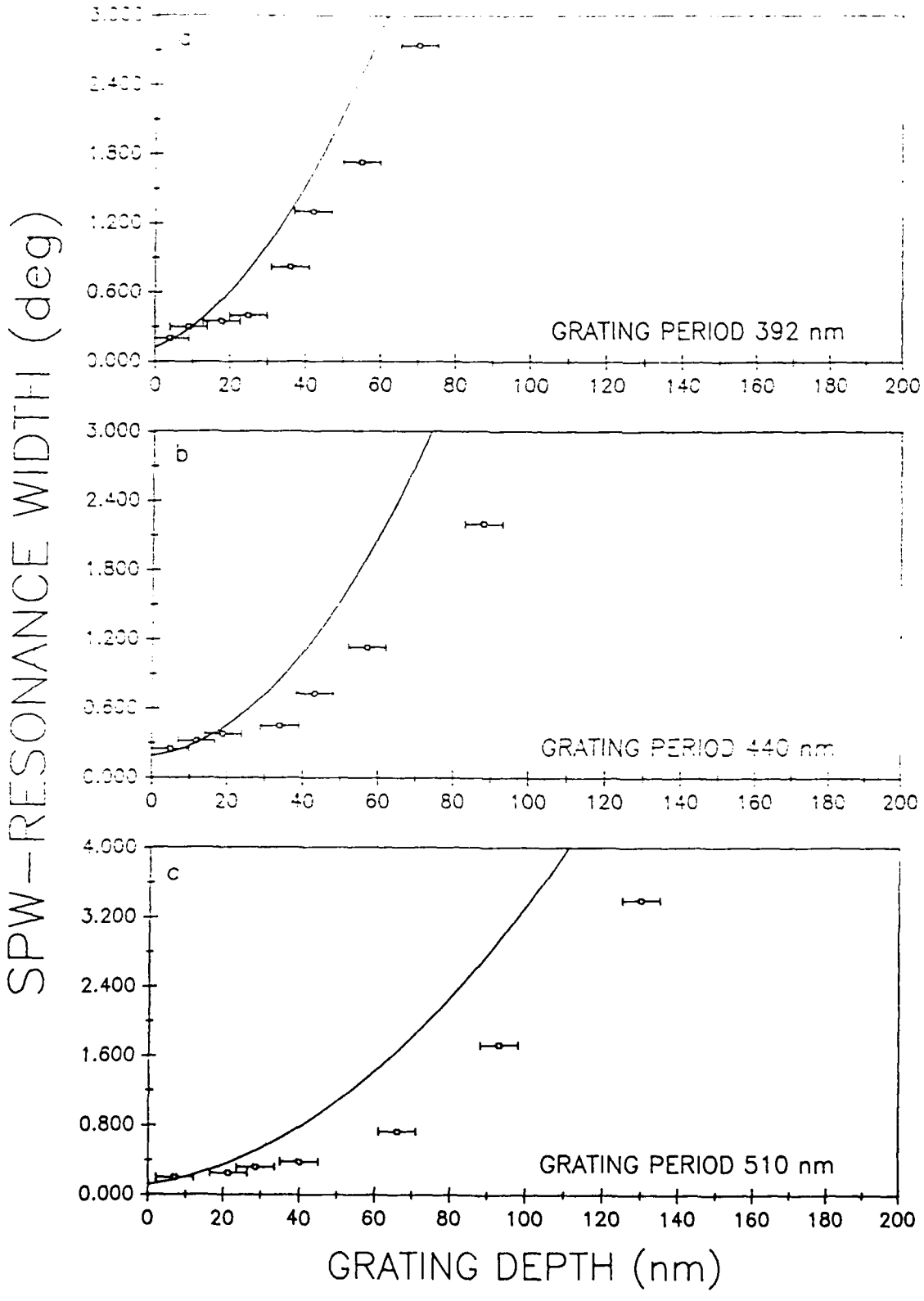
SPW–RESONANCE WIDTH (deg)
a
GRATING PERIOD 392 nm
b
GRATING PERIOD 440 nm
c
GRATING PERIOD 510 nm
0.000
0.600
1.200
1.800
2.400
3.000
0.800
1.600
3.200
4.000
0
20
40
60
80
100
120
140
160
180
200
GRATING DEPTH (nm)

Fig 6

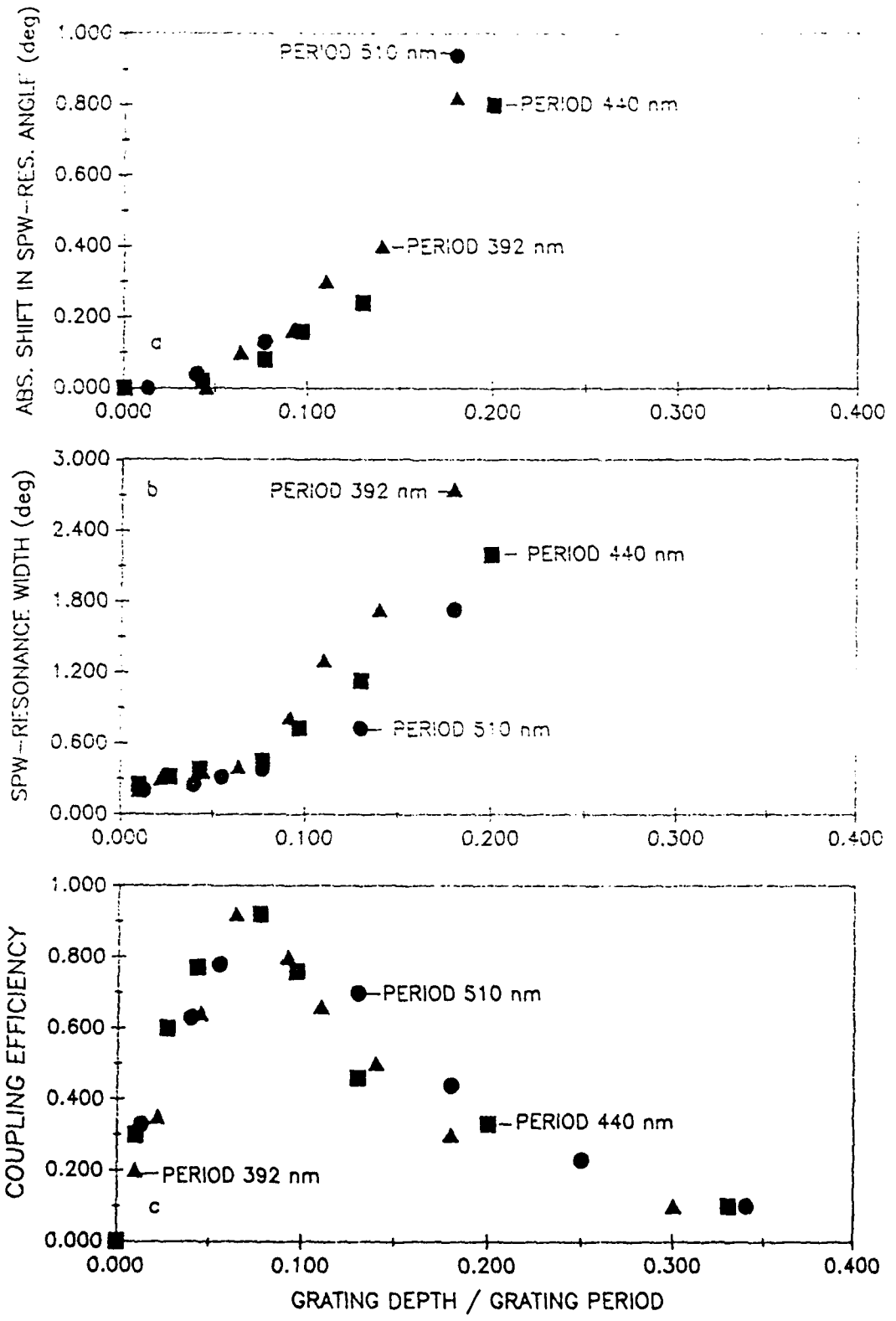
ABS. SHIFT IN SPW-RES. ANGLE (deg)
1.000
0.800
0.600
0.400
0.200
0.000
PERIOD 510 nm
PERIOD 440 nm
PERIOD 392 nm
a
0.000
0.100
0.200
0.300
0.400
SPW-RESONANCE WIDTH (deg)
3.000
2.400
1.800
1.200
0.600
0.000
b
PERIOD 392 nm
PERIOD 440 nm
PERIOD 510 nm
COUPLING EFFICIENCY
1.000
0.800
0.600
0.400
0.200
0.000
PERIOD 510 nm
PERIOD 440 nm
PERIOD 392 nm
c
GRATING DEPTH / GRATING PERIOD

Fig 8

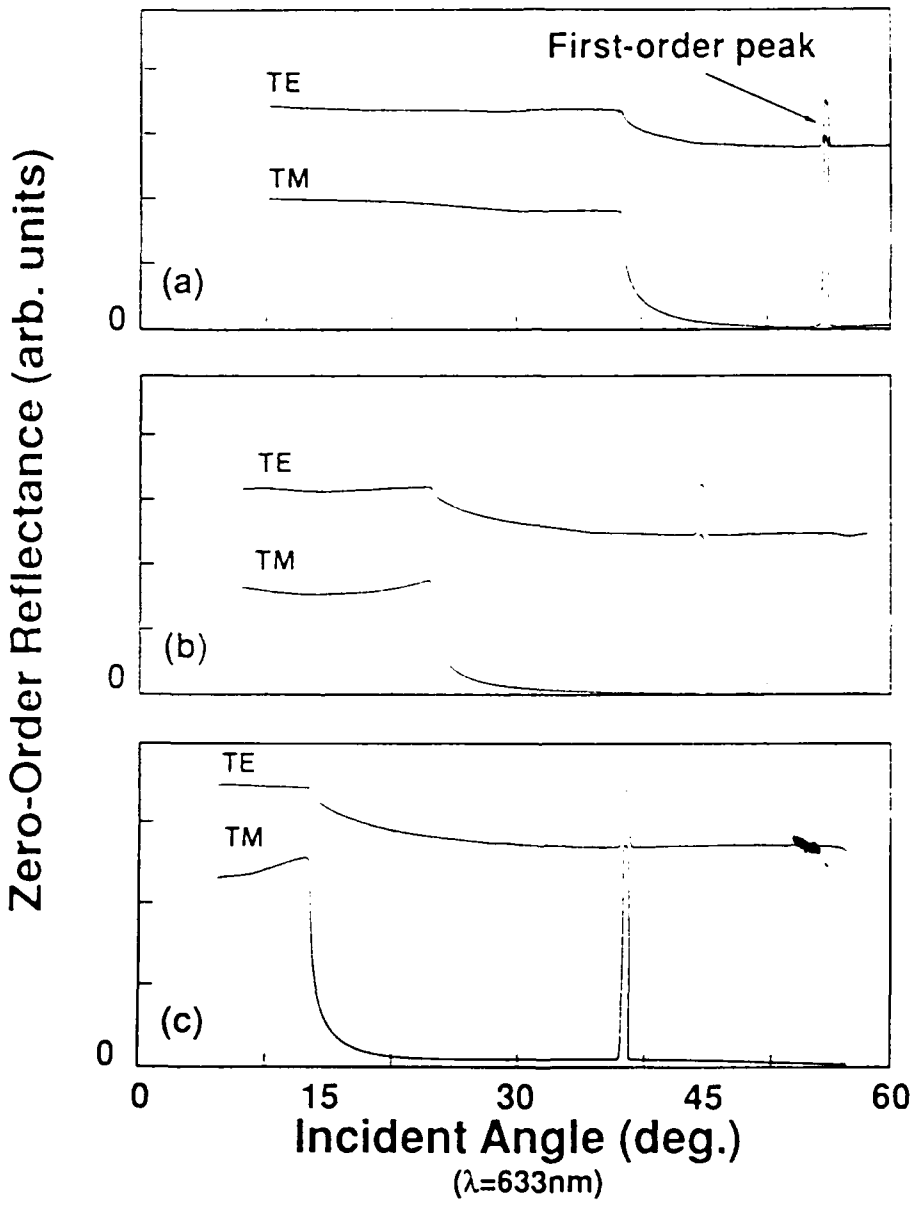
First-order peak
TE
TM
(a)
0
TE
TM
(b)
0
TE
TM
(c)
0
0
15
30
45
60
Incident Angle (deg.)
(λ=633nm)
Zero-Order Reflectance (arb. units)

a)

b)

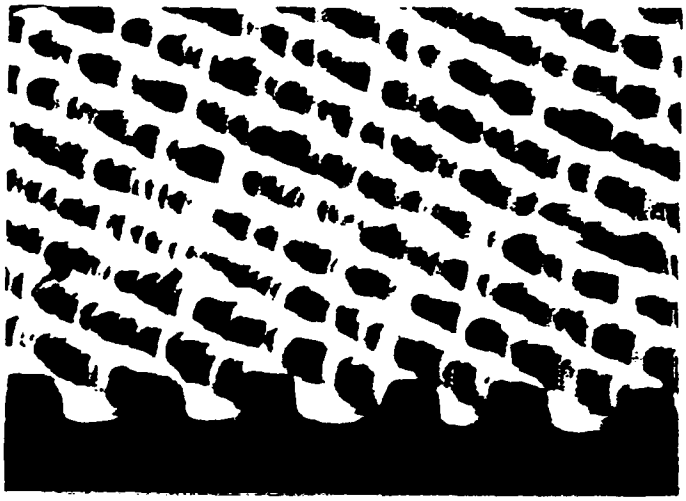

c)

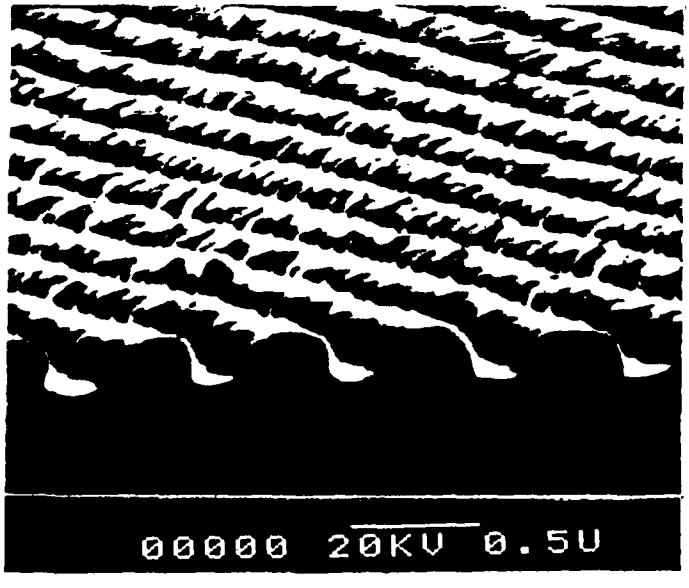

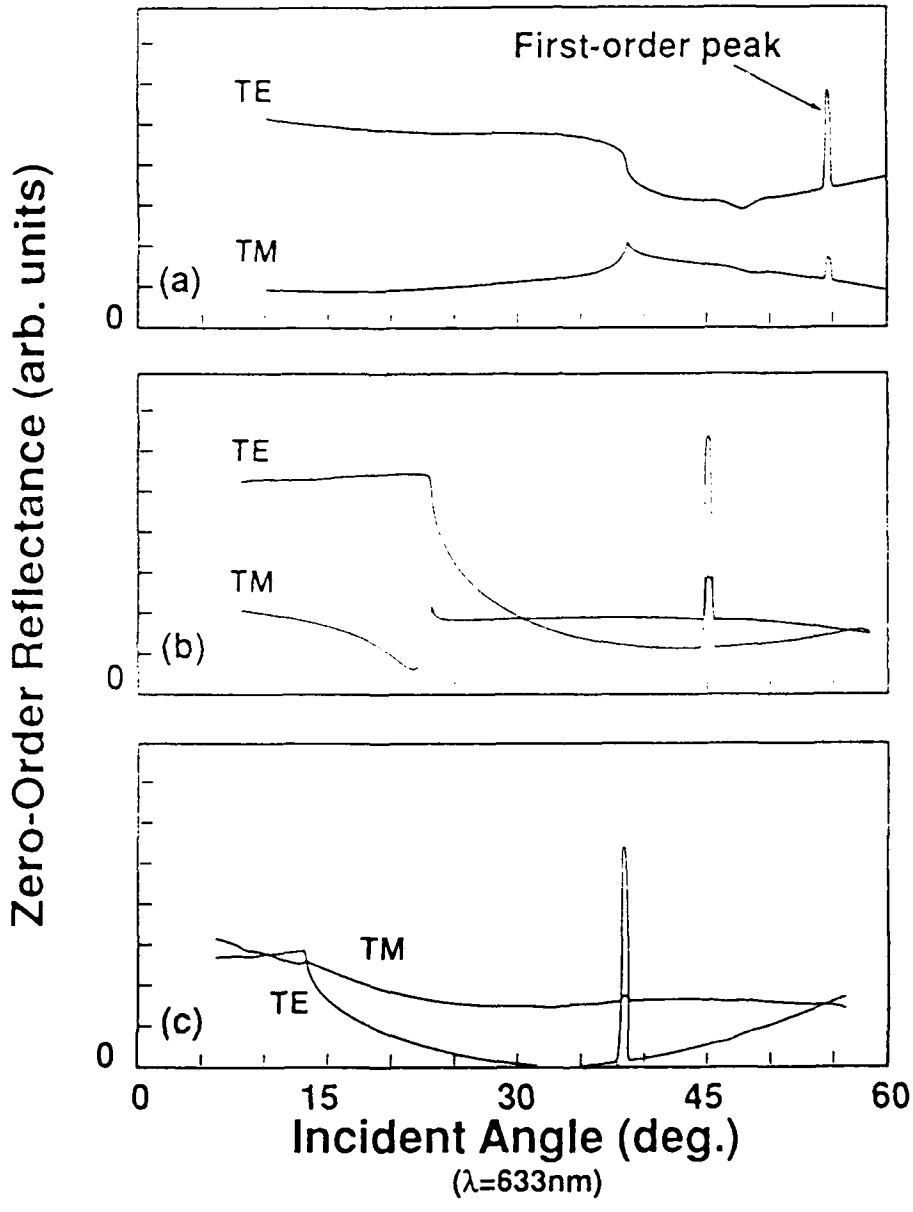
First-order peak
TE
TM
(a)
0
TE
TM
(b)
0
TM
TE
(c)
0
0
15
30
45
60
Zero-Order Reflectance (arb. units)
Incident Angle (deg.)
(λ=633nm)

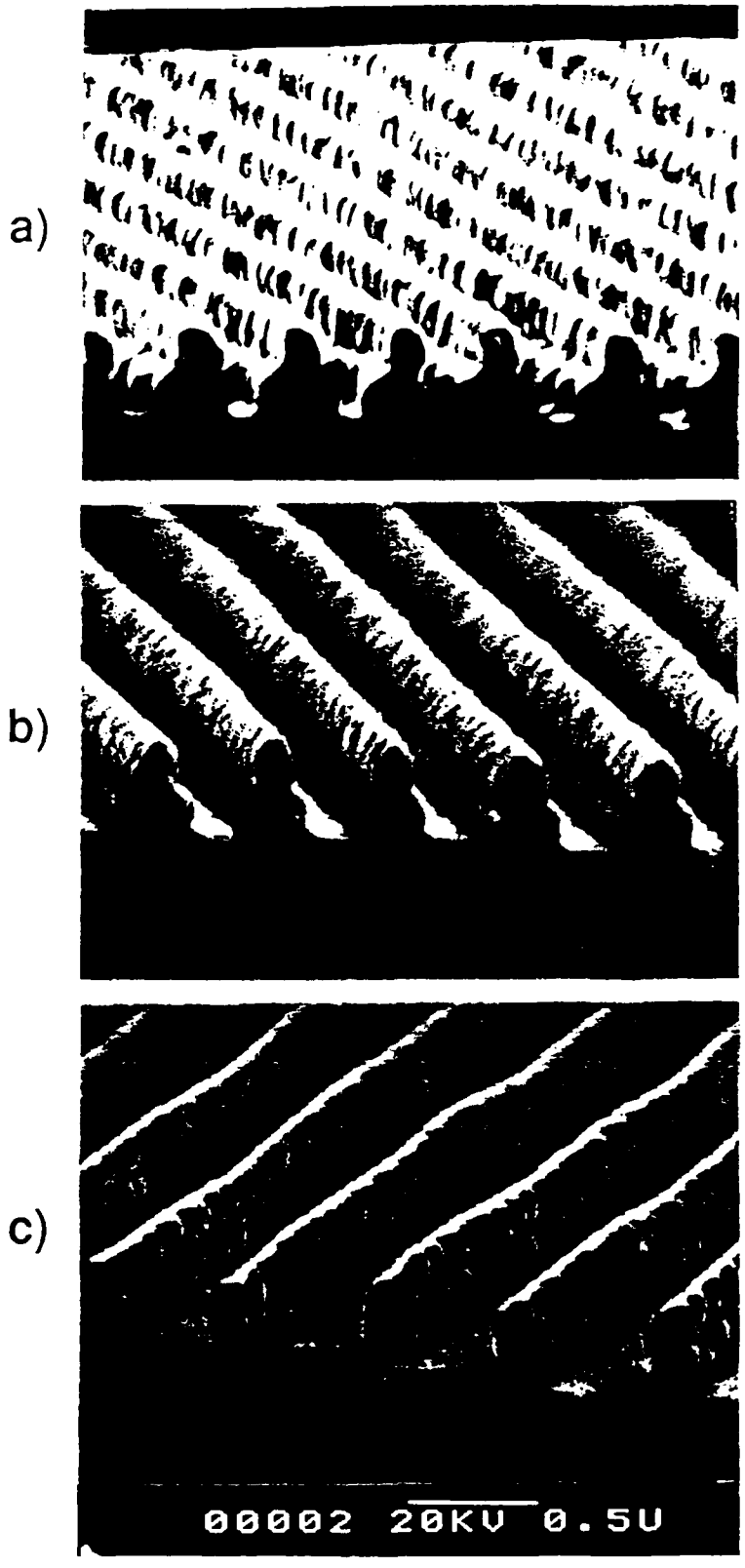

Fig. 3

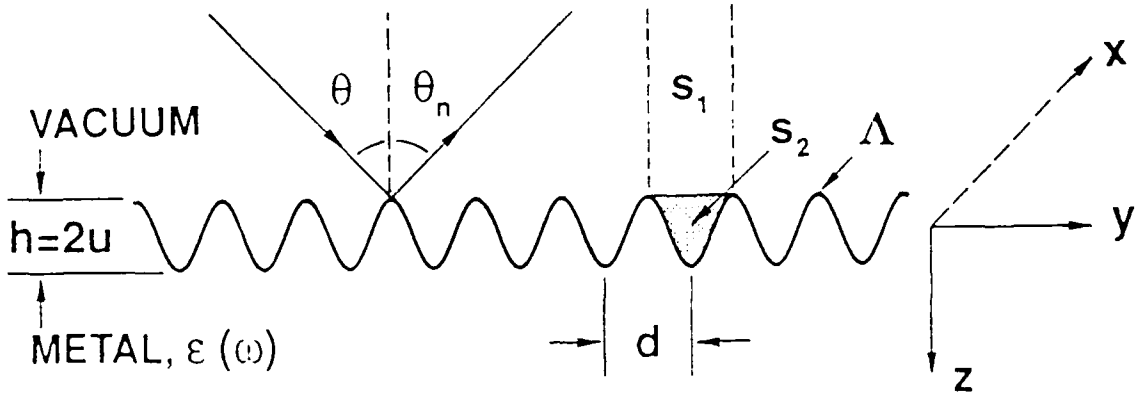

Fig (13)

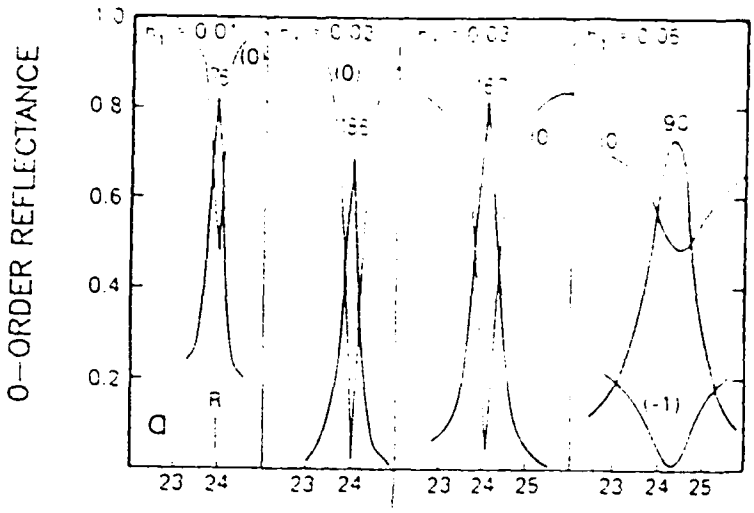
0–ORDER REFLECTANCE
1.0
0.8
0.6
0.4
0.2
a
R
(-1)
23 24
23 24
23 24 25
23 24 25
INCIDENT ANGLE (deg)

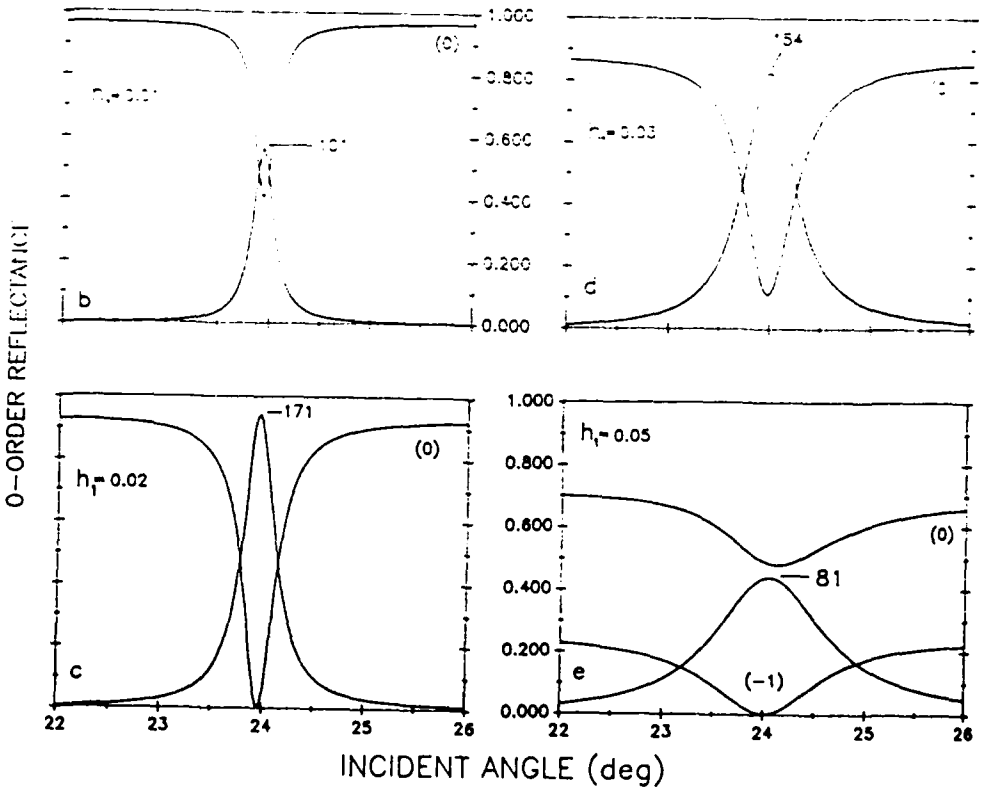
0–ORDER REFLECTANCE
1.000
0.800
0.600
0.400
0.200
0.000
b
(0)
d
154
c
171
h1= 0.02
e
h1= 0.05
81
(-1)
22 23 24 25 26
22 23 24 25 26
INCIDENT ANGLE (deg)

Fig 6

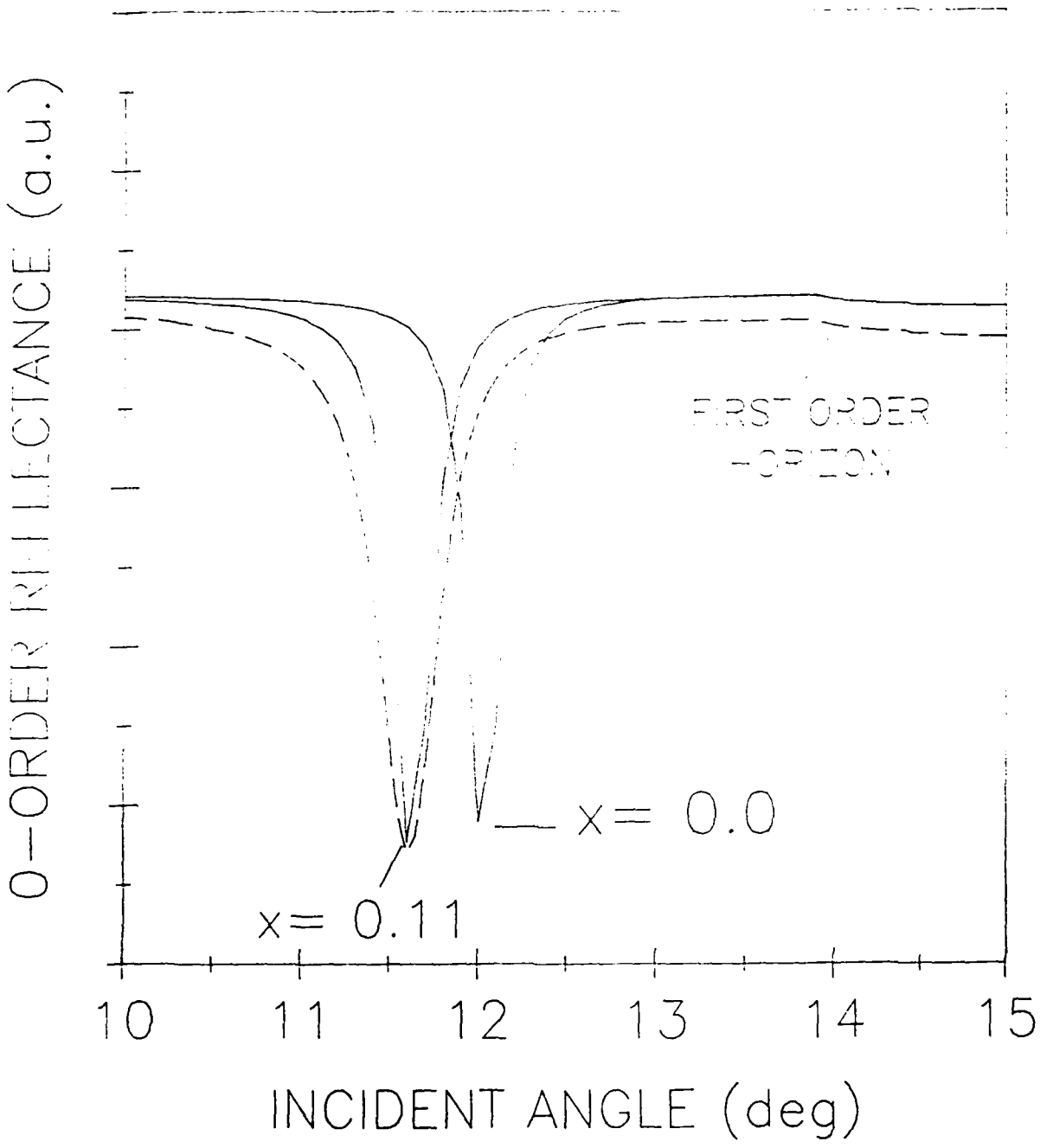
0-ORDER REFLECTANCE (a.u.)
FIRST ORDER
DIFFRACTION
x= 0.0
x= 0.11
10
11
12
13
14
15
INCIDENT ANGLE (deg)

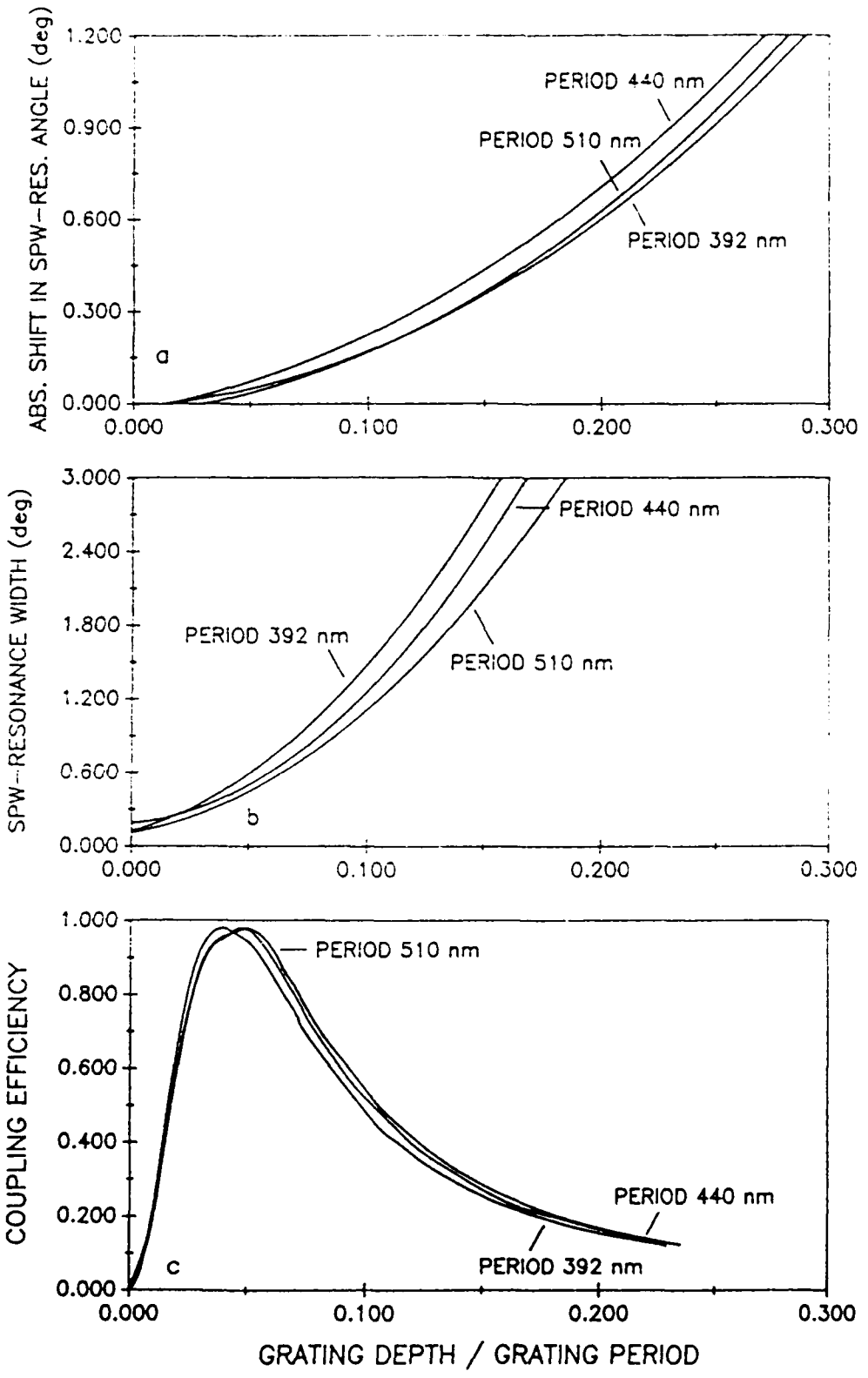
ABS. SHIFT IN SPW-RES. ANGLE (deg)
1.200
0.900
0.600
0.300
0.000
PERIOD 440 nm
PERIOD 510 nm
PERIOD 392 nm
a
0.000
0.100
0.200
0.300
SPW-RESONANCE WIDTH (deg)
3.000
2.400
1.800
1.200
0.600
0.000
PERIOD 440 nm
PERIOD 392 nm
PERIOD 510 nm
b
0.000
0.100
0.200
0.300
COUPLING EFFICIENCY
1.000
0.800
0.600
0.400
0.200
0.000
PERIOD 510 nm
PERIOD 440 nm
PERIOD 392 nm
c
0.000
0.100
0.200
0.300
GRATING DEPTH / GRATING PERIOD

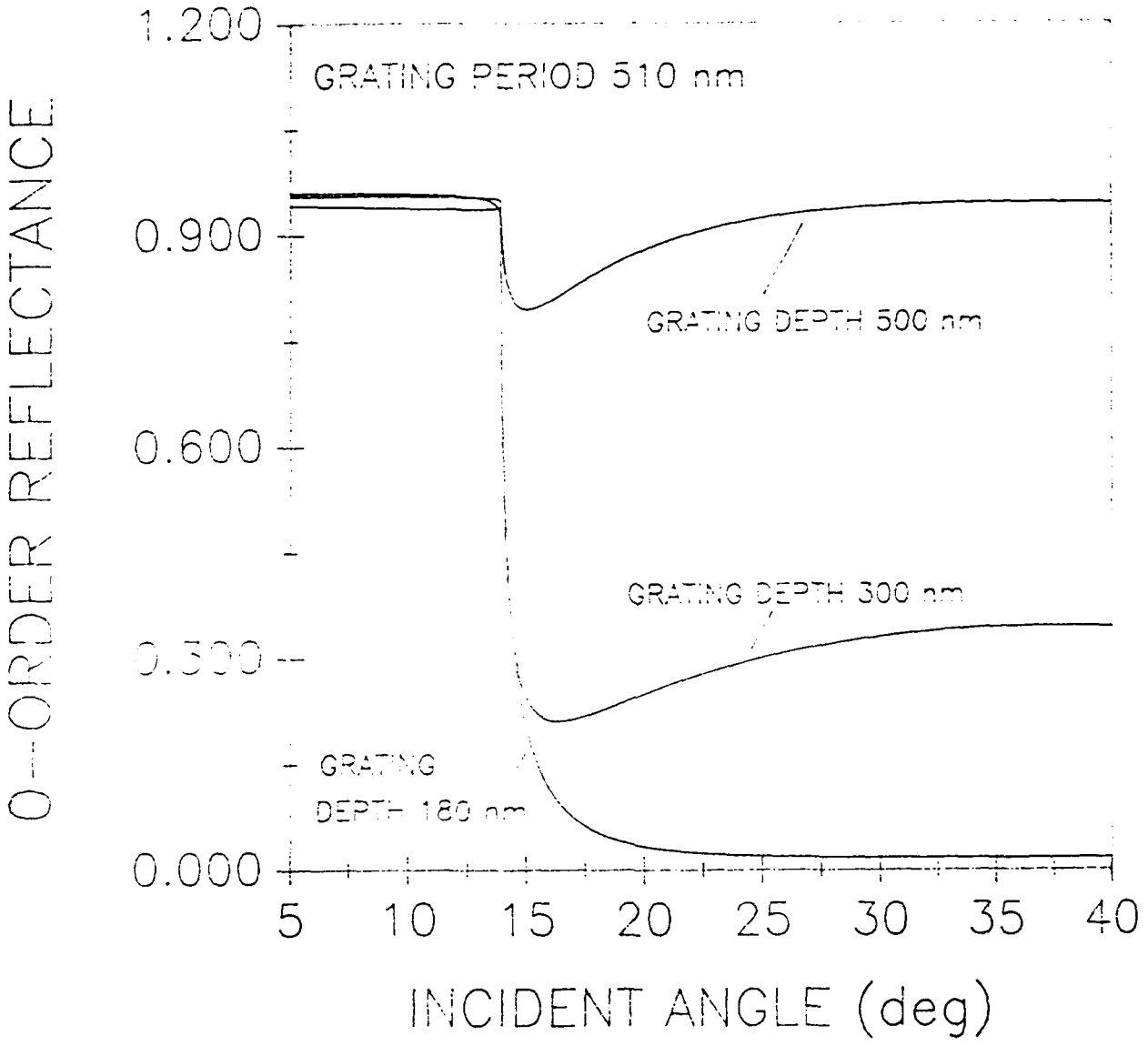
1.200
0.900
0.600
0.300
0.000
0-ORDER REFLECTANCE
GRATING PERIOD 510 nm
GRATING DEPTH 500 nm
GRATING DEPTH 300 nm
GRATING
DEPTH 180 nm
5
10
15
20
25
30
35
40
INCIDENT ANGLE (deg)

Interaction between Surface Plasma Waves and TM-Guided Modes in Metal-Clad Dielectric Waveguides

Saleem H. Zaidi and S. R. J. Brueck
Center for High Technology Materials
University of New Mexico
Albuquerque, NM 87131

Experimental results are reported for grating coupling to metal-clad dielectric waveguides that support both a surface plasma wave and a single TM-guided mode. For appropriate parameters, these modes interfere and give rise to sharp reflectivity resonances.

Interaction between Surface Plasma Waves and TM-Guided Modes in Metal-Clad Dielectric Waveguides

Saleem H. Zaidi[a] and S. R. J. Brueck[a,b]
Center for High Technology Materials
University of New Mexico
Albuquerque, NM 87131

Asymmetric metal-clad dielectric waveguides, formed by depositing a dielectric over a metal film, have a number of potential optoelectronic device applications including modulators and waveguide switches. For a proper choice of dielectric thickness, these waveguides can support two TM-resonances, a surface plasma wave[1] bound to the metal-dielectric interface and a guided mode[2]. These resonances can be phase-matched by the proper choice of parameters. Incident light can be coupled to these modes using gratings. This phase-matching is evident as an overlap in the resonance angles and interference in the coupling lineshapes.

Samples were fabricated by depositing thick (~ 100 nm) Ag films on Si substrates. Positive photoresist was then spun over the metal and a grating exposed and developed using holographic exposure techniques[3]. Zero-order, TM-polarization, reflectivity measurements as a function of incident angle were carried out at 633 nm.

Figure 1 shows the results of a series of measurements for increasing grating depth, and, consequently, decreasing average dielectric film thickness. The top trace shows two isolated resonances, a SPW mode at an incident angle of 17 degrees and a guided mode at 28 degrees. The increase in signal at 23 degrees is the result of the diffracted-order entering the collection optics and is not a variation in the zero-order reflectivity.

As the grating depth is increased, the SPW mode shifts to higher angles and the guided mode to lower angles until they overlap. For still deeper gratings, the resonances split and exhibit complex lineshapes which are due to interference phenomena between the modes. A notable feature is the very sharp resonance that occurs at ~ 17 degrees for all

of the gratings with depths beyond that required for overlap of the modes. Such sharp resonance features are especially useful for optoelectronic applications.

Detailed experimental and theoretical investigations of this coupled mode phenomenon will be reported.

References:

1. see, for example, Surface Polaritons, V. M. Agranovich and D. L. Mills, eds. (North Holland, Amsterdam, 1982)

2. I. P. Kaminow, W. L. Mammel nad H. P. Weber, Appl. Opt. *13*, 396 (1974)

3. S. H. Zaidi and S. R. J. Brueck, Appl. Opt. (to be published July 15, 1988)

---

[a] Also with the Department of Physics and Astronomy

[b] Also with the Department of Electrical Engineering

This work was partially supported by the Air Force Office of Scientific Research.

Optical Characteristics of Deeply Modulated Gratings

Saleem H. Zaidi and S. R. J. Brueck

Center for High Technology Materials

University of New Mexico

Albuquerque, NM 87131

Zero- and first-order grating reflectivities (633 nm) for periods from 380- to 840-nm with grating depths from 10- to 1000-nm are reported. Effects observed include: surface plasma-wave (SPW) coupling for deep gratings, interference between first and second-order SPW couplings, and highly efficient grating polarizers.

OPTICAL CHARACTERISTICS OF DEEPLY MODULATED GRATINGS

Experimental study of grating properties has a long history. Much of this study has been confined to gratings with sinusoidal profiles and depths less than 100 nm. Using holographically fabricated gratings (1) coated with thick Ag-films (-100nm), we report here on an experimental study of zero- and first-order reflectivities at 633 nm with special emphasis on surface plasma wave (SPW) mode couplings and grating polarization effects. The gratings studied had periods from 380 to 840 nm, depths from 10 to 1000 nm, and profiles from sinusoidal to rectangular.

For gratings with only one allowed SPW mode, it is observed that as the grating depth is increased, beyond the maximum coupling efficiency depth, the SPW coupling dip gradually decreases, the resonance angle gradually shifts and broadens. Simultaneously, the grating diffraction efficiency increases. For an optimum depth of the grating less than 1% of the light is reflected.

For gratings supporting two SPW modes, the behavior of the SPW mode couplings as a function of grating depth is complex. At an optimum depth, the two SPW modes, however, couple to form a broad minimum. The grating first-order, however, continues to exhibit strong coupling to SPW modes at well-defined angles. Further increase in the grating depth results in disappearance of all resonance characteristics. Detailed study of all these results with corresponding grating depths and periods will be reported.

Reference:

1. S. H. Zaidi and S. R. J. Brueck, Appl. Opt., July 15, 1988.

INTERACTIONS BETWEEN FIRST AND SECOND ORDER COUPLINGS TO SURFACE PLASMA WAVES

Surface plasma wave dispersion relation is investigated optically in the (+1, -2) mini-gap region by varying grating profiles. Momentum gaps are observed and are described by developing a theoretical formalism based on Rayleigh hypothesis.

INTERACTIONS BETWEEN FIRST AND SECOND ORDER COUPLINGS TO SURFACE PLASMA WAVES

Surface Plasma Wave (SPW) dispersion relation in the mini-gap region, where the unperturbed modes are degenerate, has been recently investigated, both theoretically [1] and experimentally [2]. Theoretically only energy gaps were predicted in the mini-gap region, but experimentally it was shown that both momentum and energy gaps exist [2] although optical excitation resulted only in energy gaps similar to the results obtained by Chen, et al. [3]. Here we present a detailed optical investigation of the (+1, -2) mini-gap region by varying grating depths and profiles. Momentum gaps observed were critically dependent on grating profiles.

Gratings were fabricated in positive photoresist using holographic techniques [4], and coated with ~ 100-nm silver films. The data was acquired in the form of 0-order and diffraction order reflectances versus incident angle. By adding energies in the 0-order and diffraction order, momemtum gaps were measured. For theoretical modeling, Rayleigh hypothesis was used. For sinusoidal profiles, no momentum gaps were observed. By including a second Fourier component, momentum gaps were observed, and the resulting lineshapes were in good agreement with experimental data.

Partial funding for this work was provided by the Air Force Office of Scientific Research.

REFERENCES :

1. M. G. Weber and D. L. Mills, Phys. Rev. B 34, 2893 (1986).
2. D. Heitman, N. Kroo, C. Schultz, and Z. Szentirmay, Phys. Rev. B 35 2660 (1987).
3. Y. J. Chen, E. S. Koteles, R. J. Seymour, G. J. Sonek, and J. M. Ballantyne, Solid State Comm. 41, 95 (1983).
4. Saleem H. Zaidi and S. R. J. Brueck, Appl. Opt. 27, 2999 (1988).

Authors :

Saleem H. Zaidi, M. Yousaf, and S. R. J. Brueck.

FIRST ORDER COUPLING TO SURFACE PLASMA WAVES

Using prism and grating coupling techniques, surface plasma wave effects have been used to investigate metal interfaces, metal-dielectric interfaces, and other non-linear processes [1]. Here we present a comprehensive experimental and theoretical study of first-order coupling to SPWs and the use of this technique to characterize the optical constants of metal films.

The gratings were fabricated holographically in positive photoresist [2], and coated with ~ 100-nm silver films. Data was acquired in the form of 0-order reflectance versus incident angle using a 633-nm He-Ne laser source [3]. Gratings with varying period (392 nm < d < 515 nm), depth (5 nm < h < 500 nm), and profiles were studied. Optical coupling parameters such as coupling strength and linewidth are shown to be approximately dependent on the dimensionless parameter h/d.

For theoretical modeling, the Rayleigh hypothesis was used throughout this range of parameters and profiles were assumed to be sinusoidal. The Rayleigh expansion was terminated by keeping only the resonant terms, which considerably simplified computational work. Calculations of coupling profiles are in good agreement with the experimental data.

Partial funding for this work was provided by the Air Force Office of Scientific Research.

REFERENCES:

1. Surface Polaritons, edited by V. M. Agranovich and D. L. Mills, North-Holland (1982).
2. Saleem H. Zaidi and S.R.J. Brueck, Appl. Opt. 27, 2999 (1988).
3. Saleem H. Zaidi and S.R.J. Brueck, O.S.A. annual meeting (1988).

25-WORD SUMMARY

First order grating coupling to Surface Plasma Waves is studied for a large range of parameters. A theoretical formalism based on the use of the Rayleigh hypothesis is developed. Application of this technique to characterize optical constants of metal films is discussed.

Authors :

Saleem H. Zaidi, M. Yousaf, and S. R. J. Brueck.

ELECTRIC FIELD INDUCED SECOND HARMONIC GENERATION IN PLZT

A. Mukherjee, S. R. J. Brueck† and A. Y.Wu

Center for High Technology Materials
University of New Mexico, Albuquerque, NM, 87131

ABSTRACT

The first measurements of electric-field induced second-harmonic generation in the cubic ceramic PLZT (9/65/35) are reported. A hysteresis behavior of the second harmonic signal versus electric poling field was observed and a field/no field contrast ratio of 20:1 was achieved. The area of the hysteresis loop decreased resulting in a 'slim-loop' for increasing delays between applying an external voltage and monitoring the second harmonic signal, the sample remaining irradiated by the fundamental beam.

† Also with the Departments of Electrical and Computer Engineering and Physics and Astronomy.

Optically transparent ferroelectric-oxide $Pb_{1-x}La_x(Zr_yTi_{1-y})_{1-x/4}O_3$ (PLZT) materials have been developed as shutters, light modulators, optical memories, display devices and image storage media[1-5] utilizing electrically controlled birefringence and scattering. The electrooptic (E-O) effect of the ceramic PLZT is intimately related to its ferroelectric properties. Domain reorientations and lattice distortions will affect the material's optical properties whose magnitude in general will depend on the strength and the direction of the applied field. PLZT has a perovskite structure with a transition metal (Zr or Ti) at the center surrounded by an oxygen octahedra and alkaline atoms (Pb or La) at the corners[3]. The octahedra, having dimensions of ~4 Å per side, are joined in long chains which have a nearly centrosymmetric structure in the paraelectric phase and distorted centrosymmetric structure in the ferroelectric phase[6]. Nonlinear optical interactions, such as second harmonic generation represent a fast response due to electronic motion. Here, perhaps due to the motion of electrons of the upper valence band formed by the oxygen 2p levels. Any external perturbations such as an electric field, temperature variation, or stress will bring about a change in the network of the oxygen octahedra and thus affect the sample's macroscopic optical properties. The stoichiometry of PLZT is denoted by the X Y Z notation where X is the atom percentage of La and Y Z is the zirconium titanium ratio. Second harmonic generation (SHG) experiments in PLZT of compositions 8/65/35 and 9/65/35 have been reported[7-9] and the temperature dependence studied [7,8]. Electric-field induced second-harmonic generation (EFISHG) in polydyacetylene (PDA) has been studied to investigate resonant enhancement of $\chi^{(3)}(-2\omega;\omega,\omega,0)$ and two photon generation of carriers[10] and determine the magnitude and phase of $\chi^{(3)}(-2\omega;\omega,\omega,o)$[11]. EFISHG experiments have also been reported on molecular solutions to study the molecular environment[12] and influence of carrier substitutes[13]. In this letter we report the first measurements of EFISHG on the ferroelectric oxide PLZT 9/65/35.

The E-O properties of selected compositions of PLZT were studied by Haertling and Land[2] who demonstrated that the composition 9/65/35 with neither true ferroelectric nor true paraelectric behavior (herein after referred to as quasiferroelectric) was interesting both scientifically and technologically. Studies of the dielectric and optical properties of this quasiferroelectric PLZT[14] and its phase transitions[15] suggested a electric-field-induced reversible α - β phase change at a temperature between T_t (structural phase transition temperature), 18°C,[15] and the Curie point T_c 85°C.[3]. The α-phase is paraelectric with a cubic perovskite structure and is optically isotropic[7]. It is also referred to as the state of polar short range order[14]. The β - phase is associated with the quasi ferroelectric phase with orthorhombic (distorted cubic) structure. It is also referred to as a state of polar long range order[14]. The experiments were done at room temperature (23°C) and so a quasiferroelectric behavior was expected from our sample.

This EFISHG study was done on a 0.6-mm thick polished wafer of PLZT 9/65/35 provided by Motorola. A hysteresis behavior of the SHG versus electric poling voltage and a contrast ratio (field no field) of second harmonic (SH) signal of more than 20:1 was observed. The area of the hysteresis was seen to decrease and result in a 'slim-loop' if the SH signal recording was sufficiently delayed after applying the poling voltage, the sample remaining irradiated by the fundamental beam.

The experiment is shown schematically in Fig.1. The inset shows the planar electrode pattern with a gap of 60 μm. Conventional photolithographic processes and lift-off techniques were used to fabricate these electrodes which were formed by e-beam evaporation and consisted of a 30-nm layer of Cr followed by a 300-nm layer of Au. The 1.06-μm pulse train (82 MHz repetition rate, 130-ps duration) from a cw-modelocked YAG laser provided the fundamental beam. A Fresnel-Rhomb polarization rotator and a Glan prism were used to select a linearly polarized fundamental beam of variable orientation. The beam of 3W average power was focused (~ 50-μm diameter) at

an angle of incidence of 45° on the sample using a 50-mm focal length lens. The SH signal was detected along the specular reflection direction. A lens of focal length 75 mm and aperture 25.4 mm was used to collect the second harmonic light and focus it on the active area of an uncooled photomultiplier tube (bialkali photocathode) after passing through an IR blocking filter and a band pass interference filter centered at 532 nm.

A chopper and a lock-in amplifier, with a maximum time constant of 300 ms were used in the signal detection process. The output of the lock-in amplifier was monitored by a laboratory computer system which also controlled a high voltage power supply providing the applied voltage to the sample.

In all the experimental sequences, the poling field was started with a positive voltage (arbitrarily defined) and incremented in 20 V intervals from 0 V to 360 V. The voltage was then decreased to 0 V in 20 V steps. A similar recording was taken with the opposite polarity. For the same polarisations (fundamental & SH) two sets of data were taken, with 1 second and 30 seconds delay between the application of voltage and recording SH intensity. For all of these measurements the sample was continuously illuminated by the laser source, the time delay only refers to the interval between changing the field strength and the SH measurements. Fig. 2 shows the EFISHG measurements in 9/65/35 PLZT with both fundamental & SH polarisations parallel to the poling field. Fig.2(a) shows the trace with one second delay of recording SH intensity after the application of poling voltage and Fig.2 (b) with a 30 seconds delay. From this data we see that there is a small SH signal at zero poling field. Though the sample is in α (cubic) phase, it is not strictly centrosymmetric because of the local displacement of ions away from their ideal lattice positions. Betzler and Bauerle[7] proposed a model where the local anistropy (disorder) was explained by the La^{3+}/ions (4% smaller in size than Pb^{2+} ions) being randomly located at off-center positions.

As the electric field is increased the SH intensity increases quadratically since it is proportional to[10]

[illegible] $E_\omega^2 F$ [illegible]

here $E_{2\omega}$ [illegible] field within the sample and E_ω is the field of the fundamental beam. The quadratic dependence of $I_{2\omega}$ on the fundamental intensity was confirmed. Also the SH intensity shows a slight saturation behavior at the maximum applied voltage of 300 V (~8.5 KV/cm). The scattered 2nd harmonic intensity at zero field was brightly visible to the eye. The estimation of $\chi^{(2)}$ was not possible because of the complexity of the DC field distribution inside the material along with severe polycrystalline grain boundary (~5-10μm) scattering, phase matching uncertainties, etc. However, the observed intensities, even at zero applied fields, were comparable to that from powders of KTP, suggesting that with improved material preparation such as highly oriented fine grain thin films, efficient modulatable second harmonic generation will be achieved. Increasing the voltage further caused arcing between the electrodes. The saturating poling field is about[5] 15 kV/cm and the maximum field applied here was only 8.5 KV/cm. On decreasing the field to zero the SH intensity was seen to be slightly higher than the starting value. This is likely due to remnant β - phase resulting from strains induced by cycling the field[15]. This variation of the SH intensity versus poling field is similar to the dielectric hysteresis loop reported for the same material composition by Keve & Annis[15]. Fig. 2 (b) for a large delay time of 30 s between application of the field and the SH measurement shows a 'slim-loop' behavior of the same phenomena. This recording with a considerably smaller hysteresis than the results of Fig. 2 (a) has a qualitative similarity with the high temperature behavior of the dielectric hysteresis loop[15]. A gradual decrease of the area of the hysteresis was observed versus the delay time. It was also observed that if the voltage was suddenly removed (shorted) to 0 V, the SH intensity decayed (to the 0 V value) in 30 seconds if left irradiated with the fundamental beam and over several hours if not irradiated. This is probably due to

photoinduced conductivity[18]. A more detailed study will be required to fully understand this effect.

Fig. 3 (a) and (b) shows EFISHG intensity versus applied field where the fundamental beam remained polarized parallel to field, both being in the horizontal plane, but the polarization for SH was chosen perpendicular to it. All other parameters, were the same as in Fig. 2. The overall SH signal in this case was seen to be a factor 0.36 less than for Fig. 2 where the polarization of the SH signal was parallel to the poling field. The SH intensity was dominantly horizontally polarized since the displacement of the ions due to poling and the polarization of the fundamental beam were both in the horizontal plane. The contribution of the SH signal with polarization in the vertical plane arises out of the randomly oriented microcrystallites and domain wall scattering. The influence of the randomness of microcrystallites may be accounted for in a similar manner for diacetylenes as has been discussed by Berkovic et al (19). The contribution from domain wall scattering is more complex since correlation between domains lead to an increase in the scattered intensity when a Bragg condition is fulfilled. The influence of domain scattering and effect of laser polarizations on the SH intensity may be evaluated along similar lines as for Triglycine Sulfate studied by Dolino et al (20).

A similar variation in the hysteresis was observed on delayed recording and the contrast ratio was comparable to the parallel polarization case. In Fig. 3 (b) we see an asymmetry in the SH signals of positive and negative applied fields with a greater signal on the negative poling side is observed. This is due to the remnant polarization field E_p opposing the external field E_o and so the second harmonic intensity is proportional to $(E_o + E_p)^2$. This was however not seen in the parallel polarisation (Fig.2b) case.

In conclusion, we have report EFISHG in the ceramic PLZT of composition 9/65/35 which has a quasiferroelectric (with α - β transition) behavior. The contrast ratio achieved was 20:1 which can be improved by putting a layered dielectric on the

surface allowing higher applied fields. Besides EFISHG other non-linear optical techniques such as FWM, multiphoton absorption and stimulated scattering may be used to study the electric field induced A - F phase transition in this and other quasiferroelectric ceramics. The large observed second harmonic signal indicate that these materials may be important for electro-optic applications. Highly-oriented thin film materials will enable a much more systematic study of this phenomenon; such studies are underway.

This work was partially supported by the Air Force Office of Scientific Research.

References

1. M. E. Lines and A. M. Glass, *Principles and Applications of Ferroelectrics and Related Materials*, Clarendon Press, Oxford, 1979.
2. G. H. Haertling and C. E. Land, J. Am. Cer. Soc., 54, 1 (1971).
3. G. H. Haertling, *Ceramic materials for Electronic Processing. Properties and Applications*, ed. by R. C. Buchanan, Marcel Dekkar Inc. (1986).
4. G. Wolfram, Ferroelectrics, 10, 39-42, 1976.
5. T. Kawaguchi and O. Yamazaki, JEE 55 (1984).
6. D. S. Chemla, Rep.Prog.Phys., 43 1191 (1980).
7. K. Betzler and D. Bauerle, Appl. Phys. 18, 271-274 (1979).
8. G. V. Liberts and V. Ya. Fritzberg, Phy. Stat. Sol.(a), 67, K81 (1981).
9. C.Michael, A. Sisignano , App. Phys. Lett., 24, 559 (1974).
10. P. A. Chollet, F. Kajzar and J. Messier, Thin. Sol. Films., 132, 1-10 (1985).
11. F. Kajzar, J. Messier, J. Zyss and I. Ledoux, Opt. Comm., 45, 13 (1983).
12. I. Ledoux and J. Zyss, Chem. Phys., 73, 203 (1982).
13. J.-L.Oudar, J. Chem. Phys., 67, 446 (1977).
14. K. Carl and K. Geisen, Proc. IEEE, 61, #7, July (1973).
15. E. T. Keve and A. D.Annis, Ferroelectrics, 5, 77-89 (1973).
16. V. M. Agranovich and V. L. Ginzburg, *Spatial Dispersion in Crystal Optics and the Theory of Exitons*, (John Wiley and Sons, London, 1966).
17. H. Voght, Appl. Phys., 5, 85 (1974).
18. J. M. Rouchon, M. Vergnolle and F. Micheron, Ferroelectrics, 11, 389-392 (1976).

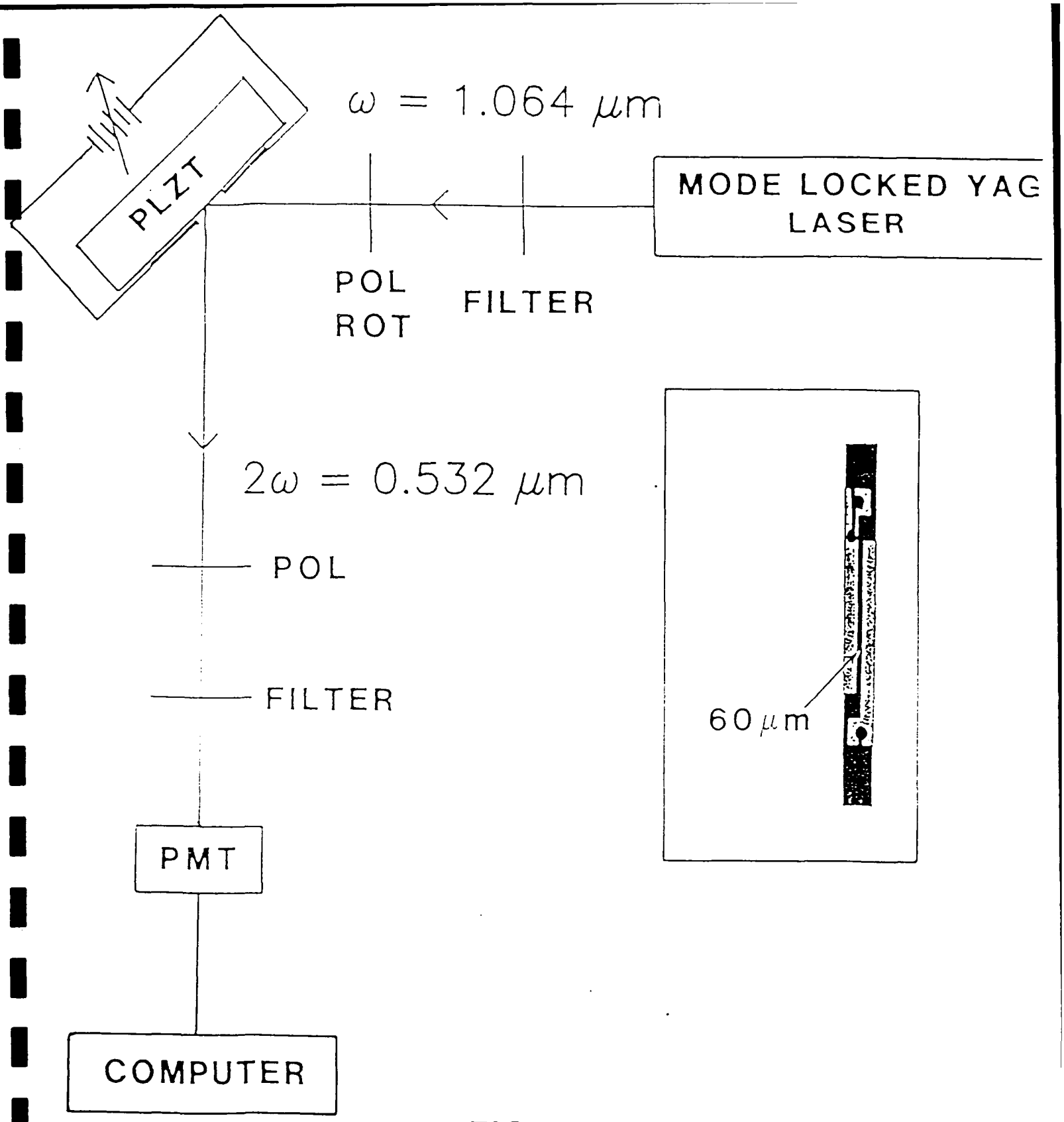
PLZT
ω = 1.064 μm
MODE LOCKED YAG LASER
POL ROT
FILTER
2ω = 0.532 μm
POL
FILTER
60 μm
PMT
COMPUTER

FIG. 1

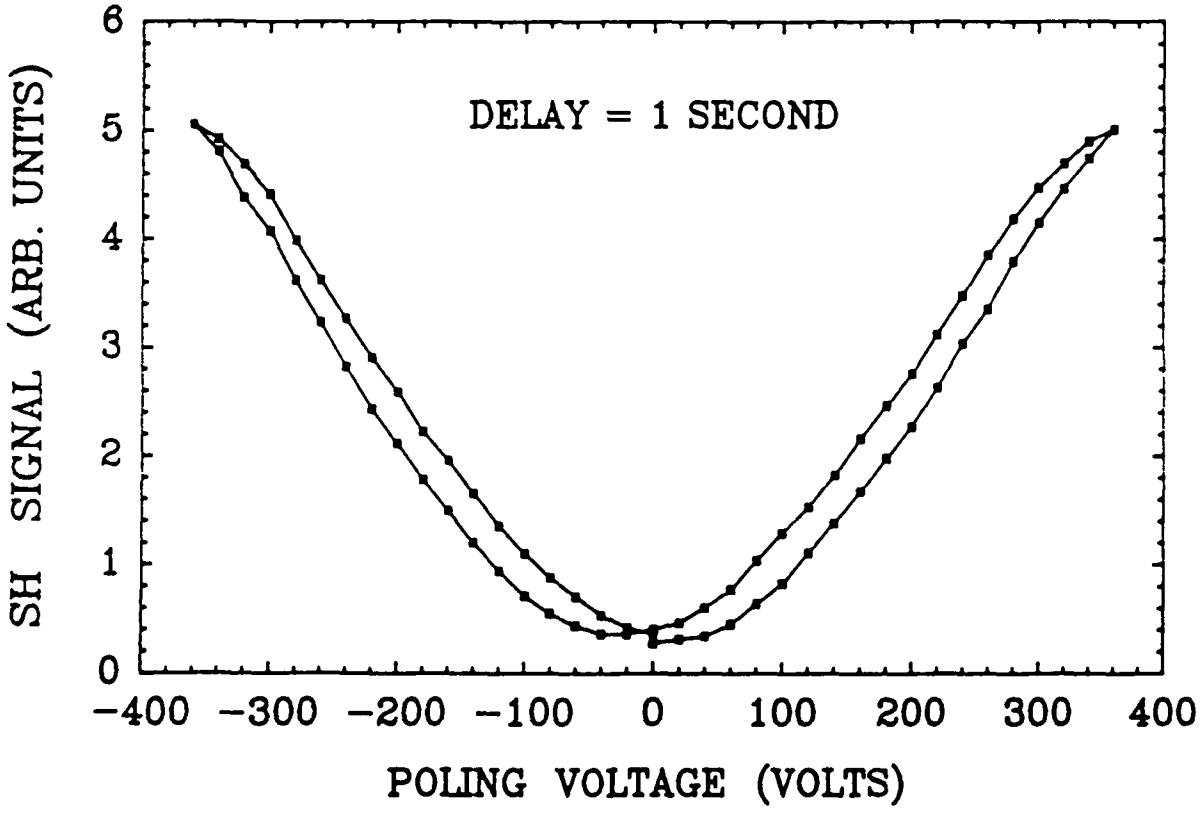
DELAY = 1 SECOND
SH SIGNAL (ARB. UNITS)
0
1
2
3
4
5
6
−400
−300
−200
−100
0
100
200
300
400
POLING VOLTAGE (VOLTS)

Fig 2a

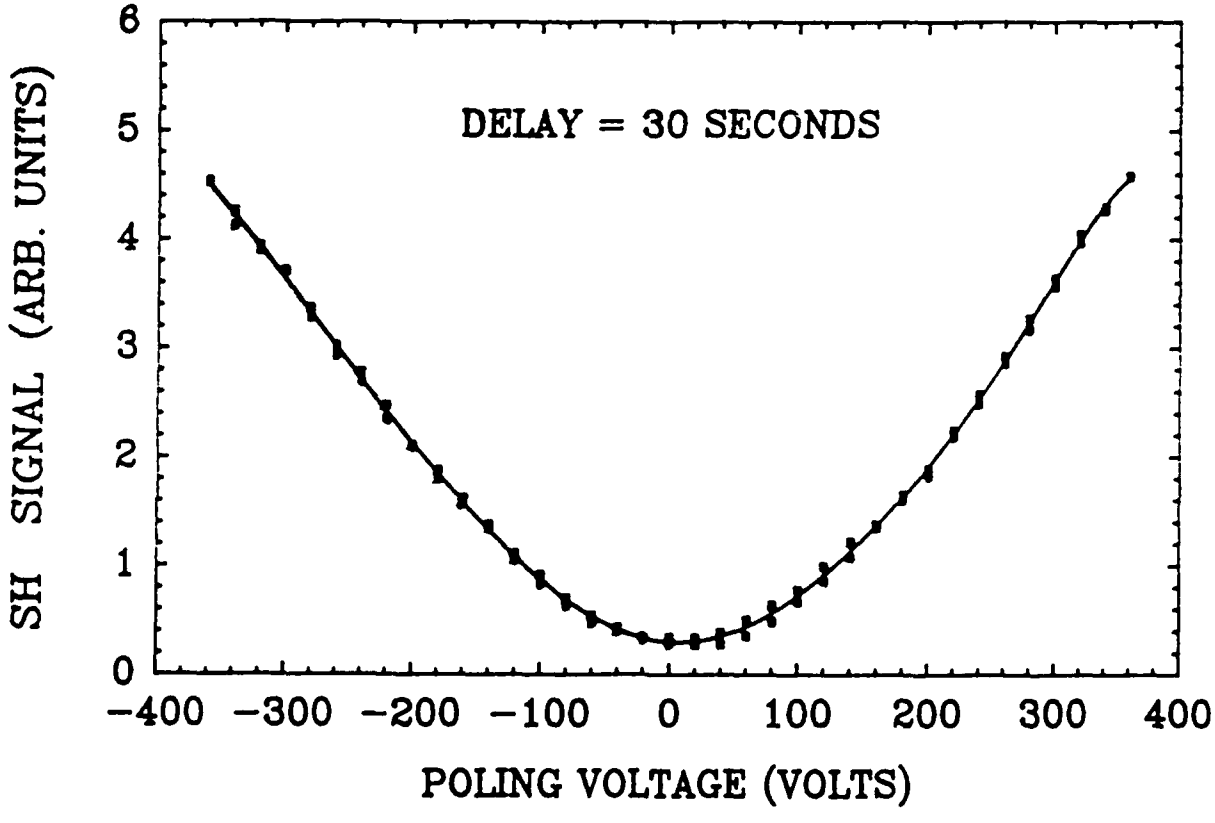
DELAY = 30 SECONDS
SH SIGNAL (ARB. UNITS)
0
1
2
3
4
5
6
−400
−300
−200
−100
0
100
200
300
400
POLING VOLTAGE (VOLTS)

Fig 2b

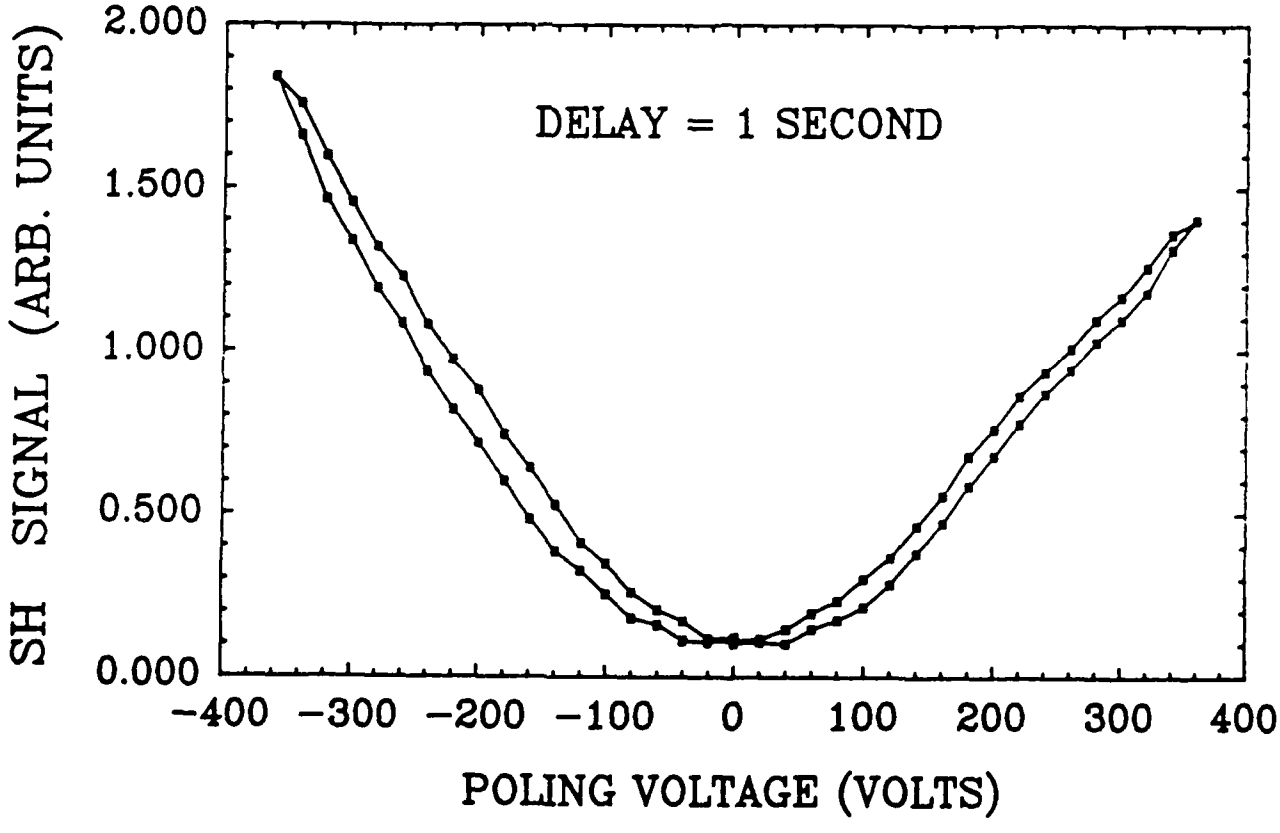
DELAY = 1 SECOND
SH SIGNAL (ARB. UNITS)
2.000
1.500
1.000
0.500
0.000
−400
−300
−200
−100
0
100
200
300
400
POLING VOLTAGE (VOLTS)

Fig 3a

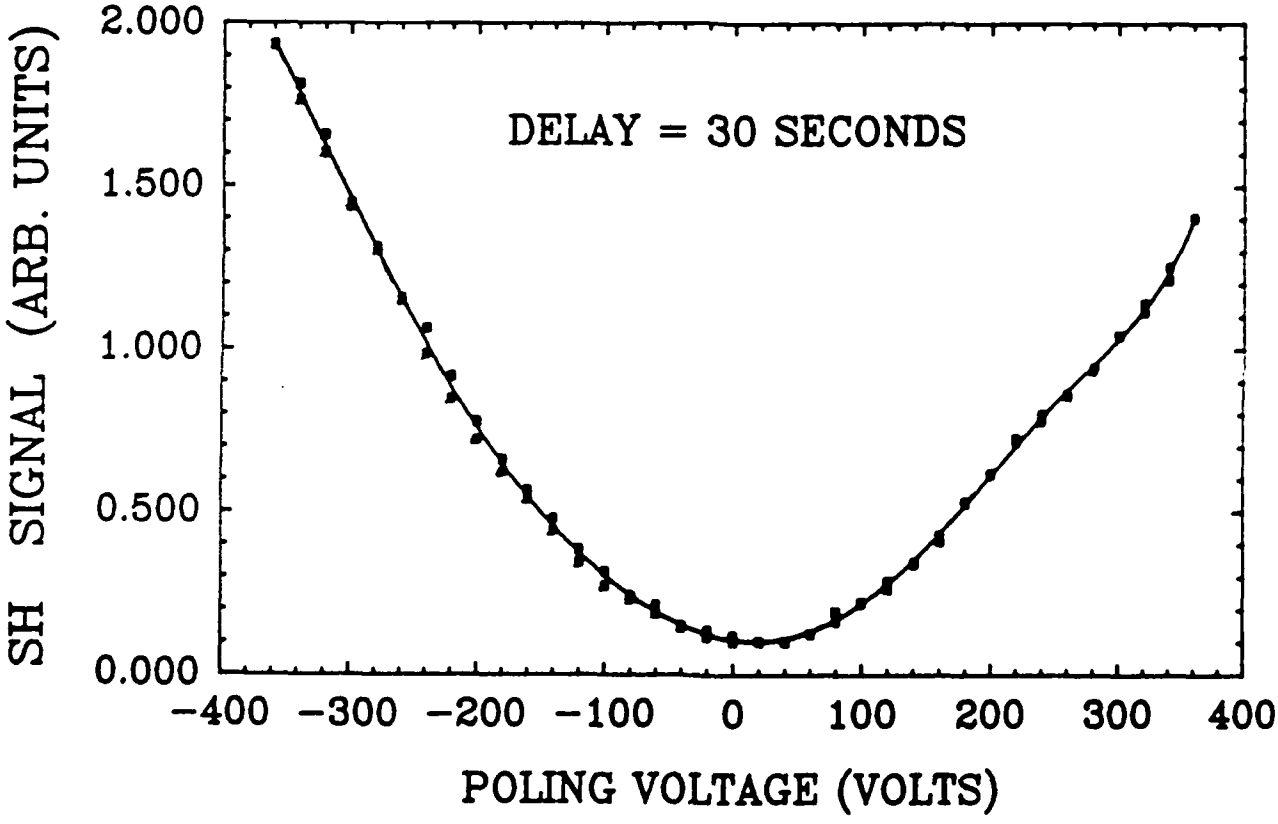
DELAY = 30 SECONDS
SH SIGNAL (ARB. UNITS)
2.000
1.500
1.000
0.500
0.000
−400
−300
−200
−100
0
100
200
300
400
POLING VOLTAGE (VOLTS)

Fig 3b

ELECTROOPTICS OF THIN FILM PLZT

A. Mukherjee, S. R. J. Brueck,* and A. Y. Wu

Center for High Technology Materials

University of New Mexico

Albuquerque, NM 87131

Abstract

We report deposition and characterization of highly oriented thin-film PLZT (28/0/100) on fused silica substrates by rf-planar magnetron sputtering. The quadratic electrooptic effect gives a birefringence of $\Delta n \sim 0.018$ at an applied field of 39 kV/mm. Optical modulation at a switching speed of < 3 ns (instrumentation limited) is achieved. Results of optically induced decay of the birefringence in these films are also reported.

* Also with the Department of Electrical Engineering and Physics.

submitted to Optics Lett.

ELECTROOPTICS OF THIN FILM PLZT

A. Mukherjee, S. R. J. Brueck, and A. Y. Wu

Center for High Technology Materials

University of New Mexico

Albuquerque, NM 87131

Ferroelectric materials are of great interest for a variety of electrooptic, piezoelectric, pyroelectric, and nonlinear optical applications. These materials, in both bulk and thin-film forms, have been used to fabricate numerous devices including sensors, memories, optical limiters, and optical switches [1-5]. Thin films of these materials are especially attractive due to the potential for monolithic integration with electronic and optoelectronic devices and systems. In addition, thin-film materials offer the potential for increased speeds, reduced voltages, and enhanced efficiencies. The family of optically transparent lanthanum-doped lead zirconate titanate (PLZT) materials have found numerous applications in optical devices [1]. Bulk PLZT materials have been used for optical storage [2], protective limiters, and spatial light modulators. Thin films of PLZT have been used for binary waveguide switches [4,5]. These quarternary materials, $Pb_{1-x}La_x(Zr_yTi_z)_{1-x/4}O_3$ usually represented as PLZT (x/y/z), are known to exhibit large electrooptic effects [5]. For the same applied field, the birefringence of PLZT (28/0/100) is several times larger than that of $LiNbO_3$, a material in widespread use for optical waveguide switches [3,6]. Future applications of these materials depend on improved film quality and improved understanding of the electrooptic and nonlinear optic material parameters.

There have been several reports of the growth of PLZT thin-films, predominantly, epitaxial growth by sputtering on $SrTiO_3$, Al_2O_3, and MgO substrates (cf. Ref. 3 and references therein). Here, we report, for the first time, the growth of highly oriented PLZT (28/0/100) films on fused silica substrates by rf-planar magnetron sputtering. Characterization of the electrooptic properties of these films including: electrooptic coefficient, very fast (~ ns, instrumentation limited) electrooptic switching speeds, and optical-intensity dependent photorefractive decay of the birefringence are also reported.

PLT films were prepared using a 17-cm diameter planar magnetron sputtering system. The sputtering target was pressed PLT powder with an excess of PbO. Sputtering media was an ultrahigh purity oxygen and argon gas mixture with a ratio of O_2/Ar ranging from 0/100 to 50/50 and a sputtering pressure varying between 5 and 10 mTorr. An optically polished fused silica substrate was maintained at 500 ~ 600 °C during the deposition using a resistance heater. The deposition rate was about 1000 ~ 2000 Å/hr for a rf power of 100 - 200 W. After deposition, X-ray diffraction scans showed highly- oriented growth with a (100) direction normal to the substrate as shown in Fig. 1. Note the absence of any additional X-ray peaks. The absorption edge, measured by optical transmission, is at 370 nm and the material is transparent throughout the visible - near infrared spectral region. The refractive index measured at 632 nm was ~ 2.5.

It has been reported by Haertling and Land [1] that an electric-field induced reversible structural phase transition (paraelectric <-> ferroelectric) occurs at room temperature for PLZT of compositions 9/65/35 and 28/0/100 and that these materials have large quadratic electrooptic coefficients R leading to a strong birefringence,

$$\Delta n = -(1/2)\, n^3\, R\, E^2$$

These initial investigations were focussed on the composition 28/0/100 due to the relative ease of deposition of a film with uniform composition [3]. Planar interdigitated electrodes (30 nm of Cr and 300 nm of Au) having a separation and width of 8 μm were evaporated on 500-nm thick films of PLZT(28/0/200) grown on fused silica substrates.

Birefringence was measured in transmission through the film with the electrodes oriented at 45° to the polarizer/analyzer axes. The (field on) / (field off) ratio of transmission at 514.5-nm wavelength at an average power density of 10 kW/cm^2 through crossed polarizers versus electric field is shown in Fig. 2. A dominant Kerr or quadratic electrooptic effect was seen. The birefringence (magnitude) of 0.018 at an applied field of 39 kV/mm was estimated from the rotation of polarization through the film. For the same field strengths, the linear birefringence of $LiNbO_3$ is several times smaller. From this data, the quadratic electrooptic coefficient R was estimated to be 0.06 x 10^{-16} $(m/V)^2$, in agreement with the value given in Ref. [3]. Using Glan polarizers with extinction ratio 10^5:1 the (field on) / (field off) ratio achieved at a field of 39 kV/mm is 40:1. At fields greater than 40 kV/mm, electrical breakdown in the electrodes was observed.

Optical switches based on electrooptic birefringence modulation in a total internal reflection (TIR) configuration in channel waveguides fabricated from PLZT thin films on sapphire have been reported by Wasa et al [5] and Higashino et al [4]. They reported low drive voltages (4.7 V) and multi-GHz speeds. Here we report optical switching on propagation perpendicular to the film plane [7]. The experimental set up is identical to

that used in measuring birefringence i.e. beam propagating perpendicular to the film through an interdigitated electrode pattern. A pulse generator comprised of a charged transmission line and a mercury switch generated voltage pulses of up to 5 kV with a rise time of ~ 2 ns. The switched voltage pulse and the transmitted optical pulse are shown in Fig. 3. The upper trace shows the applied voltage pulse (85 V) of width ~ 75 ns and a risetime of ~ 2 ns. The lower trace shows the transmission as detected by a fast avalanche photodiode with a characteristic rise time of 3.5 ns. The time delay between the traces results from the transit time of an extra length of cable and is not an intrinsic effect. The response is clearly instrumentation limited. Note also that the turn-off time of the birefringence follows the turn-off of the voltage. This rapid decay, comparable to the rise time, is advantageous for many applications. The undershoot of the voltage pulse is due to cable reflections. The fast response in these thin films is in sharp contrast to previous results in bulk [8] (*10 μs - 100 ms*) and in thin-film memory applications [9] (~ 50 ns). The improvement in temporal response may be due to improved material quality, so that the dominant effect is lattice distortion rather than domain wall reordering. Ultrafast measurements of the PLT response are being pursued in our laboratories. Clearly PLZT thin films offer very fast speeds, high contrast, high damage thresholds (no damage was observed at 5 GW/cm^2) and integration capabilities with existing Si and III-V semiconductor devices. With these attractive features PLZT thin films should become an important material for integrated optic applications.

Photorefractive phenomena have been observed in a wide range of electrooptic materials [10]. These are manifested as a space charge field that builds up across illuminated regions. Many studies have been reported on photorefractive effects in multiple-beam grating experiments such as two-beam coupling and four-wave mixing. These phenomena also occur in single beam experiments where the space charge field

builds up on the scale of the beam diameter rather than on the scale of the grating period as in the multiple beam case [11]. Because the induced space charge field opposes the applied field, the result is a reduction of the observed birefringence [12-14].

This optically induced decay in the birefringence is shown in Fig. 4. A 100-MHz train of 70 ps pulses at 532 nm was focussed at a peak intensity of 50 MW/cm^2 (average intensity 350 kW/cm^2) between a pair of planar electrodes. As before, the transmission of the beam propagating perpendicular to the film through crossed polarizers is shown. A voltage pulse was applied resulting a field of 7 kV/mm in the material. The transmission showed the typical very fast rise, instrumentation limited in Fig. 4, but decayed in a ms timescale. The field was applied at t = 1 ms and maintained to beyond 10 ms. The birefringence decay can be attributed to the optical generation of free carriers, their drift and diffusion in the external field and trapping at impurity sites causing an internal space charge field E_i opposing the external applied field. E_i increases until a uniform current flows across both the illuminated and unilluminated regions of the film. The fact that E_i does not cancel the external field can be seen from the remnant birefringence at long times. The optical origin of this decay process was evident from a strong laser intensity dependence of the decay rate.

A similar decay is observed for the electric-field induced second harmonic generation in these films; a strong dependence of the decay rate of the second harmonic signal on the incident laser power density is observed. A detailed study is being carried out on the intensity dependent generation of space charge fields resulting in the decay of both the field-induced second-harmonic generation and the birefringence, since both phenomena depend directly on the optically induced space charge field.

In conclusion, we report the deposition of highly oriented thin films of PLZT on fused silica substrates. The quadratic electrooptic effect in these films results in a birefringence of 0.018 at an applied field of 39 kV/mm. Instrumentation-limited response of the electrooptic effect was found to be $\leq$ 3.5 ns. Optically induced decay of birefringence due to photorefractive effects in these films is also reported.

Acknowledgements

The authors would like to thank Drs. M. Avinor, G. Haertling, C. E. Land and G. C. Valley for helpful discussions. This work was partially supported by the Air Force of Scientific Research and by the Air Force Weapons Laboratory.

FIGURE CAPTIONS

Fig 1. X-ray diffraction pattern of PLZT (28/0/100) thin films on fused silica substrates.

Fig 2. Field on/field off transmission ratio through crossed polarizers at 514.5-nm wavelength versus applied electric field.

Fig 3. High speed switching of electric-field-induced birefringence. The upper trace shows the applied voltage pulse (85 V) and the lower trace shows the transmission through a 500-nm PLZT (28/0/100) film between crossed polarizers.

Fig 4. Optical field induced decay of birefringence in presence of the applied electric field. The time-averaged incident laser intensity at 532 nm was 350 kW/cm^2.

REFERENCES

1. G. H. Haertling, and C. E. Land, J. Am. Ceram. Soc. 54,1, 1971.

2. M. E. Lines, and A. M. Glass, "*Principles and Applications of Ferroelectrics and Related Materials*," Clarendon Press, Oxford, 1979.

3. H. Adachi, T. Mitsuyu, O. Yamazaki, and K. Wasa, J. App. Phys. 60, 2, 1986.

4. H. Higashino, T. Kawaguchi, H. Adachi, T. Makino, and O. Yamazaki, Jap. Jour. App. Phys. Vol. 24, 284, 1985.

5. K. Wasa, O. Yamazaki, H. Adachi, T. Kawaguchi, and K. Setsune, J. Lightwave Tech. LT-2, 5, 710, 1984.

6. T. Kawaguchi, H. Adachi, K. Setsune, O. Yamazaki, K. Wasa, App. Opt., 23, 13, 2187, 1984.

7. A. Mukherjee, S. R. J. Brueck, and A. Y. Wu, Paper #ThH2, CLEO, Baltimore, Maryland, April 24-28, 1989.

8. G. Wolfram, Ferroelectrics, Vol. 10, 39, 1976.

9. J. F. Scott, L. Kammerdiner, M. Parris, S. Traynor, V. Ottenbacker, A. Shawabkeh, and W. F. Oliver, J. Appl. Phys. 64, 787, 1988.

10. *Electrooptic and Photorefractive Materials*, Ed. P. Günter, Proceedings of the International School of Material Science and Technology, Erice, Italy, July 6-17, 1986, Springer Proceedings in Physics, Vol. 18, Springer-Verlag.

11. N. V. Kukhtarev, V. B. Markov, S. G. Odulov, M. S. Soskin, and V. L. Vinetskii, Ferroelectrics, Vol. 22, 949, 1979.

12. J. M. Rouchon, M. Vergnolle, and F. Micheron, Ferroelectrics, Vol. 11, 389, 1976.

13. A. E. Krumins, E. E. Klotins, V. I. Dimza, U. Yu. Ilyin, and V. J. Fritsberg, Ferroelectrics, Vol. 18, 21, 1978.

14. R. C. Hughes and R. J. Sokel, J. Appl. Phys., 52, 6743 1981.


PLT
(200)
PLT
(100)
X-Ray Intensity
50
45
40
35
30
25
20
X-Ray Diffraction Angle 2θ (Degree)

Figure 1

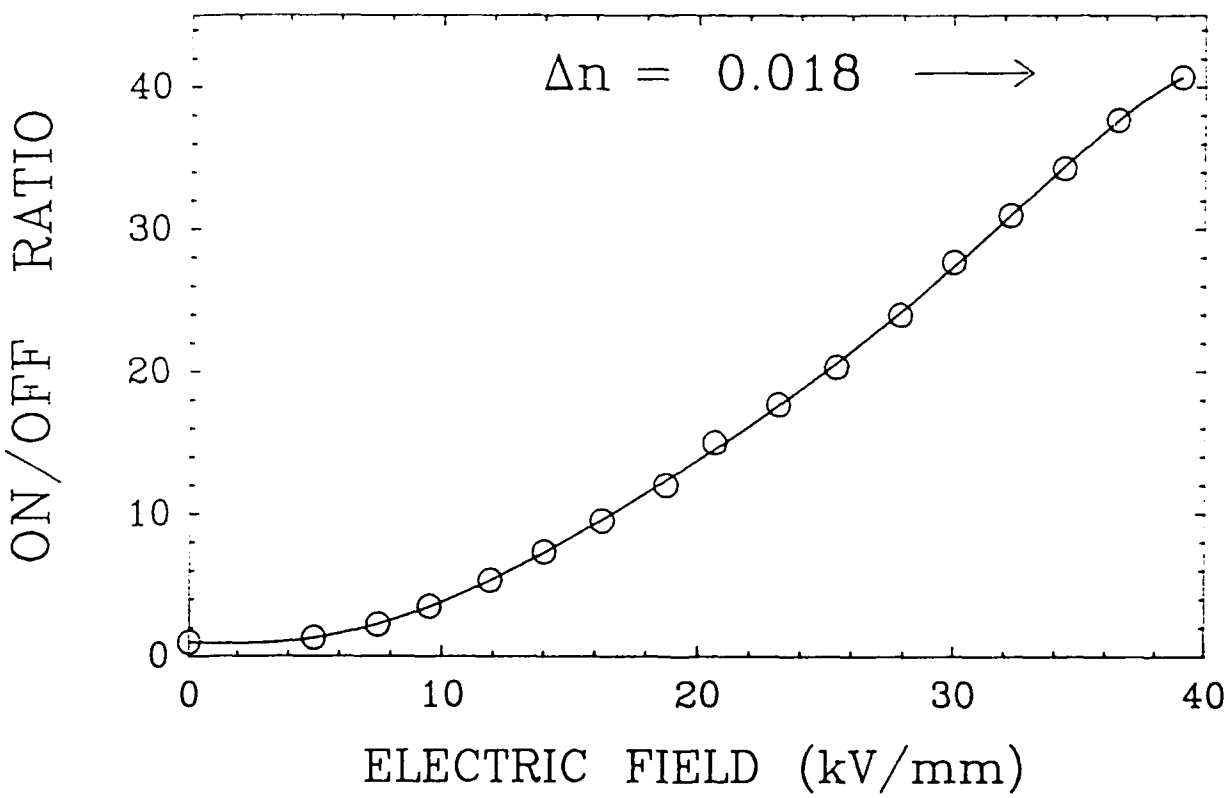

Fig. 2

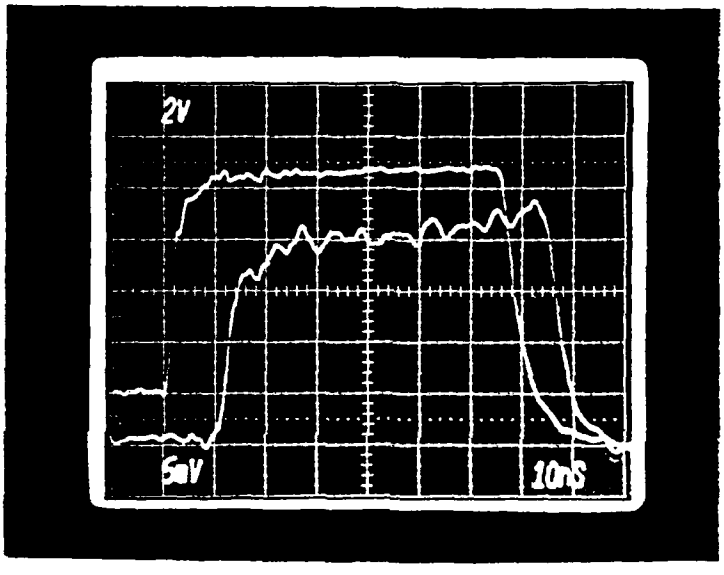

Fig. 3

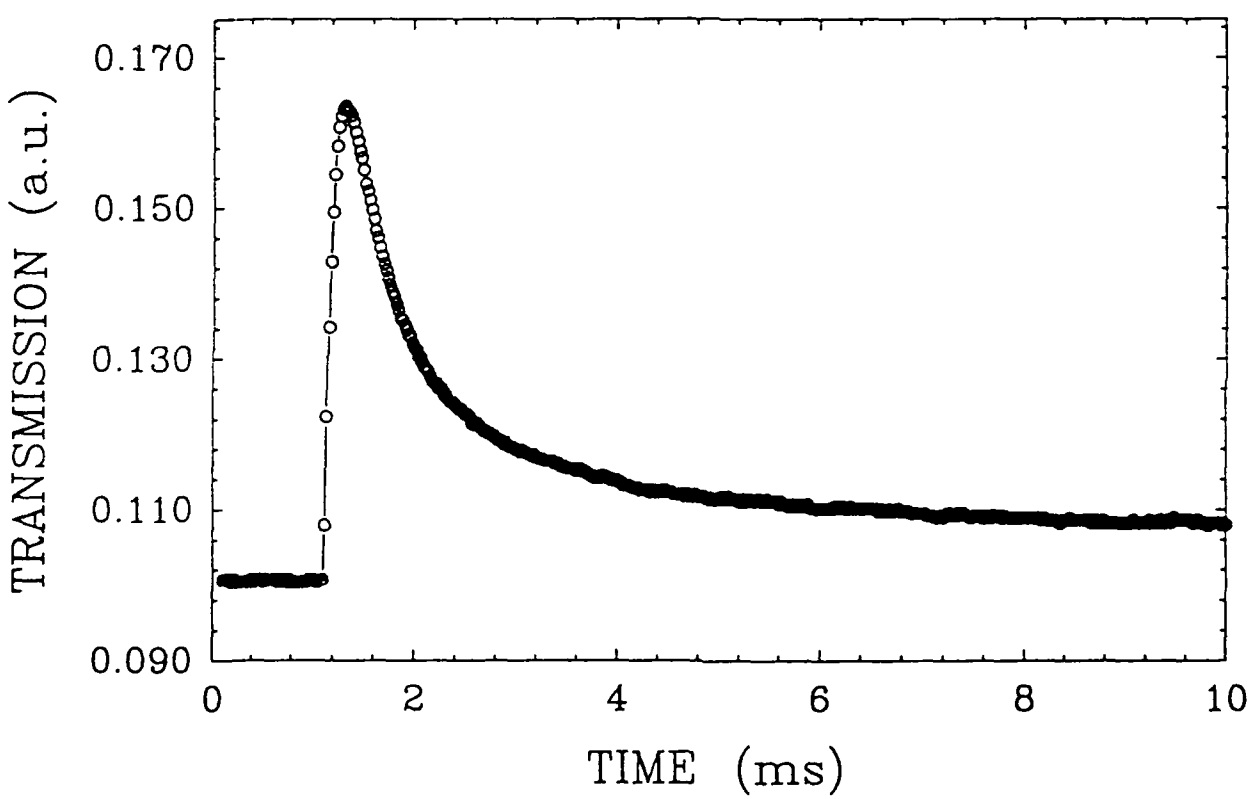

Fig. 4

MF15-1

DC FIELD INDUCED SECOND-HARMONIC GENERATION IN PLZT 9/65/35*

A. Mukherjee, S. R. J. Brueck and A.Y. Wu
Center for High Technology Materials
University of New Mexico, Albuquerque, NM, 87131

Centrosymmetry of molecular aggregates having a center of inversion can be broken by applying an external DC electric field and even-order nonlinear optical processes can be studied. Electric field induced second-harmonic generation (EFISHG) has been studied in centrosymmetric polydiacetelene (PDA) to investigate resonant enhancement of $\chi^{(3)}$ $(-2\omega;\omega,\omega,0)$ and two photon generation of carriers[1] and determine the phase and value of $\chi^{(3)}$ $(-2\omega;\omega,\omega,0)$ [2]. EFISHG experiments have also been reported on molecules in solution to study the molecular environment[3] and influence of carrier substituents[4]. In this paper, we report the first EFISHG measurements in optically transparent, ferroelectric oxide PLZT (La- doped lead zirconate titanate) ceramic materials.

PLZT has a perovskite structure with a transition metal (Zr or Ti) at the center surrounded by an oxygen octahedra with Pb or La at the corners[5]. Due to a strong electrooptic effect, PLZT materials have been used as shutters, modulators, memories and other devices[5]. PLZT is stoichiometrically written in x/y/z notation where x stands for the atom percentage of La, and y/z for the zirconium/titanium ratio. Selected compositions of PLZT were studied by Haertling and Land[6] who demonstrated that the composition 9/65/35 having quasiferroelectric (neither true ferroelectric nor true paraelectric) behaviour was interesting from both scientific and application points of view. At room temperature, PLZT 9/65/35 undergoes an electric field induced reversible displacive phase transition α to β, where α represents a cubic paraelectric phase and β a distorted cubic ferroelectric phase[7].

The EFISHG measurements were carried out on a 9/65/35 PLZT wafer of thickness 0.6 mm at room temperature and in an air ambient. A hysteresis behavior of SHG signal versus poling field was observed. The contrast ratio achieved was 20:1 and the area of the hysteresis was seen to decrease to a 'slim-loop' if the SH signal recording was sufficiently delayed after applying the poling voltage, the sample remaining irradiated by the fundamental beam.

The 1.06μm modelocked pulse train (82 MHz, 130 ps duration pulses) from a cw-modelocked YAG laser served as the fundamental beam. A polarization rotator and a Glan prism were used to select a linearly polarized fundamental beam of variable orientation. A beam of 3W average power was focused (50μm diameter) at 45° angle of incidence on the region between two planar electrodes on the surface of the wafer. The SH signal was observed along the specular reflection direction. A lens was used to collect the SH light and focus on the active area of an uncooled photomultiplier tube. An IR blocking filter, an interference filter, and a polarizer were used to select a linearly polarized component of the SH signal. Conventional photolithographic and metalization processes were used to deposit 30 nm of Cr and then 300 nm Au strips as electrodes on the wafer surface. The electrodes had a gap of 60μm and were 1.5 mm long.

The poling was started with a positive voltage from 0V to 360V and down to 0V in steps of 20V. At each step there was a delay, Δt, between the application of the poling field and the SHG measurements. The same procedure was followed to trace out

the negative poling branch. For the same set of polarizations (fundamental and SH) two sets of data were taken, with Δt = 1s (Figs.1a and 2a) and 30 seconds (Figs.1b and 2b). Fig. 1 shows the EFISHG traces with both fundamental and SH polarizations being parallel to poling field and Fig. 2 shows the traces with the fundamental beam having parallel polarization and SH having perpendicular polarization with respect to the poling field.

From these data we see that there is a small SH signal at the starting zero poling field. Though the sample is nominally in the α (cubic) phase it is not strictly centrosymmetric because of polar microregions associated with lattice defects, impurities and local deviations from stoichiometry. We see that the SH intensity increases quadratically as the poling field is increased. This is consistent with EFISHG as a third order process with the SH intensity being proportional to

$$I^{2\omega} \propto \left| \chi^{(3)}(-2\omega;\omega,\omega,0)\, E_\omega{}^2 E_l \right|^2$$

where E_ω is the fundamental field and E_l is the local DC electric field. The quadratic dependence of $I^{2\omega}$ with the fundamental intensity was also confirmed. Weak saturation behavior can be seen at the maximum poling voltage of 360V (~ 60kV/cm). Though the saturating poling field is much higher than this, a further increase in poling voltage caused arcing between the electrodes. This could be avoided with an improved sample preparation and the addition of a dielectric layer on the surface allowing higher poling fields and greater contrast ratio. On decreasing the poling field to zero the SH intensity was a little higher than the starting value. This may be due to the remnant β - phase resulting from strains induced by poling. The decrease of the area of hysteresis on delay time is analogous to the 'slim-loop' behavior of dielectric hysteresis reported at higher temperatures[8]. If the poling circuit was suddenly opened, it was observed that the decay of the SH intensity took about 30 seconds under irradiation with the fundamental beam and several hours if not irradiated. This is possibly due to photoinduced conductivity and needs a more detailed study to fully understand this effect. Field-induced birefringence measurements in the same configuration will also be reported.

In Fig. 2 we see an asymmetry in the SH signals of positive and negative poling fields. This is because of the remnant spontaneous polarization resulting a residual polarization field E_p opposing the external field E_0 and so the local field E_l becomes proportional to (E_0 + E_p) for the negative poling. This was not seen in the parallel SH case (Fig. 1). Also in Fig 2. we observe a shift in the minimum of SH intensity away from zero poling field.

In conclusion, we report the first measurements of EFISHG in ceramic PLZT 9/65/35. A minimum contrast ratio 20:1 was observed. We have grown highly oriented thin films of PLZT on various substrates in our laboratories and results on these materials will also be presented. In addition to EFISHG, other field-induced nonlinear optical processes such as FWM, stimulated scattering, and multiphoton absorption are being studied in these thin films.

References

1. P. A. Chollet, F. Kajzar and J. Messier, Thin Sol. Films 132, 1-10 (1985)

2. F. Kazar, J. Messier, J. Zyss and I. Ledoux, Opt. Comm. 45, 13 (1983).

3. I. Ledoux & J. Zyss, Chem. Phys. 73 (1982).

4. J.-L. Ouder, J. Chem. Phys. 67, 446 (1977).

5. T. Kawaguchi & O. Yamazaki, JEE Jan, (1984)

6. G. H. Haertling & C. E. Land, J. Am. Cer. Soc. 54, 1 (1971)

7. K. Carl & K. Geisen, Proc. IEEE, Vol 61, #7, July (1973)

8. E. T. Keve & A. D. Annis, Ferroelectrics 5, 77-89 (1973)

* Partial support for this work was provided by the Air Force Office of Scientific Research.

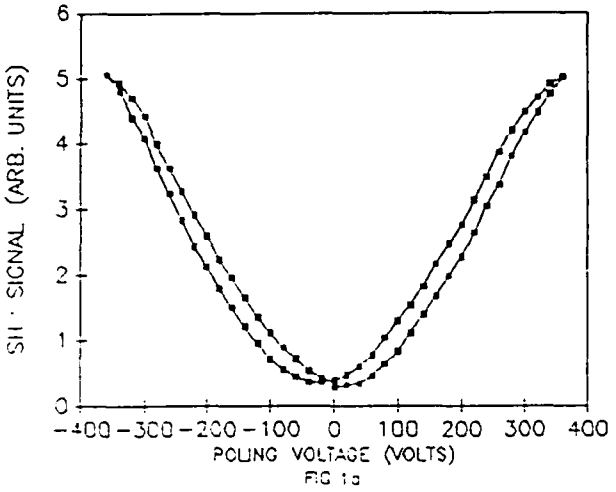

FIG 1a

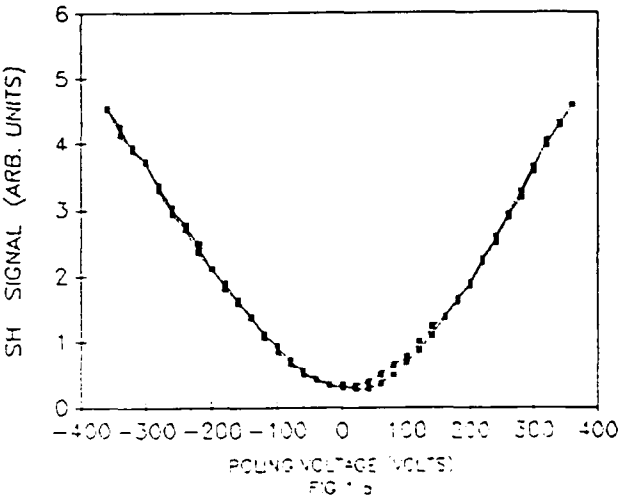

FIG 1b

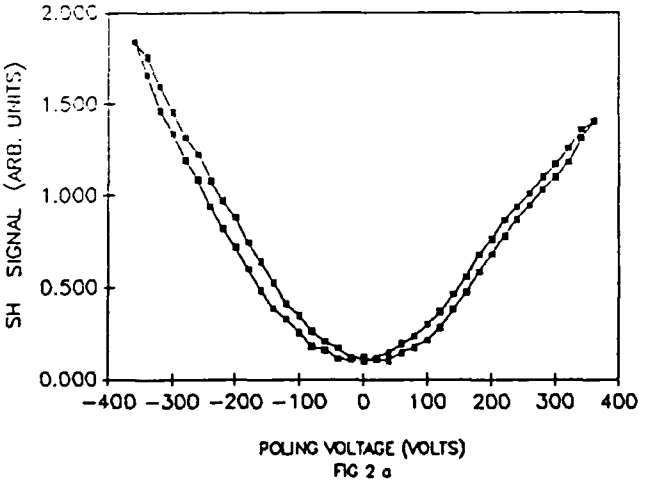

FIG 2a

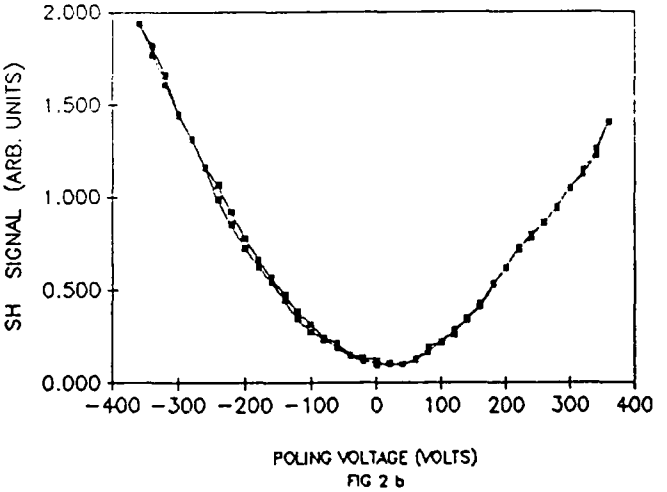

FIG 2b

Thursday MORNING

27 April 1989 THH

CONVENTION CENTER ROOM 310

10:30 AM Nonlinear Optics: 2

Duncan G. Steel, University of Michigan, Presider

THH1 Second harmonic generation in a new organic nonlinear chalcone derivative crystal

G. J. ZHANG, T. KINOSHITA, K. SASAKI, Keio U., Dept. Electrical Engineering, 3-14-1 Hiyoshi, Yokohama 223, Japan; Y. GOTO, A. NAKAYAMA, Nippon Oil & Fats Co., Japan.

Some organic polymer materials with large delocalized π-electron systems exhibit extremely large nonlinearities compared with inorganic nonlinear materials. However, application research has been restricted because of the following:

(1) The largest second harmonic generation tensor component is not phase matchable. (2) The bulk crystal is not easy to prepare. (3) There often is a strong absorption in the useful SHG wavelength region making it unsuitable as a nonlinear optical material. (4) In general the mechanical or physical properties (deliquescence, volatility) of the organic materials make them difficult to handle.

We present nonlinear optical properties and methods of crystal growth for a new organic nonlinear optical material, a chalcone derivative

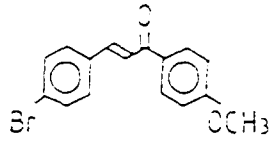

The material gives large nonlinear optical effects which can compare with 2-methyl-4-nitroaniline (MNA).[1] Optically transparent and mechanically stable bulk crystals of ~4 X 10 X 10 mm were prepared by solution growth with precise temperature control over one month. The principal axis directions and cleavage plane are shown in Fig. 1. X-ray diffraction analysis shows that the crystal belongs to the point group m, space group Pc with a = 15.898 Å, b = 7.158 Å, c = 5.983 Å, and β = 97.19°. The second harmonic polarization P is given as

$$P_x = d_{11}E_x^2 + d_{12}E_y^2 + d_{13}E_z^2 + 2d_{15}E_zE_x,$$

$$P_y = 2d_{24}E_yE_z + 2d_{12}E_xE_y,$$

$$P_z = d_{15}E_x^2 + d_{24}E_y^2 + d_{33}E_z^2 + 2d_{13}E_xE_z.$$

The cleavage plane is used for SHG and refractive index measurement. From ellipsometric measurements combining the cleavage plane (normal to the y axis) with the fast growth plane (normal to the z axis), the anisotropic refractive index along the principal axis has been determined.

A Q-switched Nd:YAG laser (λ = 1.064 μm) was used for second harmonic generation. It was found that the figure of merit of this crystal for the component d_{11} is ~400 times larger than d_{31} of $LiNbO_3$.

The anisotropic absorption edge of the crystal advantageously extends to the UV region as shown in Fig. 2. For light polarized parallel to the z axis it shows a slightly larger absorption than for orthogonally polarized light. The coarser cleaved surface for the fundamental ray at normal incidence yields a gourdlike SHG pattern as shown in Fig. 3. This pattern completely obeys the type 1 critical phase matching SHG of Hobden's classification.[2] The SHG pattern is projected on a screen at the back of the crystal and photographed. The SHG signal is quite strong and coherent. The melting point of the crystal is 159.5°C and exhibits no deliquescence or sublimation in air. Furthermore, it has a high optical damage threshold and is transparent even at the near UV region.

(Invited paper, 25 min)

1. B. F. Levine, C. G. Bethea, C. D. Thurmond, R. T. Lynch, and J. L. Bernstein, J. Appl. Phys. **50**, 2523 (1979).
2. M. V. Hobden, J. Appl. Phys. **38**, 4365 (1967).

THH2 Electrooptics of thin film PLZT

A. MUKHERJEE, STEVE R. J. BRUECK, A. Y. WU, U. New Mexico, Center for High Technology Materials, Albuquerque, NM 87131.

Integrated optic devices such as high speed waveguide switches are essential components for modulation and multiplexing operations in optical communication and signal processing. Thin films of the optically transparent ferroelectric oxide $Pb_xLa_{1-x}(Zr_yTi_{1-y})_{1-x/4}O_3$ (PLZT) materials have very large electrooptic effects and are very promising materials for fabricating such devices. Deposition, characterization, and TIR switch operation in thin film PLZT has been reported by Adachi *et al.*[1] and Higashino *et al.*[2] We report on the deposition of highly oriented (100) PLZT (28/0/100) thin films on a variety of substrates, very fast switching of electric-field-induced birefringence, and the first measurements of electric-field-induced second harmonic generation in these films.

Thin films (500 nm thick) of PLZT (28/0/100) were deposited on heated (600°C) fused silica substrates in a rf planar magnetron sputtering system. The x-ray diffraction of these films suggests that these films are highly oriented with (100) direction normal to the substrate. Planar interdigitated electrodes (30 nm of Cr and 200 nm of Au) were evaporated on the films. Films were also deposited on Si and Al_2O_3 substrates.

To demonstrate the electric-field-induced birefringence, the films were sandwiched between crossed polarizers with the electric field oriented at 45° with respect to the transmission axes of both polarizers. The field-on/field-off ratio of transmission of an Ar-ion laser beam (514.5 nm) through crossed polarizers vs electric field is shown in Fig. 1. The electrooptic effect showed a dominant Kerr effect, and the quadratic electrooptic coefficient was estimated to be 0.6 X 10^{-16} (m/V)^2, which is in agreement with the value estimated in Ref. 1. Note the birefringence shift of $\Delta n = -0.018$ at an electric field of 68 kV/cm. The switching speed measured is shown in Fig. 2. The upper trace shows the applied voltage pulse (85 V) of ~75-ns width and ~2-ns rise time. The lower trace shows the transmission as detected by a fast avalance photodiode with a characteristic rise time of 3.5 ns. The time delay between these traces is due to the cable transit time and is not an intrinsic effect. Clearly, the response is instrumentation limited. Note also that the birefringence follows the turn-off time of the voltage, being comparable to the rise time is advantageous for many applications. The higher speed of operation is expected in these films, and measurements are under way to establish material limitations.

The first measurements of electric-field-induced second harmonic generation in these films are shown in Fig. 3. The fundamental beam was a train of mode-locked 1.06-μm pulses of 100-ps duration and 82-MHz repetition rate. The second harmonic signal has been normalized to the residual signal at the zero external field. The second harmonic signal at the zero external field is weak reflecting the pseudocubic nature of PLZT (28/0/100). The application of an electric field induces a displacement of the oxygen octahedra from the symmetric position about the Zr (or Ti) sites breaking the inversion symmetry of the medium. Note the 3 orders of magnitude enhancement of the second harmonic signal at the maximum applied field. The quadratic dependence of the second harmonic signal on the applied electric field E_{ac} arises out of the third-order susceptibility, namely,

$$I^{2\omega} \propto |\chi^{(3)}(-2\omega;\omega,\omega,0)E_{ac}E_{dc}|^2.$$

In contrast to the birefringence, the second harmonic signal displays a complex temporal dependence on long time (millisecond) scales. The signal shows a large initial susceptibility along with an intensity-dependent decay (typically 50 ms at 6 MW/cm^2) to a lower steady state value. Detailed measurements of the polarizations, optical power, and applied electric field dependences of these features are presented.

In summary: We have reported very fast switching (detection limited to ~3 ns) in transmission through crossed polarizers and, we believe, the first measurements of electric-field-induced second harmonic generation in thin film PLZT materials. The polarization and power dependences of the fundamental beam on the peak, decay, and steady state values of the second harmonic signal in the presence of an external field reported here may provide clues to a better microscopic modeling of the nonlinear susceptibilities of these ferroelectric thin films. Uses in integrated optics and spatial light modulators are discussed. (12 min)

1. H. Adachi, T. Mitsuyu, O. Yamazaki, and K. Wasa, Appl. Phys. **60**, 736 (1986).
2. H. Higashino, T. Kawaguchi, H. Adachi, T. Matsuno, and O. Yamazaki, Jpn. J. Appl. Phys. **24**, 284 (1985) Suppl. 24-2.

THH3 Sensitivity of two-core fiber coupling to light-induced defects

M. A. SAIFI, Y. SILBERBERG, H. FOUCKHARDT, ANDREW M. WEINER, M. J. ANDREJCO, Bellcore, 331 Newman Springs Rd, Red Bank, NJ 07701-7020.

The nonlinear directional coupler based on the intensity-dependent refractive index is a potentially important device for all-optical signal processing in ultrahigh bit rate communication networks. Since it was originally proposed by Jensen[1] several applications as a logic gate, pulse compressor, and optical transistor have been proposed. In a dual core optical fiber nonlinear directional coupler, all-optical switching in the femtosecond regime has been demonstrated.[2] It is well known that for complete power transfer in the linear regime, the two cores of a directional coupler should have identical propagation constants and a length preferably equal to one coupling length. The matching of the propagation constants can be obtained by fabricating a two-core fiber with identical core and cladding parameters. Switching is then achieved by perturbing the coupling with the intensity-dependent change in the refractive index of the input core.

We report on a small but discernible permanent change in the refractive index of the germania-doped silica glass fiber subjected to high intensity femtosecond pulses at 620 nm. We believe the refractive index change is associated with several germania related defect centers. The defect related change in the refractive index has been recognized, since reflection[3] gratings in germania-

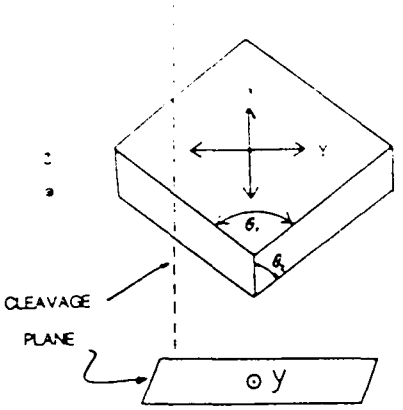

THH1 Fig. 1. Single crystal shape and principal axes directions for the chalcone derivative.

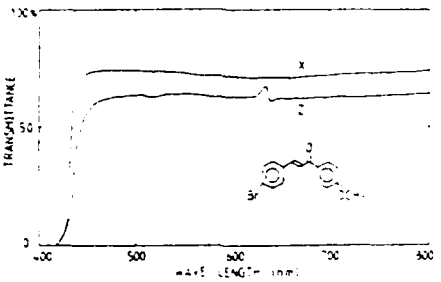

THH1 Fig. 2. Anisotropic transmission curves of the chalcone derivative crystal

THH1 Fig. 3. Gourdlike SHG signal pattern from the chalcone derivative crystal on a perpendicularly positive screen at the back of the crystal.

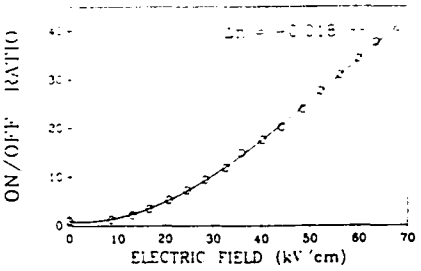

THH2 Fig. 1. Field-on/field-off ratio of the transmission of an Ar laser beam (514.5 nm) through crossed polarizers vs applied electric field.

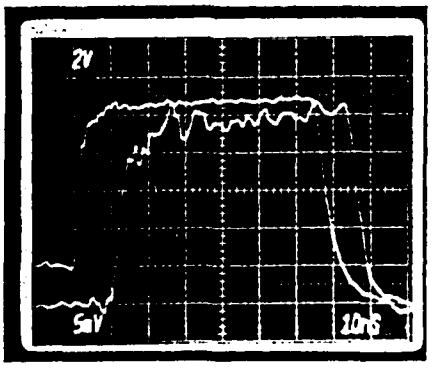

THH2 Fig. 2. High speed birefringence switching. The upper trace shows the applied voltage (85-V) pulse, and the lower trace shows the transmission of a 0.5-μm thick PLZT film through crossed polarizers.

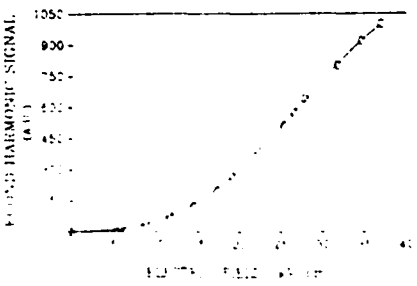

THH2 Fig. 3. Electric-field-induced second harmonic generation in thin film PLZT (28/0/100)

NOVEL WAVELENGTH-RESONANT OPTOELECTRONIC STRUCTURE AND ITS APPLICATION TO SURFACE-EMITTING SEMICONDUCTOR LASERS

Indexing terms: Semiconductor lasers, Integrated optics, Semiconductor devices and materials

An optimised design for optoelectronic devices which depends on the interaction between an electromagnetic standing wave and the carrier population is described. The structure consists of quantum well layers spaced at one half the wavelength of a selected optical transition in quantum wells. This spatial periodicity allows the amplifying or absorbing medium (quantum wells) to coincide with the peaks of the standing wave optical field in the Fabry–Pérot cavity. In such a periodic medium, the gain or absorption for the selected wavelength is enhanced by a factor of two compared to a uniform medium. This concept was applied to fabricate a surface-emitting semiconductor laser in the GaAs/AlGaAs system. Lasing was achieved with the shortest gain medium length (320 nm) ever reported.

Introduction: Many optoelectronic devices utilise interaction of a standing electromagnetic wave with an amplifying or absorbing semiconductor medium. This interaction is not spatially uniform, but is strongest at the antinodes of the standing-wave optical field and vanishes at the nulls. Thus, if for example the medium is amplifying, the carriers located in the vicinity of the antinodes are depleted by the interaction, while excess carriers may accumulate around the nodes. This problem was investigated in the early days of semiconductor lasers[1] as a possible mechanism for their multimode operation. Even though fast carrier diffusion restores spatial homogeneity, the gain of the medium is not fully utilised when single-frequency light is generated. To eliminate this problem, we propose here a new multilayer structure that maximises the medium gain by confining the carriers to the antinode regions. In amplifying media this will also reduce the amplified spontaneous emission (ASE) due to carriers otherwise present near the nodes. In particular, we apply this concept to demonstrate that surface-emitting (SE) lasers with reduced threshold can be built and we report successful operation of optical pumped AlGaAs GaAs SE laser.

Device concept: Consider a multilayer structure which involves a series of very thin layers (quantum wells) separated by relatively thick spacers, as shown schematically in Fig. 1. The bars represent single quantum wells or groups of multiple quantum wells kept very close together. For the interaction with light to be limited to the quantum well (QW) medium, the spacer thickness has to match one half of the selected wavelength in the medium, corresponding to a particular transition in the QW. Moreover, the phase of the reflected wave from the material surface must be such that peaks of the standing wave optical field coincide with the periodic QW medium.

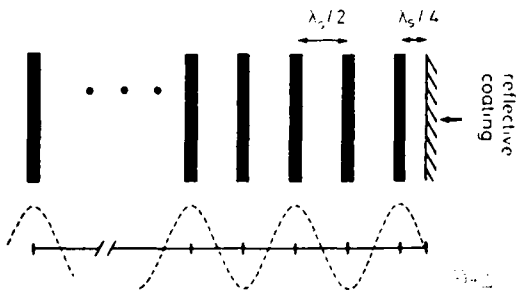

Fig. 1 *Schematic diagram of periodic structure to enhance interaction between standing-wave optical field and charge carriers*

λ_s is resonant wavelength in spacer medium

To illustrate the effect of the periodic QW medium on interaction with a standing-wave pattern we consider the case of amplifying medium in a Fabry–Pérot (FP) cavity (an analogous argument could be presented for absorptive medium). For a medium nonuniform along the resonator axis direction (z), the integrated gain $G(\lambda)$ is given by

$$G(\lambda) = \int_0^L a(z) \sin^2\left(\frac{2\pi m(z) z}{\lambda}\right) dz \qquad (1)$$

where L is the resonator length, $a(z)$ and $m(z)$ are longitudinal profiles of material gain and refractive index, and λ is the free-space wavelength of the standing wave. For a uniform medium, the integral (eqn. 1) gives $G(\lambda) = aL/2$, that is only half of the available material gain is utilised. Consider now a periodic gain medium illustrated in Fig. 1, with single quantum wells separated by $\lambda_s = \lambda_r/2n_2$, where n_2 is the refractive index of spacer material (we ignore here the phase shift in the QW). As shown in Fig. 2, $G(\lambda)$ has a resonance at λ_r which enhances the available gain. The discrimination for

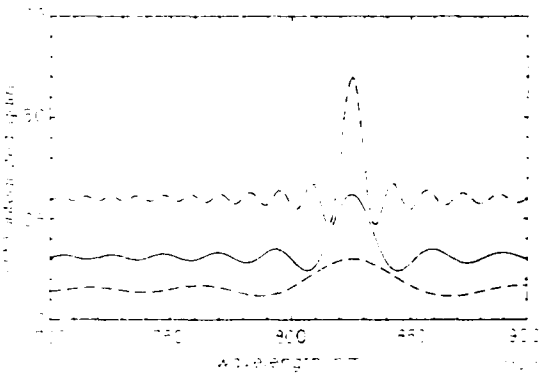

Fig. 2 *Integrated relative gain of periodic medium consisting of single quantum wells separated by spacers matched to half-wavelength at 825 nm*

15 wells; 30 wells; 60 wells

the resonant wavelength improves with the increasing number of QW layers. This is analogous to the situation where the resolution of a grating is improved by illumination of a larger area (more lines). Away from the resonance, $G(\lambda)$ approaches the limit of $Ng_1L_2/2$, same as for the uniform-gain medium (N, g_1, and L_2 are the number of QW layers, gain, and thickness of each QW, respectively). At the resonant wavelength the integrated gain coefficient $G(\lambda_r)$ is a factor of two larger.

Surface emitting laser: The proposed structure has potential for applications in various optoelectronic devices such as lasers, amplifiers, modulators, low threshold optical bistable switches, photodetectors, *etc.* In the remaining part of this letter, we demonstrate its usefulness for vertical-cavity SE lasers. Previously reported vertical-cavity SE lasers[2–4] suffer from high thresholds and low efficiencies caused by short active-cavity lengths (typically a few μm), significant ASE in the direction transverse to the lasing axis, and lack of confinement of carriers and optical fields.

Apart from enhanced integrated gain, the proposed structure has additional appeal for SE lasers because it reduces the ASE. Since the spacer medium around the nodes of the optical field contains no free carriers, the spontaneous emission loss is reduced and longitudinal spatial hole burning is eliminated.

Experiment: As an initial demonstration of the wavelength-resonant structure, we have fabricated an MBE-grown GaAs/AlGaAs SE laser cavity consisting of 32 GaAs 10 nm thick quantum wells separated by 120 nm thick $Al_{0.25}Ga_{0.75}As$ spacers. The top end AlGaAs spacer, on which Al coating was deposited to increase the reflectivity, had 60 nm thickness to account for the phase change of reflected light. The Al-coated side was bonded to a piece of glass for support and the GaAs substrate was removed by standard selective chemical etching which stopped at an AlAs GaAs short period superlattice. The total thickness of the processed sample (and the length of FP cavity) was $\sim 4.3\,\mu$m. It is worthwhile to point out that the structure does not act as a distributed feedback laser, calcu-

lations including the effects of refractive index and gain yield the total reflectivity smaller than 1%.

The structure was optically pumped using a 10 Hz pulsed dye laser operating at 680 nm, with a 7 ns pulsewidth. A monochromator was used to separate the pump beam and a photomultiplier was employed for detection. Experimentally determined threshold for room temperature lasing was 6 MW cm^{-2}. We have thus demonstrated a semiconductor laser with the active medium length of only 320 nm; previously, the shortest reported length was 1·5 μm for a multiple QW active region.[3] Fig. 3 shows both room temperature and 77 K data well above threshold. By comparing with absorption spectra,

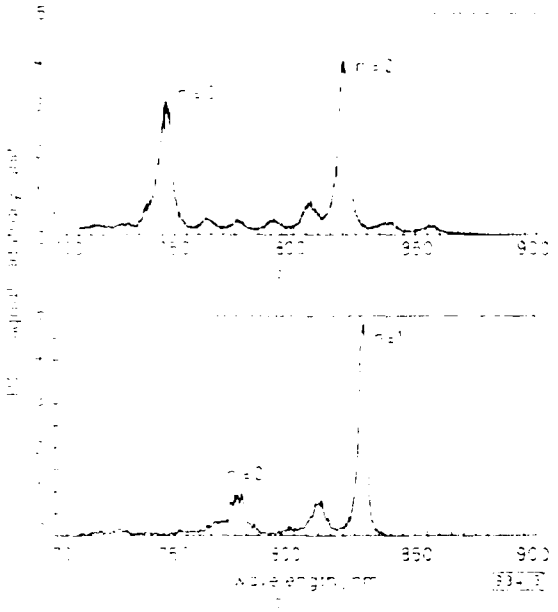

Fig. 3 *Spectra of SE laser optically pumped well above threshold*
a Room temperature, $P = 4{\cdot}8P_{th}$; $E_{in} = 580$ nJ; ×0·05
b 77 K, $P \simeq 10P_{th}$, $E_{in} = 820$ nJ; ×0·02

we assigned room temperature lasing spectra to $n = 2$ and 3 transitions. Emission around 820 nm ($n = 2$) corresponds to the resonant wavelength selected in the design of the structure. Emission at $n = 3$ is attributed to higher material gain caused by higher density of states. At 77 K, the bandgap widens and the resonant wavelength is close to $n = 1$ transition at 830 nm, as illustrated in Fig. 3.

Conclusions. We have described a new optoelectronic structure which enhances the interaction between a standing-wave optical field and charge carriers. A factor of two improvement in gain absorption is predicted. We implemented the design to fabricate a surface-emitting GaAs AlGaAs laser and have demonstrated the lasing action by optical pumping. The total thickness of the structure was ~4·3 μm with cumulative active-medium length of only 320 nm, which is the shortest ever reported.

Acknowledgments. We thank Dr. William Streifer of Spectra Diode Laboratories for his valuable comments. This work was partially supported by the U.S. Air Force Office of Scientific Research.

M. Y. A. RAJA
S. R. J. BRUECK
M. OSIŃSKI
C. F. SCHAUS
J. G. McINERNEY

Center for High Technology Materials
University of New Mexico
Albuquerque, NM 87131, USA

T. M. BRENNAN
B. E. HAMMONS

Sandia National Laboratory
PO Box 5800
Albuquerque, NM 87185, USA

27th June 1988

References

1 STATZ, H., TANG, C. L., and LAVINE, J. M.: 'Spectral output of semiconductor lasers', *J. Appl. Phys.*, 1964, **35**, pp. 2581–2585
2 KINOSHITA, S., and IGA, K.: 'Circular buried heterostructure (CBH) GaAlAs GaAs surface emitting lasers', *IEEE J. Quantum Electron.*, 1987, **QE-23**, pp. 882–888
3 GOURLEY, P. L., and DRUMMOND, T. J.: 'Visible, room-temperature, surface-emitting laser using an epitaxial Fabry–Perot resonator with AlGaAs AlAs quarter-wave high reflectors and AlGaAs GaAs multiple quantum wells', *Appl. Phys. Lett.*, 1987, **50**, pp. 1225–1227
4 OGURA, M., HSIN, W., WU, M.-C., WANG, S., WHINNERY, J. R., WANG, S. C., and YANG, J. J.: 'Surface-emitting laser diode with vertical GaAs/GaAlAs quarter-wavelength multilayers and lateral buried heterostructure', *Appl. Phys. Lett.*, 1987, **51**, pp. 1655–1657

Surface-emitting, multiple quantum well GaAs/AlGaAs laser with wavelength-resonant periodic gain medium

M. Y. A. Raja,[a] S. R. J. Brueck,[a,b] M. Osiński,[a,b] C. F. Schaus,[b]
and J. G. McInerney[b]
Center for High Technology Materials, University of New Mexico, Albuquerque, New Mexico 87131
T. M. Brennan and B. E. Hammons
Sandia National Laboratories, P. O. Box 5800, Albuquerque, New Mexico 87185

(Received 18 May 1988; accepted for publication 23 August 1988)

A novel surface-emitting semiconductor laser with a vertical resonator, extremely short gain length, and enhanced gain at a specific design wavelength has been demonstrated. The gain medium consists of a series of GaAs quantum wells separated by AlGaAs spacers whose thicknesses are chosen to be one-half the wavelength of a particular transition in the quantum wells. This structure forces the antinodes of the standing-wave optical field to coincide with the gain elements, enhancing the gain and frequency selectivity in the vertical direction and substantially reducing amplified spontaneous emission. We have achieved optically pumped lasing with a threshold of 6 MW/cm^2 at room temperature in a molecular beam epitaxially grown structure of thickness 4.3 μm, of which only 320 nm provided gain.

Semiconductor lasers which emit from the surface[1–4] rather than the end facets hold promise for monolithic optoelectronic integration,[5] optical chip-to-chip interconnection, and for high-power large area two-dimensional arrays.[6] GaAs/AlGaAs and other ternary and quaternary III-V compound semiconductors are most attractive for such applications. Realization of these systems, however, has been impeded by the limitations of existing surface-emitting (SE) laser designs, particularly the high thresholds and low efficiencies of devices with vertical (normal to the chip plane) resonators. These problems are mostly due to the short length of the gain medium ($\sim 2\,\mu$m) compared to the transverse dimensions, lack of carrier and optical confinement, and the generation of competitive amplified spontaneous emission (ASE) in the transverse direction. On the other hand, the short cavity length ($\sim 5\,\mu$m) of SE laser results in a large Fabry–Perot (FP) mode spacing which favors single longitudinal mode operation of these devices.

In this letter, we report a novel GaAs/AlGaAs optoelectronic structure which optimizes the overlap between the gain medium and the optical field of a selected lasing mode. The result is an anisotropic and strongly wavelength-selective gain medium; the gain for the selected mode is enhanced over other longitudinal modes and ASE in the transverse direction is substantially reduced. Consequently, the efficiency will be higher and the lasing threshold lower than in a conventional double heterostructure or multiple quantum well (MQW) gain medium of the same length. Our preliminary data for pulsed dye laser optical pumping at 77 and 300 K confirm these expectations.

The most important feature of the new structure is that the position of very thin active regions is arranged such that they coincide with antinodes of a vertical standing-wave pattern at the lasing wavelength. Figure 1 illustrates the structure schematically, with the black lines representing the GaAs quantum wells (active regions) separated by passive AlGaAs spacers. The spacer thickness is $\lambda/2$, where $\lambda(=\lambda_0/\mu)$ is the wavelength of room-temperature emission from the quantum wells propagating in the AlGaAs medium (i.e., λ_0 is the free-space wavelength corresponding to a selected transition in the GaAs quantum wells and μ is the AlGaAs index of refraction at this wavelength). In this geometry, the periodic MQW gain medium is aligned with the antinodes of the electric field of the standing-wave pattern set by the FP cavity. When the MQW period is matched to the emission wavelength, there is no possibility of longitudinal spatial hole burning because the gain medium coincides with the peaks of optical field. The spatial overlap integral between an optical field and the gain elements is enhanced in the vertical direction at a specific wavelength determined by the period of the gain medium, hence the gain in this structure is both anisotropic and wavelength selective which should favor single longitudinal mode operation. The usual spatial average over a squared sinusoidal function to determine the effective gain along the resonator axis does not apply to this structure, which results in a factor of two enhancement in gain coefficient compared to conventional SE lasers. Moreover, since there is no gain medium between the peaks of electric field of the lasing radiation, the ASE around the nodes of standing-wave pattern is eliminated which will result in higher external efficiency. This new design should then improve considerably the performance of SE lasers.

The particular structure used in our experiments consisted of 32 10-nm-thick GaAs quantum wells, separated by $Al_{0.25}Ga_{0.75}As$ spacers each 120 nm thick grown by molecular beam epitaxy. To account for the phase shift of reflected radiation the thickness of the end spacer was $\lambda/4$, with an Al coating deposited to enhance the reflectivity[7] to $R_1 \simeq 75\%$. The device was then epoxied Al-side down onto a glass slide and the GaAs substrate was removed by standard mechanical polishing and selective chemical etching techniques. A 20-period superlattice of alternating 2.5 nm AlAs/GaAs layers was not removed by this process. The output mirror of the vertical cavity was formed by the uncoated sample/air

[a] Also with the Department of Physics and Astronomy, University of New Mexico.
[b] Also with the Department of Electrical and Computer Engineering, University of New Mexico

 0003-6951/88/441678-03$01.00

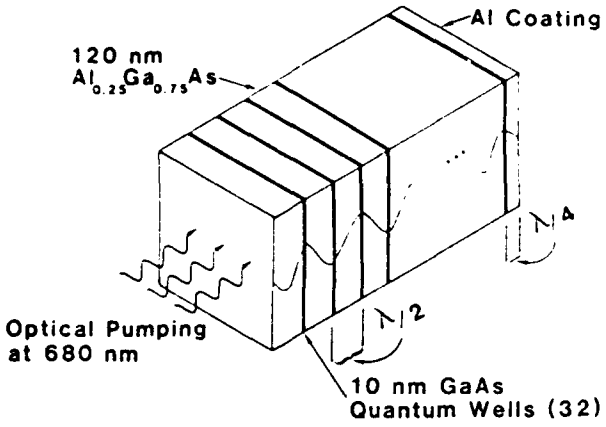

FIG. 1. Schematic diagram of surface-emitting MQW laser structure with wavelength-resonant periodic gain medium. Thick lines represent GaAs quantum wells. λ is the wavelength of GaAs quantum well emission propagating in the AlGaAs spacer medium.

interface, with $R_2 \simeq 30\%$. The total thickness of the processed structure was $\sim 4.32\ \mu$m as confirmed by the FP mode spacing observed in transmission spectra.

Figure 2 shows a room-temperature intensity-transmission spectrum of an uncoated sample (no Al reflector) for the region between $\lambda = 1000$ and 700 nm. Clear $n = 1$, 2, and 3 electron-hole excitonic features are exhibited at $\lambda = 858$, 815, and 762 nm, respectively. Also apparent are FP fringes whose separation can be used to estimate the thickness of the entire structure.

Optical pumping studies were carried out using a cw Ar-ion laser and a pulsed tunable dye laser pumped by a frequency-doubled Q-switched YAG laser, while a monochromator, cooled GaAs photomultiplier, and a computer-controlled data acquisition system were employed for detection.

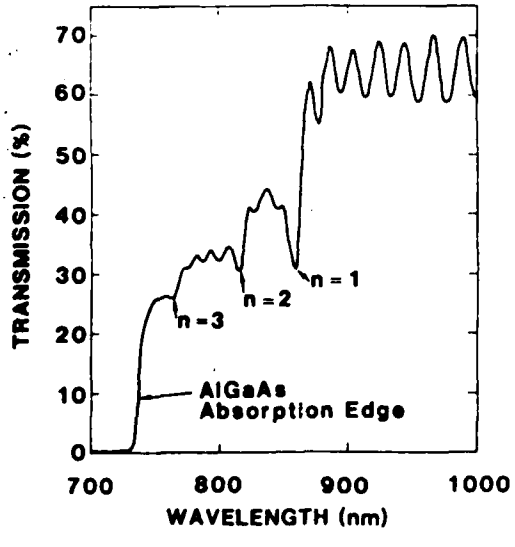

FIG. 2. Spectrophotometer scan of the laser structure bonded to a microscope slide, with the GaAs substrate removed. Electron-heavy hole excitonic features corresponding to allowed quantum states are indicated.

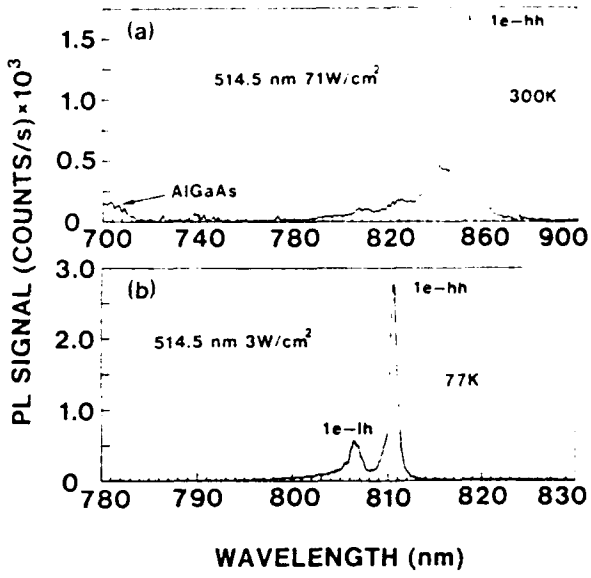

FIG. 3. Low-intensity cw photoluminescence from the SE laser structure using 514.5 nm Ar-ion laser excitation at (a) 300 K, 71 W/cm² and (b) 77 K, 3 W/cm². Heavy- and light-hole excitonic peaks are indicated.

Figure 3 shows cw photoluminescence (PL) data taken at room temperature and 77 K using an Ar-ion pump source at 514.5 nm which excited a few quantum wells near the surface of the sample. Prominent features of the room-temperature PL spectrum are $n = 1$, electron-heavy hole excitonic peak with superimposed FP modes. At 77 K, heavy-hole (1 e-hh) and light-hole (1 e-lh) peaks are clearly resolved. The width of the heavy-hole excitonic peak (1.8 meV at 77 K) agrees with the recent theoretical calculations.[8] The quality and uniformity of the structure is evidenced by the absence of any structure at the peak, even at 0.1 nm resolution. The splitting between heavy-hole and light-hole transitions is ~ 9.5 meV (5 nm), close to the predicted value based on the envelope function approximation.[9] The PL data obtained using a cw dye laser pump source at 710 nm, which excited all 32 quantum wells, showed a remarkable uniformity of the quantum wells without any noticeable broadening over the results shown in Fig. 3.

Lasing was achieved at 77 K and at room temperature when the device was pumped with 7 ns pulses at 10 Hz from a tunable dye laser operating at 680 nm. Figure 4 shows emission spectra at 300 K for increasing pump pulse energy, beginning just below the lasing threshold. The progression from broadband spontaneous PL to stimulated emission at $n = 2$ and $n = 3$ subband transitions is evident. The PL spectrum near the threshold is much broader than at low excitation levels as a result of band-filling effects. A sharp transition from broadband spontaneous PL to stimulated emission was observed at ~ 140 nJ pulse energy (corrected for reflection from the sample surface and the window losses). Since the pump pulse was focused into a $\sim 20\ \mu$m spot, the room-temperature threshold intensity was ~ 6 MW/cm². At 77 K lasing occurred at a comparable threshold energy, but the lasing transition involved $n = 1$ subbands whose wavelength at this temperature closely matches the periodicity of the gain medium.

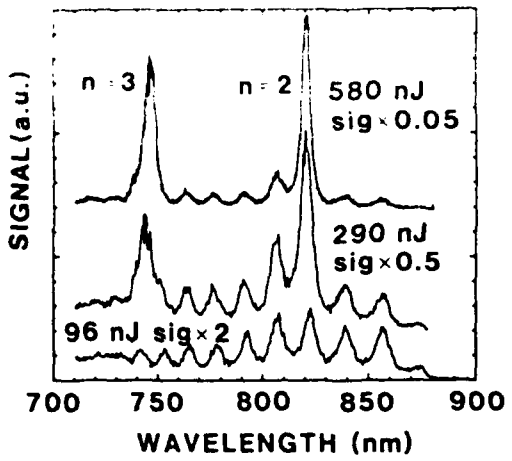

FIG. 4. Emission spectra of the SE laser structure pumped using 680 nm line of a pulsed dye laser (10 Hz with 7 ns pulse duration) at different pulse energies.

Further reduction in the threshold is possible by incorporating high-reflectivity stacks, possibly epitaxially grown at the same time as the gain medium[3,10] which will improve the cavity Q at the desired emission wavelength. This will also obviate the necessity for GaAs substrate removal and bonding to a supporting substrate.

As pointed out above, the alignment of the peaks of the optical standing-wave field with the half-wave-spaced quantum well gain media results in an optimal overlap integral between the lasing mode and the spatial gain distribution in the vertical direction and at the desired wavelength. The usual sine-square averaging in calculating the overlap between a standing wave and a uniform gain medium is therefore absent, and the effective gain is increased by a factor of 2. This is confirmed by a simple single-mode density-matrix calculation[11] for our structure.

It is important to recognize that the wavelength-resonant SE laser described in this letter is not a distributed feedback (DFB) structure.[12] Predominantly, this is because the quantum well gain regions are very thin relative to the optical wavelength. A straightforward calculation of the power reflectivity induced by each quantum well shows that the reflectivity is only $\sim 4\times 10^{-4}$, with main contribution due to gain rather than the real part of the refractive index. Thus the reflectivity is only 1.2% for all 32 wells and the cavity is dominated by the end mirrors and not by DFB effects. It is interesting to speculate on growing a similar structure composed of alternating $\lambda/4$ sections of AlGaAs. Such a structure would have unique quantum optical characteristics.

In summary, we have fabricated and demonstrated the operation of an optically pumped surface-emitting GaAs/AlGaAs laser with a vertical resonator. This laser features a series of GaAs quantum wells separated by half-wave AlGaAs spacers, with the resulting anisotropic and highly dispersive gain medium. Such a novel structure offers several potential advantages over comparable bulk devices, notably lower threshold, higher efficiency, reduced spontaneous emission, better spectral and power-handling capabilities. The total length of the active medium was only 320 nm, which to our knowledge is the shortest ever reported for any laser. Various means of reducing the room-temperature threshold of 6 MW/cm^2 for pumping at 680 nm are suggested. This structure also has potential applications as low-threshold high-speed optical bistable switching device and as a periodic gain medium for correlated spontaneous emission lasers.[13] We are in the process of fabricating similar structures with integrated high reflectors grown as epitaxial multilayers of AlAs and AlGaAs between the substrate and the SE laser structure. We are also investigating electrical pumping schemes for this novel surface-emitting laser.

We are grateful to Dr. W. Streifer, Spectra Diode Laboratories, for valuable comments. We also thank Professor M. O. Scully and Dr. M. S. Zubairy, Center for Advanced Studies, Department of Physics and Astronomy, University of New Mexico, for helpful discussions. This work was supported by the U. S. Air Force Office of Scientific Research.

[1] I. Melngailis, Appl. Phys. Lett. 6, 59 (1965).
[2] S. Kinoshita and K. Iga, IEEE J. Quantum Electron. QE-23, 882 (1987).
[3] P. L. Gourley and T. J. Drummond, Appl. Phys. Lett. 50, 1225 (1987).
[4] M. Ogura, W. Hsin, M. C. Wu, S. Wang, J. R. Whinnery, S. C. Wang, and J. J. Yang, Appl. Phys. Lett. 51, 1655 (1987).
[5] H. Matsueda, J. Lightwave Technol. LT-5, 1382 (1987).
[6] J. Nitta, Y. Koizumi, and K. Iga, *Technical Digest Conference on Lasers and Electro-Optics*, San Francisco, 9–13 June 1986 (Optical Society of America, Washington, DC, 1986), paper FO4, p. 382.
[7] H. A. Macleod, *Thin Film Optical Filters* (Adam Hilger, London, 1979), p. 74.
[8] D. A. Broido, E. S. Koteles, C. Jagannath, and J. Y. Chi, Phys. Rev. B 37, 2725 (1988).
[9] F. Laruelle and B. Etienne, Solid State Commun. 65, 565 (1988).
[10] M. Ogura, T. Hata, N. J. Kawai, and T. Yao, Jpn. J. Appl. Phys. 22, L112 (1983).
[11] See, for example, M. Sargent III, M. O. Scully, and W. E. Lamb, Jr., *Laser Physics* (Addison–Wesley, Reading, MA, 1974).
[12] H. Kogelnik and C. V. Shank, J. Appl. Phys. 43, 2327 (1972).
[13] J. Krause and M. O. Scully, Phys. Rev. A 36, 1771 (1987).

MOCVD GROWTH OF GaAs/AlGaAs WAVELENGTH RESONANT PERIODIC GAIN VERTICAL CAVITY SURFACE-EMITTING LASER

Indexing terms: Semiconductor lasers, Vapour deposition

The first all-semiconductor GaAs/AlGaAs vertical cavity laser incorporating wavelength resonant periodic gain layers grown by metalorganic chemical vapour deposition is reported. The optically pumped structure exhibits a threshold of 0·5 nJ at 852 nm for 720 nm pulsed excitation and energy conversion efficiencies up to ~6%. The output linewidth is ≤0·4 nm FWHM with single longitudinal mode oscillation. An output of 0·43 nJ (~60 mW) is demonstrated at 300 K.

Introduction: It has recently been reported[1,2] that a resonant periodic gain (RPG) medium is useful for reduction of threshold pump requirements in vertical cavity surface-emitting lasers (VCSELs). Previous reports[1,2] have been based on materials grown by molecular beam epitaxy (MBE). However, the use of metalorganic chemical vapour deposition (MOCVD) as a growth technique for these, and related structures,[3] is desirable owing to its characteristic accelerated growth rates and high-quality optical device materials. In this letter we describe a new laser structure grown by MOCVD which incorporates both distributed feedback (DFB) and the RPG medium to form the active region, while epitaxial multilayer reflectors (MLRs) provide cavity mirrors. The considerations for successful materials growth of VCSELs incorporating the RPG with DFB, as well as preliminary test results, are reported.

Design considerations: Several important considerations must be made. First, the periodicity of the RPG must match half the lasing wavelength λ_0 which, in turn, must match the gain of the $n = 1$ QW transition. Secondly, the MLRs must be designed such that the reflectivity peak aligns with λ_0. Thirdly, the phase of the optical standing wave, fixed by the optical thickness of the 159 MOCVD layers, must allow the amplitude peaks (antinodes) to spatially overlap the QWs of the RPG. These conditions place stringent demands on material uniformity and reproducibility. The optical thicknesses of the DFB and MLR layers should be $\frac{1}{4}\lambda_0$, where λ_0 must be within the tolerance of the gain spectra which is typically less than ±5 nm. This translates to a layer thickness tolerance of ±0·6%. Excessive deviation from this will result in unacceptably high thresholds due to gain mismatch. Also, the MOCVD material must be capable of providing QW heterostructures with high quantum efficiency, and smooth and abrupt interfaces. We use the periodic nature of the gain layers to provide additional DFB as shown in Fig. 1. The MLRs are designed to provide 99·7 and 99·95% reflectivity for the output coupler (right) and reflector (left), respectively. The centre layer of the RPG medium provides a $\frac{1}{4}\lambda$ thickness needed for aligning the optical standing wave to the RPG. This structure incorporates another unique feature important for both optical and electrical pumping applications. The larger Al mole fraction in the mirrors increases the bandgap by several kT at room temperature over that in the active region. This allows for a reduction in optical pump absorption

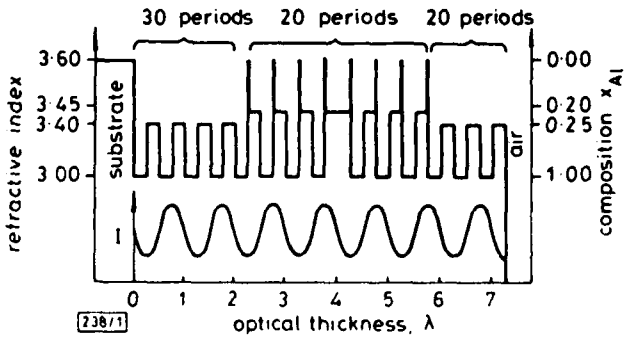

Fig. 1 *Illustration of RPG/DFB VCSEL*
Also shown is optical field intensity corresponding to cavity mode

in the mirrors, while maintaining active region pumping efficiency. Finally, for electrically pumped diodes, it will help confine injected carriers to the QWs and adjoining $Al_xGa_{1-x}As$ layers.

Material growth: Epitaxial layers were grown at 100 torr in a horizontal MOCVD reactor at 725°C in hydrogen. The carrier flow was 10 slm. Trimethylgallium (−10 ± 0·1°C) and trimethylaluminium (17 ± 0·1°C) from CVD Inc.* were used with arsine from Phoenix Research Inc.† as reactant sources. The metalorganic sources were maintained at 880 ± 3 torr independent of process pressure and monitored by capacitance manometers. The growth rate was 50 nm/min except in the QWs, where it was 40 nm/min. The V/III ratio was maintained at 50 (62·5 for QWs). A 20 s growth stop was incorporated into each interface in order to change flows. The reaction chamber was etched at 900°C in HCl vapour prior to each run. A rectangular flow channel and inclined susceptor was used to achieve thickness uniformities of ±2% over 90% of a 50 nm diameter substrate.

Characterisation: Materials were characterised using room-temperature photoluminescence at 5 kW/cm² HeNe laser excitation and IR reflectivity using a spectrophotometer. Optical pumping of the device structure was carried out using an experimental set-up which has been reported elsewhere.[1] The input pump energy takes into account loss due to the focussing optics and surface reflection. Conversion efficiency was determined using a calibrated Si photodiode.

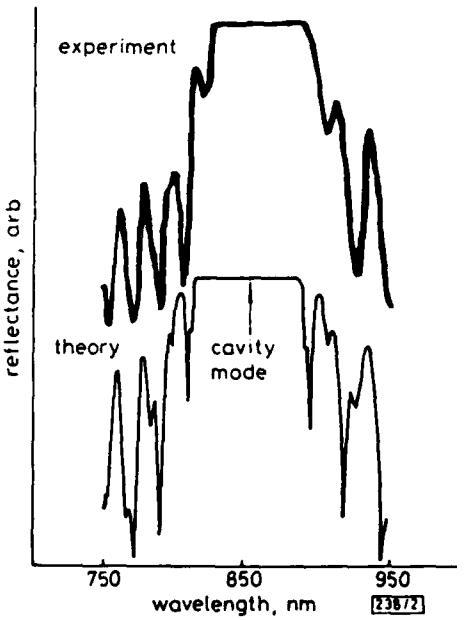

Fig. 2 *Experimental and theoretical curves for as-grown device structure*

Results and discussion: Careful calibration of the individual layer thicknesses consistently led to periodic structures with the reflectance peak centred at λ_0. The result is that 40–50% of the wafer area has a λ_0 which falls under the allowable gain spectra of the QWs. The final device structure has the reflectance spectrum shown in Fig. 2. The cavity mode is seen as a small dip in the theoretical reflectivity curve. The experimental curve shows good agreement with theory, with some loss in resolution. This is due to the 1 cm² measurement area, over which thickness nonuniformities of ±0·2% become significant. The lasing threshold for pulsed excitation was determined for various pump wavelengths as shown in Fig. 3. The threshold is the point at which a sharp peak (~0·4 nm FWHM) was observed to clearly dominate over the spontaneous emission background spectra. The pumping threshold attains a minimum value at 720 nm, which is between the bandgap energies of $Al_{0·20}Ga_{0·80}As$ and $Al_{0·25}Ga_{0·75}As$. This

* CVD Inc., Danvers, MA, USA
† Phoenix Research Inc., La Mesa, CA, USA

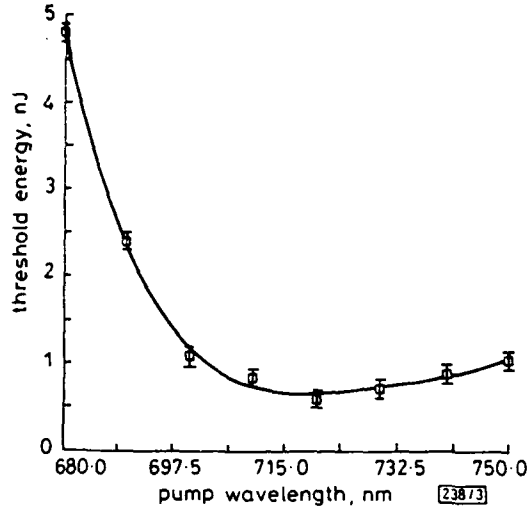

Fig. 3 *Threshold pump energy for different pump wavelengths*
MOCVD grown, RPG/DFB VCSEL; pulsed dye laser, 25 μm spot

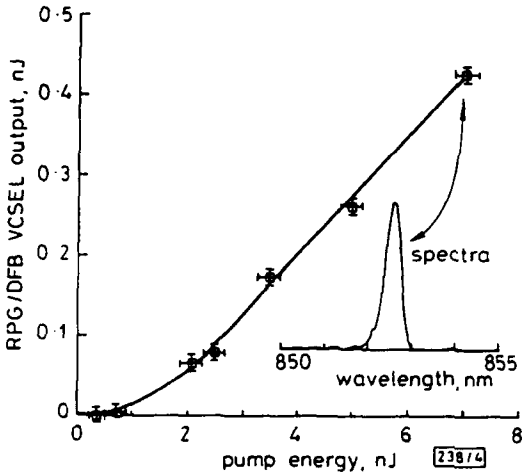

Fig. 4 *Optical energy output against input curve at 720 nm and spectral output above threshold*
MOCVD grown, RPG/DFB VCSEL

illustrates the effectiveness of the absorption in the RPG/DFB region where the MLR is transparent. At shorter wavelengths the pump radiation is absorbed in the MLR, while at longer wavelengths it is not absorbed efficiently by the RPG/DFB region.

Fig. 4 shows the output energy against input energy at 720 nm pump wavelength. The overall power conversion efficiency is ~6% at 0·43 nJ output power. The small loss of pumping efficiency due to absorption in the MLR and transmission through the RPG/DFB region has been taken into account. The laser linewidth did not broaden significantly with pump power. It is expected that both the efficiency and threshold will improve substantially, when transverse optical and carrier confinement is achieved and the spot size is reduced for injection pumped structures.

Conclusion: A novel GaAs/$Al_xGa_{1-x}As$ vertical cavity surface-emitting laser with resonant periodic gain combined with distributed feedback is demonstrated. The MOCVD growth process exhibits the high degree of control and reproducibility required for thickness and composition control to within less than 1% over ~45% of a 50 mm-diameter substrate. With a cumulative gain length of 200 nm and a pumping threshold of 0·5 nJ at 720 nm for a 25 μm spot, the device exhibits a single stable longitudinal mode output at 852 nm with a 0·4 nm FWHM, and conversion efficiencies up to ~6%. Further experiments are aimed at demonstrating 300 K CW operation of injection pumped devices.

Acknowledgment: We thank Min Juang and Kang Zheng for their help with the MOCVD crystal growth, and J. McInerney and M. Osiński for stimulating discussions. This work was partially supported by the Air Force Office of Scientific Research.

C. F. SCHAUS
H. E. SCHAUS
S. SUN
M. Y. A. RAJA
S. R. J. BRUECK

Center for High Technology Materials
University of New Mexico
Albuquerque, NM 87131, USA

19th January 1989

References

1 RAJA, M. Y. A., BRUECK, S. R. J., OSINSKI, M., SCHAUS, C. F., MCINERNEY, J. G., BRENNAN, T. M., and HAMMONS, B. E.: 'Surface-emitting, multiple quantum well GaAs/AlGaAs laser with wavelength-resonant periodic gain medium', *Appl. Phys. Lett.*, 1988, 53, pp. 1678–1680
2 CORZINE, S. W., GEELS, R. S., SCOTT, J. W., COLDREN, L. A., and GOURLEY, P. L.: 'Surface-emitting lasers with periodic gain'. Lasers & Electro-Optics Society annual meeting, Conf. Proc., 1988, Paper OE1.2, pp. 5–7
3 OGURA, M., HSIN, W., WU, M. C., WANG, S., WHINNERY, J. R., WANG, S. C., and YANG, J. J.: 'Surface-emitting laser diode with vertical GaAs/AlGaAs quarter-wavelength multilayers and lateral buried heterostructure', *Appl. Phys. Lett.*, 1987, 51, pp. 1655–1657
4 CASEY, H. C., and PANISH, M. B.: 'Heterostructure lasers, Part A: fundamental principles' (Academic, San Diego, 1978), p. 44

with each wavelength driven by 150mW of RF power, resulting in a conversion efficiency of ~70% per wavelength selected. Independent CW signals generated from five frequency synthesisers were used to select the five independent optical wavelengths simultaneously.

The filtered optical beam was then coupled back into a single-mode fibre for detection by a commercial transimpedance receiver (optimised at 2.4Gb/s baseband). The input and output optical spectra are shown in Fig. 2. The total fibre-to-fibre (single-mode) insertion loss of the IAOTF, including the 2dB insertion loss of the bulk polarisers, was 8.7dB.

Fig. 3 shows the worse-case power penalty, the eye pattern at a BER of 10^{-9}, and the RF spectrum of the detector output

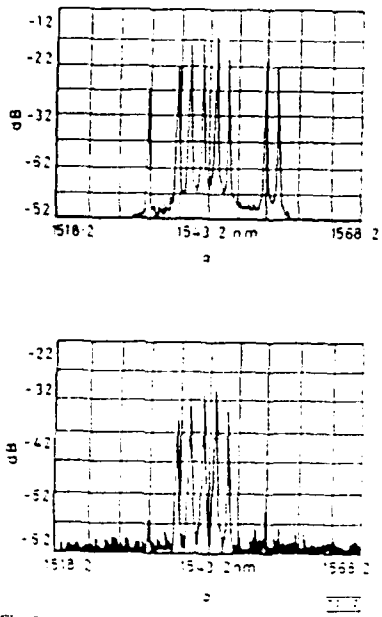

Fig. 2
a Input optical spectrum
b Output optical spectrum

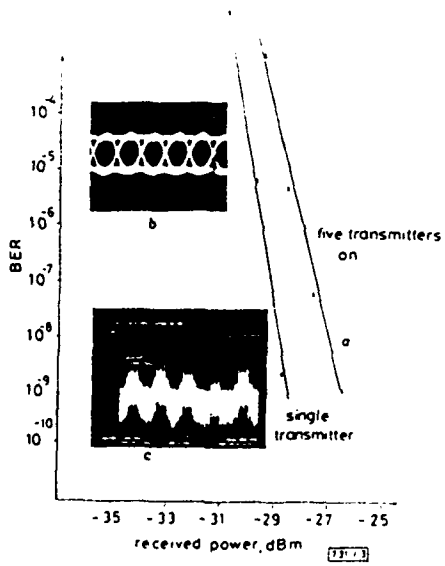

Fig. 3
a Worst case power penalty
b Eye pattern at BER = 10^{-9}
c RF spectrum of detector output

which contains all five subcarrier channels. The worse case power penalty corresponds to the 1.2GHz subcarrier channel of the 1.5422μm transmitter (the middle of the five selected wavelengths), and was measured to be 2.2dB. About 1dB of the penalty was accounted for by the coherent heterodyne effect[5,6] that arose from the five RF driving frequencies interacting with a single optical wave in the IAOTF. The rest of the penalty was probably due to the imperfections in the RF synthesiser chain that caused further coherent heterodyne degradation.

Conclusion: We have demonstrated simultaneous, independent, five-wavelength filtering using an integrated-optic acousto-optic tunable filter with a wavelength separation of 2.2nm. The worst-case power penalty due to the coherent heterodyne effect is less than 2.2dB at this wavelength separation, demonstrating the feasibility of dense multiple-wavelength operation.

K. W. CHEUNG
S. C. LIEW
C. N. LO
Bellcore
445 South Street, Morristown, NJ 07960-1910, USA

D. A. SMITH
J. E. BARAN
J. J. JOHNSON
Bell Communications Research
331 Newman Springs Road, Red Bank, NJ 07701, USA

28th March 1989

References

1 CHEUNG, K. W., LIEW, S. C., and LO, C.: 'Experimental demonstration of a multiwavelength optical network with microwave subcarriers', *Electron. Lett.*, 1989, 25, pp. 381–382
2 CHEUNG, K. W., SMITH, D. A., BARAN, J. E., and HEFFNER, B. L.: 'Multiple channel operation of an integrated acousto-optic tunable filter', OFC'89, paper ThB, Houston 1989
3 HEFFNER, B. L., SMITH, D. A., BARAN, J. E., YEVICK, A., and CHEUNG, K. W.: 'Improved acoustically-tunable optical filter on x-cut $LiNbO_3$', *Electron. Lett.*, 1988, 24, pp. 1562–1563
4 LIEW, S. C., and CHEUNG, K. W.: 'A broadband optical network based on hierarchical multiplexing of wavelengths and RF subcarriers'. To appear in ICC'89 Proceeding, Boston, Massachusetts, 1989
5 WAY, W. I., and CASTELLI, C.: 'Simultaneous transmission of 2Gbit/s digital data and ten FM-TV analogue signals over 16.5km SM fibre', *Electron. Lett.*, 1988, 24, pp. 611–613
6 CHOY, M. M., CHEUNG, K. W., SMITH, D. A., and BARAN, J. E.: 'Coherent crosstalk mechanism in multi-wavelength switching of an integrated acousto-optic tunable filter', CLEO'89, paper FG2, Baltimore, Maryland, 1989

HIGH-EFFICIENCY CW OPERATION OF MOCVD-GROWN GaAs/AlGaAs VERTICAL-CAVITY LASERS WITH RESONANT PERIODIC GAIN

Indexing terms: Semiconductor lasers, Refractive index profiles, Vapour deposition

A GaAs/AlGaAs vertical-cavity surface-emitting laser with resonant periodic gain has been grown by metal-organic chemical vapour deposition. The as-grown structure exhibits an optically pumped CW threshold below 15mW at 300K and a single-ended power efficiency up to 45%. Fundamental Gaussian and higher-order modes are observed with spectral widths (FWHM) as low as 0.27Å.

Introduction: Applications in optical communications, computing, solid-state laser pumping and high-power 2D arrays will benefit from the development of semiconductor lasers which emit normal to the wafer surface. Of the currently available approaches (grating coupling, turning mirrors and vertical cavities), the vertical cavity surface emitting laser (VCSEL)[1] places the most stringent demands on material quality. However, the benefits gained from VCSELs include

the potential for planar diode fabrication, stable single-mode oscillation, low-divergence circular output beam, very small area and simple extendability to 2D arrays. It has been proposed[2] and recently demonstrated[3-5] that a resonant periodic gain (RPG) medium is useful for reduction of threshold pump requirements in VCSELs. These reports have indicated that improved performance is obtained, but low efficiencies and high thresholds have precluded use in practical applications. Recently however, independent studies[6] have demonstrated RPG VCSELs by molecular beam epitaxy (MBE) which exhibit optically pumped, CW, room-temperature operation. In this letter, we describe growth by metal-organic chemical vapour deposition (MOCVD) and properties of an improved low-threshold, high-efficiency and narrow-linewidth optically pumped VCSEL which has operated CW at room temperature.

Experimental: The MOCVD apparatus used is of the conventional low-pressure horizontal design. The radial injection manifold is pressure-balanced with zero dead space design. The main and vent carrier flows are split equally between source channels at the injection values. The chamber is load-locked to atmosphere via a nitrogen-purged glove box. Computer control with 10 ms loop times allows precise timing of control parameters. Details of the growth parameters have been reported elsewhere.[4]

Materials were characterised by using room temperature photoluminescence at 5 kW/cm^2, HeNe-laser excitation and IR reflectivity. Lasing results were obtained with CW dye laser excitation (700–750 nm) focussed onto the wafer using a microscope objective which also served to collect the VCSEL laser radiation.[5] The wafer was mounted on a glass slide with double-sided tape. Power and efficiency measurements were made with a cross-calibrated power meter. Spectral measurements were performed using a 1 m double monochromator with resolution 0·1 Å. The input pump power takes into account attenuation owing to measured surface reflection, as well as the 15% calculated loss owing to absorption in the front mirror and transmission through the active region.

Design considerations: The RPG VCSEL structure refractive index and composition profile are shown in Fig. 1. The optical thickness of the multilayer reflector (MLR) layers are one-quarter of the lasing wavelength corresponding to the $n = 1$ quantum well transition. One-half wavelength spacing is used in the active region where 20 quantum wells are placed at the optical antinodes, also indicated in the Figure. In a previous report,[4] we had taken advantage of the periodic nature of the gain layers to provide additional distributed feedback (DFB) in the active RPG region. Although the design of Reference 4 provides stronger cavity feedback and should reduce the threshold, the active region forms a compound cavity with the MLRs. The result is that the mode of the active DFB region and the MLR cavity mode must be exactly coincident to realise the benefits of a DFB active region. This requires thickness tolerances better than ±0·05% between layers for the DFB and MLR regions. It is therefore preferable to reduce the effect of DFB in the RPG region to eliminate these cavity mode-matching requirements. In the present case of uniform active region barriers, the active region feedback, although significant, is much reduced. The MLRs on either side of the RPG are designed to provide reflectivities of 99·95% (30·5 periods on the GaAs substrate) and 99·7% (20 periods terminating in air) for the high-reflector and output coupler, respectively. The increased Al mole fraction in the mirrors (Fig. 1) reduces the optical pump absorption while maintaining active region pumping efficiency.

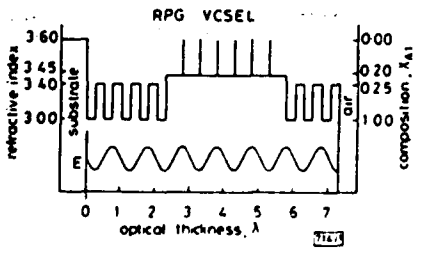

Fig. 1 *Illustration of epitaxial structure in which the number of periodic layers has been reduced to simplify interpretation*

Also shown is standing-wave electric field corresponding to resonant mode of gain medium

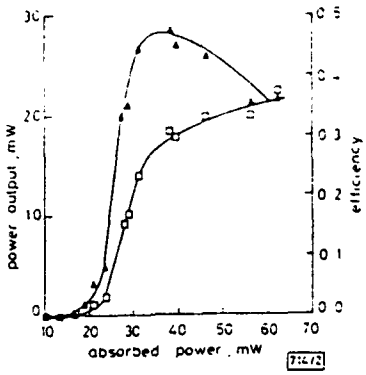

Fig. 2 *Optical power output against input for 739 nm CW excitation using 20 × pump focussing objective*

□ P_{in} ▲ E_{ff}

Results and discussion: The CW lasing threshold was determined for various pump wavelengths. The threshold attained a minimum value below 15 and 25 mW at 739 nm for 20× and 5× pump focussing objectives, respectively. At shorter wavelengths, the pump radiation is absorbed in the output coupler MLR and at longer wavelengths, it is absorbed less efficiently by the RPG region. Variations in the layer thicknesses over the substrate area were also observed to cause changes in threshold and shifts in the lasing wavelength.

Fig. 2 shows the output power against input power at 739 nm pump wavelength. The overall single-ended power conversion efficiency is ~45% at 18 mW output power. The dominant transverse mode output is observed to change as the pump power is increased, evolving from fundamental Gaussian to higher orders. Kinks are observed in the output power corresponding to these mode changes making it difficult to measure differential quantum efficiency. Heating is evident as the roll-over in the curve at higher powers. Typical output spectra are shown in Fig. 3, indicating the characteristic spectral broadening and red-shifting with increasing pump power. Uing 5× and 20× focussing objectives for the pump, the near-field FWHM is 26 and 7 μm, respectively. Both the near and far-field patterns follow fundamental Gaussian distributions at low pump powers, with near diffraction-limited beam divergences.

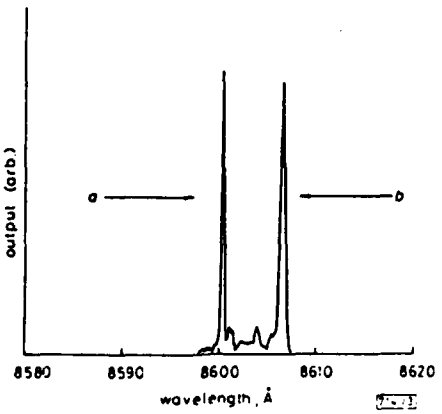

Fig. 3 *Spectral output for different pump powers at 739 nm, using 5 × pump focussing objective*

a FWHM 0·27 Å, 31·5 mW pump
b FWHM 0·35 Å, 42 mW pump

Conclusion: A GaAs A... emitting laser with resona... MOCVD. Optically pum... threshold pump power an... 15 mW and 0·27 Å, respect... ments in performance o... Our devices lase CW at ... powers of over 20 mW a... expected with heat-sinkin... the carriers and the optica...

Acknowledgments: We w... Kang Zheng at the Uni... their help with the MOC... Sandia National Laborat... MBE-grown device result... also at UNM, for help in... was partially supported by ... fic Research.

C. F. SCHAUS
M. Y. A. RAJA
J. G. McINERNEY
H. E. SCHAUS
S. SUN
M. MAHBOBZADEH
S. R. J. BRUECK

Center for High Technology M... University of New Mexico... Albuquerque, NM 87131, USA

References

1 IGA, K., KOYAMA, F., and K... ductor lasers', *IEEE J. Qu...*
2 RAJA, M. Y. A., BRUECK, S. R. J., BRENNAN, T. M., and ... resonant optoelectronic ... lasers', *Electron. Lett.*, 19...
3 CORZINE, S. W., GEELS, R. ... GOURLEY, P. L.: 'Surface-em... Ann. Meeting of IEEE L... Clara, Calif., Oct. 1988, pa...
4 SCHAUS, C. F., SCHAUS, H. ... S. R. J.: 'MOCVD growth ... periodic gain vertical cavi... 1989, 25, pp. 538–539
5 RAJA, M. Y. A., BRUECK, S. R. J., BRENNAN, T. M., and ... surface-emitting semicond... (Special issue on semicond...
6 GOURLEY, P. L., BRENNAN, ... GEELS, R. S., YAN, R. H., SC... efficiency TEM_{00} continuo... emitting lasers with half-w... 1989

Ka-BAND HIGH POW... HETEROSTRUCTURE...

Indexing terms: Semic... sistors, Field-effect tran...

A 0·25 μm gate-length... pseudomorphic heteros... and efficiency is rep... 658 mW with 3·2 dB p... ciency.

Introduction: Ka-Band G... have exhibited high outpu... amplifiers have demonstrate... with 3 dB gain and 11% p... output power at 34 GHz wi... Pseudomorphic high electr... have recently demonstrate... power normalised to gate w... rable FETs,[3] but the power...

Conclusion: A GaAs:$Al_xGa_{1-x}As$ vertical-cavity surface-emitting laser with resonant periodic gain has been grown by MOCVD. Optically pumped power conversion efficiency, threshold pump power and spectral linewidth values of 45%, 15 mW and 0.27 Å, respectively, represent substantial enhancements in performance over previously described structures. Our devices lase CW at room temperature delivering output powers of over 20 mW at 860 nm. Improved performance is expected with heat-sinking and lateral confinement of both the carriers and the optical mode.

Acknowledgments: We would like to thank Min Juang and Kang Zheng at the University of New Mexico (UNM) for their help with the MOCVD crystal growth, P. L. Gourley of Sandia National Laboratories for helpful discussions of his MBE-grown device results prior to publication, and L. Rose, also at UNM, for help in optical measurements. This work was partially supported by the US Air Force Office of Scientific Research.

C. F. SCHAUS
M. Y. A. RAJA
J. G. McINERNEY
H. E. SCHAUS
S. SUN
M. MAHBOBZADEH
S. R. J. BRUECK

Center for High Technology Materials
University of New Mexico
Albuquerque, NM 87131, USA

22nd March 1989

References

1 IGA, K., KOYAMA, F., and KINOSHITA, S.: 'Surface emitting semiconductor lasers', *IEEE J. Quantum Electron.*, 1988, 24, pp. 1845–1855
2 RAJA, M. Y. A., BRUECK, S. R. J., OSINSKI, M., SCHAUS, C. F., MCINERNEY, J. G., BRENNAN, T. M., and HAMMONS, B. E.: 'Novel wavelength-resonant optoelectronic and its application to surface emitting lasers', *Electron. Lett.*, 1988, 24, pp. 1140–1142
3 CORZINE, S. W., GEELS, R. S., SCOTT, J. W., COLDREN, L. A., and GOURLEY, P. L.: 'Surface-emitting lasers with periodic gain' Proc. Ann. Meeting of IEEE Lasers and Electro-Optics Society, Santa Clara, Calif., Oct. 1988, paper OE1.2, pp. 5–7
4 SCHAUS, C. F., SCHAUS, H. E., SUN, S., RAJA, M. Y. A., and BRUECK, S. R. J.: 'MOCVD growth of GaAs:AlGaAs wavelength resonant periodic gain vertical cavity surface-emitting laser', *Electron. Lett.*, 1989, 25, pp. 538–539
5 RAJA, M. Y. A., BRUECK, S. R. J., OSINSKI, M., SCHAUS, C. F., MCINERNEY, J. G., BRENNAN, T. M., and HAMMONS, B. E.: 'Resonant periodic gain surface-emitting semiconductor lasers', *IEEE J. Quantum Electron.* (Special issue on semiconductor lasers), to be published June 1989
6 GOURLEY, P. L., BRENNAN, T. M., HAMMONS, B. E., CORIZINE, S. W., GEELS, R. S., YAN, R. H., SCOTT, J. W., and COLDREN, L. A.: 'High efficiency TEM_{00} continuous-wave (Al, Ga)As epitaxial surface-emitting lasers with half-wave periodic gain', *Appl. Phys. Lett.*, 1989

Ka-BAND HIGH POWER PSEUDOMORPHIC HETEROSTRUCTURE FET

Indexing terms: Semiconductor devices and materials, Transistors, Field-effect transistors, Power semiconductor devices

A 0·25 μm gate-length, 900 μm gate width doped-channel, pseudomorphic heterostructure FET with high output power and efficiency is reported. At 35 GHz, output power is 658 mW with 3·2 dB power gain and 24% power-added efficiency.

Introduction: Ka-Band GaAs MESFET power transistors have exhibited high output powers: FET-based monolithic amplifiers have demonstrated 1·1 W output power at 28 GHz with 3 dB gain and 11% power-added efficiency,[1] and 0·6 W output power at 34 GHz with 2·8 dB gain and 9% efficiency.[2] Pseudomorphic high electron mobility transistors (HEMTs) have recently demonstrated higher power density (output power normalised to gate width) and efficiencies than comparable FETs,[3] but the power levels reported to date have been low (< 150 mW), limited by device gate width. In this letter, we present results for a large gate width, pseudomorphic, heterostructure FET (HFET). The device is denoted as an HFET, rather than a HEMT, since doping has been added to the GaInAs channel, thereby reducing the electron mobility.

Device description: The pseudomorphic HEMT, formed by adding a thin layer of GaInAs to the conventional AlGaAs:GaAs HEMT, provides improved RF power performance as a result of a larger conduction band discontinuity and the improved confinement afforded by the quantum well.[4] Recently, several workers have reported that the addition of doping within the GaInAs quantum well of a pseudomorphic HEMT can increase device transconductance and current density, and that the associated degradation in electron mobility does not adversely affect device performance since the saturated velocity, which is more important, remains unchanged.[5,6]

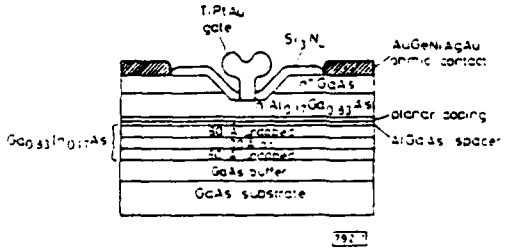

Fig. 1 *Cross-section of doped-channel pseudomorphic HFET*

A channel cross-section of the doped-channel pseudomorphic HFET used in this work is given in Fig. 1. A 30 Å-thick region in the centre of the 150 Å GaInAs layer has been doped at a concentration of $3·5 \times 10^{12}$ cm^{-2}. Additional carriers are provided by a layer of Si planar doping in the AlGaAs, separated from the GaInAs by a 45 Å-thick undoped AlGaAs spacer. The InAs mole fraction and the AlAs mole fraction in the modulation doped layer are both 15%. Hall measurements of this wafer at 300 K yielded electron mobility of 2800 cm^2 Vs and sheet density N_s of $3·5 \times 10^{12}$ cm^{-2}.

A 0·25 μm-long T-shaped cross-section gate is employed to obtain high gain with low series resistance. A low-resistance gate structure is essential in a large power transistor since it allows longer gate fingers, and hence ultimately higher output power. The 900 μm gate width HFET is shown in Fig. 2. The device consists of two cells, each containing six 75 μm gate fingers. The source electrodes are interconnected with plated air-bridges and source grounding is accomplished with via-holes etched through the 50 μm-thick substrate.

Performance: **The transistors display a maximum transconductance of 550 mS/mm and full-channel current of 800 mA/mm (measured at $V_{ds} = 2$ V, $V_{gs} = 1$ V). The power performance was measured at 35 GHz using a test fixture with E-field probe waveguide/microstrip transitions and microstrip**

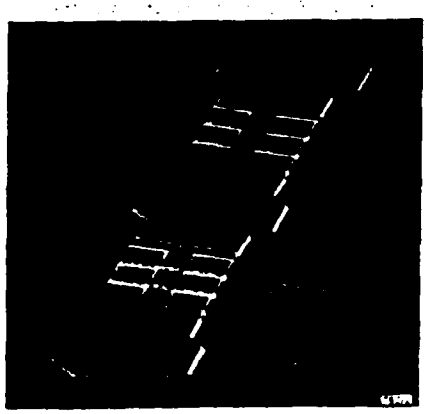

Fig. 2 *Power HFET with 0·25 μm × 900 μm gate*

Resonant Periodic Gain Surface-Emitting Semiconductor Lasers

MOHAMMAD YASIN A. RAJA, STEVEN R. J. BRUECK, MEMBER, IEEE, MAREK OSIŃSKI, SENIOR MEMBER, IEEE, CHRISTIAN F. SCHAUS, MEMBER, IEEE, JOHN G. McINERNEY, MEMBER, IEEE, THOMAS M. BRENNAN, AND B. EUGENE HAMMONS

Abstract—A novel surface-emitting semiconductor laser structure with a vertical cavity, extremely short gain medium length, and enhanced gain at a specific design wavelength is described. The active region consists of a series of quantum wells spaced at one half the wavelength of a particular optical transition in the quantum wells. This spatial periodicity allows the antinodes of the standing wave optical field to coincide with the gain elements, enhancing the frequency selectivity, increasing the gain in the vertical direction by a factor of two compared to a uniform medium or a nonresonant multiple quantum well, and substantially reducing amplified spontaneous emission. Optically pumped lasing was achieved in a GaAs/AlGaAs structure grown by molecular beam epitaxy, with the shortest gain medium (310 nm) ever reported. Various other optoelectronic devices which depend on the interaction between an electromagnetic standing wave and a carrier population distribution can also benefit from this concept.

I. Introduction

SEMICONDUCTOR lasers which emit from the top (epitaxial) surface [1]–[8] rather than from the end facets are of considerable interest for a variety of applications such as monolithic optoelectronic integrated circuits [9], optical chip-to-chip interconnects, optical logic devices [10], and high-power large-area two-dimensional arrays [11]. Progress in the development of these systems, however, has been impeded by the limitations of existing surface-emitting laser designs, particularly the high thresholds and low efficiencies of devices with vertical (normal to the chip plane) resonators, which are well suited for forming two-dimensional arrays. These problems are mostly due to short active-region lengths (typically $\sim 2\ \mu m$) compared to transverse dimensions, lack of carrier and optical confinement, and the generation of competitive amplified spontaneous emission (ASE) in the transverse direction. On the other hand, the short cavity lengths ($\sim 5\ \mu m$) of surface-emitting lasers result in large Fabry–Pérot mode spacings which favor single longitudinal mode operation of these devices.

Vertical cavity surface-emitting lasers developed so far have exhibited inferior performance as compared to conventional edge-emitting lasers. This has led to the introduction of alternative geometries whereby the active regions are configured in the same way as in edge-emitting lasers, but the radiation is directed towards the surface either by 45° mirrors [12], [13] or by second-order distributed Bragg reflectors [14]–[16]. While some of these designs have been successful in achieving low threshold, high efficiency, and large output power, their fabrication involves rather complicated processing. In contrast, the vertical-cavity surface emitters offer potentially higher packing density, larger emitting areas, better beam quality, unconstrained arrangement of emitters, and planar integration with easy batch processing and on-wafer probe testing.

In this paper, we describe implementation of the novel concept [17]–[19] of a vertical-cavity resonant periodic gain (RPG) surface-emitting laser with a uniquely engineered gain medium which affects the fundamental physical processes taking place in the device. This design creates an optimal overlap between the periodic gain medium and the standing wave optical field of the lasing mode. In conventional vertical-cavity surface-emitting lasers, the active medium is either uniform [3] or uses closely packed multiple quantum wells (MQW's) with no correlation between their periodicity (i.e., the quantum well spacing) and the optical standing wave [4]. The effective interaction length is therefore half of the total physical length of the gain medium, due to the averaged squared sinusoid in the overlap integral [19]. The RPG structure makes use of quantum wells with half-wave spatial periodicity, arranged within a Fabry–Pérot cavity so that the antinodes of the standing wave in the cavity coincide with the quantum-well regions. The result is an anisotropic and strongly wavelength-selective gain medium. The effective gain for

Manuscript received October 27, 1988; revised January 27, 1989. This work was supported in part by the U.S. Air Force Office of Scientific Research and by the National Science Foundation.

M. Y. A. Raja is with the Center for High Technology Materials and the Department of Physics and Astronomy, University of New Mexico, Albuquerque, NM 87131.

S. R. J. Brueck is with the Center for High Technology Materials, the Department of Electrical and Computer Engineering, and the Department of Physics and Astronomy, University of New Mexico, Albuquerque, NM 87131.

M. Osiński is with the Center for High Technology Materials, the Department of Electrical and Computer Engineering, and the Department of Physics and Astronomy, University of New Mexico, Albuquerque, NM 87131, on leave at the Research Center for Advanced Science and Technology, University of Tokyo, Meguro-ku, Tokyo 153, Japan.

C. F. Schaus and J. G. McInerney are with the Center for High Technology Materials and the Department of Electrical and Computer Engineering, University of New Mexico, Albuquerque, NM 87131.

T. M. Brennan and B. E. Hammons are with Sandia National Laboratories, Albuquerque, NM 87185.

IEEE Log Number 8927327.

0018-9197/89/0600-1500$01.00 © 1989 IEEE

the resonant mode is enhanced over that of other longitudinal modes, and ASE in the transverse direction is substantially reduced. Consequently, the lasing threshold should be lower and the overall power efficiency higher than in a conventional double-heterostructure (DH) or MQW gain medium of the same gain length. Our preliminary data for pulsed-dye-laser optical pumping at 77 and 300 K confirm these expectations.

In Section II, the concept of the RPG medium is described in some detail and its potential is examined for several optoelectronic device applications, with emphasis on vertical-cavity surface-emitting lasers. Fabrication of GaAs/GaAlAs vertical-cavity RPG lasers and of conventional structures used for comparative study is described in Section III. Section IV considers a combination of the RPG medium and a high-Q Fabry–Pérot resonator, with specific examples of structures described in Section III. Section V presents, interprets, and discusses various experimental results using our prototype devices. A comparison to conventional surface-emitting structures is given in Section VI. Finally, a summary and conclusions are presented in Section VII.

II. Device Concept

Many optoelectronic devices utilize interaction of a standing electromagnetic wave with an amplifying or absorbing semiconductor medium. This interaction is not spatially uniform, but is strongest at the antinodes of the standing-wave optical field and vanishes at the nulls. For example, if the medium is amplifying, the carriers located in the vicinity of the antinodes are depleted by the interaction, while excess carriers may accumulate around the nodes. This phenomenon was investigated in the early days of semiconductor lasers [20] as a possible cause for their multimode operation. Even though fast carrier diffusion restores spatial homogeneity, the gain of the medium is not fully utilized when single-frequency light is generated. To eliminate this problem, a new multilayer structure has been proposed [17]–[19] which maximizes the modal gain by confining the carriers to the antinode regions. In amplifying media, this will also reduce amplified spontaneous emission (ASE) due to carriers otherwise present near the nodes. This new design is particularly attractive for vertical-cavity surface-emitting lasers, leading to considerably improved performance. In particular, it should reduce the threshold and may well turn out to be an important step towards achieving the room-temperature CW operation of electrically pumped devices.

The most important feature of the new structure is that the position of the periodic quantum-well active regions is arranged such that they coincide with antinodes of a vertical standing wave pattern at the lasing wavelength. Fig. 1 illustrates the RPG structure schematically, with a series of localized gain regions separated by relatively thick passive spacers. The gain regions, represented by thick lines, consist of single quantum wells or groups of quantum wells kept very close together. The spacer thickness determines the resonant wavelength (λ_r in free space) at which the interaction of the optical field with the gain distribution is maximized. As indicated in Fig. 1, the thickness of each spacer (approximately $\lambda_r/2\mu_s$ where μ_s is the refractive index of the spacer material) is chosen such that the entire structure has an optical periodicity of $\lambda_r/2$. For a properly designed structure, λ_r should correspond to a particular transition in the quantum wells. In addition, the end reflectors of the cavity should be placed so that the antinodes of the optical standing-wave field coincide with the wells.

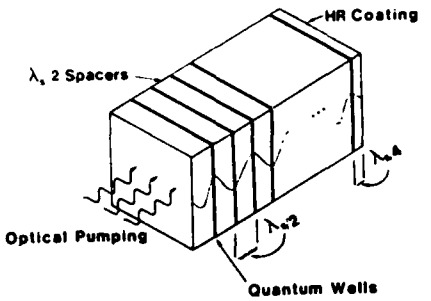

Fig. 1. Schematic diagram of a resonant periodic gain (RPG) structure designed to enhance the interaction between a standing-wave optical field and a charge carrier distribution. The thick lines represent localized gain regions (quantum wells), and $\lambda_r = \lambda_r/\mu_s$ is the resonant wavelength in the spacer medium.

The structure described above has several advantages. First, since the gain medium only exists at the peaks of the standing-wave optical field, the spatial overlap integral between the optical field and the gain elements is enhanced in the vertical direction (normal to the quantum-well planes) at the resonant wavelength determined by the spatial periodicity of the gain medium. Hence, the gain in this structure is both anisotropic and wavelength selective. Second, charge carriers generated or injected tend to remain within the quantum wells and cannot accumulate in the spacer regions, thus eliminating the possibility of longitudinal spatial hole burning. Combined with enhanced spectral discrimination, this should ensure stable single-frequency operation, provided that the transverse modes can be controlled, possibly by built-in index steps or by an external cavity. Moreover, loss of carriers through spontaneous emission is considerably reduced because the spacer medium around the nodes of the optical field contains no free carriers; this should result in a lower threshold and improved overall power efficiency.

The RPG laser structure also offers the possibility of increased differential quantum efficiency, especially for materials in which Auger effects or other nonradiative recombination processes are significant. Even though the carrier density in an ideal laser above threshold remains clamped at its threshold value, the presence of nonradiative effects which are superlinear in the radiative recombination rate will cause lower quantum efficiencies at higher carrier densities. The RPG structure permits lower threshold carrier densities, with correspondingly lower carrier loss (leakage and nonradiative recombination) rates.

In recent years, extensive use has been made of MQW semiconductor heterostructures for various optoelectronic

devices in which light propagates in a direction normal to the planes of the quantum wells [21]. The concept of a resonant periodic gain (or absorption) active medium can be applied to these devices, offering promises of improved performance. Promising candidates include amplifiers, modulators [22]-[25], wavelength- and phase-sensitive photodetectors [26], bistable etalons for low-threshold optical switching [27], saturable excitonic absorbers for mode-locking applications [28], self-electrooptic-effect devices (SEED's) [29], and nonlinear elements for wave mixing [30] and phase conjugation. In each case, the spatial overlap integral between the standing-wave optical field in the resonator and the MQW active medium is of primary interest, as it is this quantity which determines the effective interaction length and hence the threshold and overall efficiency of the device. It follows that optimization of this overlap integral at a specific design wavelength is extremely important.

The fundamental quantum optical effects of resonant periodic gain (or loss) structures are also interesting to contemplate. One fertile area of study is modification of spontaneous emission spectra in lasers and other high-power optoelectronic devices. For example, the RPG structure can be used as the amplifying medium for a correlated spontaneous emission laser [31]. It is also possible that the periodicity in the refractive index may inhibit spontaneous emission as well as suppress ASE. A tremendous reduction in the threshold of semiconductor lasers has been predicted as a result of inhibition of spontaneous emission [32] in artificially engineered structures with full three-dimensional half-wave periodicity in the refractive index of the active medium.

To illustrate the effect of the RPG structure on the interaction between a standing-wave electromagnetic field and the active medium, we consider a spatially inhomogeneous amplifying medium in a Fabry–Pérot cavity, noting that an analogous argument holds for an absorptive medium. Since the medium is nonuniform along the resonator (z) axis, the integrated gain factor $G(\lambda) = gL_{\text{eff}}$ (the product of the gain per unit length and the effective gain length) of the structure is given by

$$G(\lambda) = \int_0^L g(z) \sin^2\left(\frac{2\pi\mu(z)z}{\lambda}\right) dz \qquad (1)$$

where λ is the free-space wavelength of the standing wave optical field, L is the length of the cavity, and $g(z)$, $\mu(z)$ are the longitudinal profiles of the material gain per unit length and of the refractive index, respectively. For a uniform medium, the integral (1) gives $G(\lambda) = gL/2$, that is, only half of the available material gain is utilized. Consider now the periodic gain medium illustrated in Fig. 1, with single quantum wells separated by $D = \lambda_r/2\mu_s$ where μ_s is the refractive index of the spacer material (for simplicity, we ignore the phase shift in the quantum well). As shown in Fig. 2, $G(\lambda)$ has a resonance at λ_r which enhances the available gain. The discrimination against nonresonant wavelengths improves with increasing number of quantum-well layers, a situation analogous to the resolution of a grating being improved by illumination of a larger area which includes more grating periods. Away from the resonance, $G(\lambda)$ approaches the limit of $Mg_1L_z/2$, equal to the integrated gain in a uniform gain medium (M, g_1, and L_z are the number of quantum-well layers, gain, and thickness of each quantum well, respectively). At the resonant wavelength, however, the integrated gain coefficient $G(\lambda_r)$ is *enhanced by a factor of two* compared to a conventional medium of equal gain length.

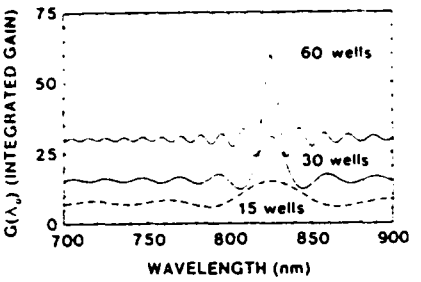

Fig. 2. Integrated relative gain spectrum $G(\lambda)$ of RPG media consisting of various numbers of single quantum wells separated by half-wave spacers, each designed for $\lambda_r = 825$ nm. $G(\lambda)$ is normalized so that gL_z, the gain coefficient for a single QW, is unity.

Apart from enhanced integrated gain, the proposed structure has additional appeal for surface-emitting lasers because the gain anisotropy reduces the ASE. As discussed above, the effective gain coefficient at the resonant wavelength in the vertical direction is twice as high as that in the transverse direction. It follows that the transverse ASE is reduced by a factor of two, so that the RPG laser has a reduced threshold and increased overall power efficiency compared to conventional structures with nonresonant gain media.

It is important to recognize that the RPG laser is not a distributed feedback (DFB) structure in the usual sense [2], [33] because the quantum-well gain regions are very thin relative to the optical wavelength. A straightforward calculation shows that the power reflectivity of each quantum well is only $\sim 4 \times 10^{-4}$, with the main contribution due to the gain rather than the real part of the refractive index. For structures such as those described in Section III below, with ~ 30 quantum wells separated by half-wave spacers, the detailed cavity calculations described in Section IV indicate some changes in the overall cavity resonance due to multiple reflections. However, these are small compared to strong DFB resonances.

III. Device Fabrication

All wafers were grown using a computer-controlled Varian Gen II molecular beam epitaxy (MBE) system, equipped with a reflection high-energy electron diffraction (RHEED) apparatus, a residual gas analyzer (RGA), an infrared pyrometer, and a 2-in rotating substrate holder. A transition chamber is situated between the introduction chamber and the MBE growth chamber which has a base pressure of 6×10^{-11} torr with the group III and dopant

sources idling at 700°C. Unintentionally doped GaAs grown in this system is routinely p-type with residual impurity concentrations of $\sim 2 \times 10^{14}$ cm^{-3}.

Polished (100) GaAs substrates were cleaned [34] and mounted with indium on a molybdenum holder. After evacuation to 1×10^{-8} torr in the introduction chamber, they were transferred into the transition chamber (which idles at 1×10^{-9} torr) where they were outgassed at 250°C for 1 h to remove any H_2O vapor. The samples were then transferred into the growth chamber after all fluxes had been established. Surface thermal oxides were desorbed at 580–600°C and the substrate was heated momentarily to approximately 700°C under sufficient arsenic flux to maintain a (2×4) surface reconstruction. Beam fluxes were adjusted with an ion gauge in the growth position to achieve growth rates of ~ 1 μm/h and ~ 3 μm/h for GaAs and AlAs, respectively, at substrate temperatures $T_s < 675$°C.

All aluminum-containing layers were grown at $T_s > 700$°C to increase photoluminescence efficiency and avoid the forbidden region of GaAs/AlGaAs structures [35]. Due to the nonunity sticking coefficient of gallium [36] at these temperatures, precise growth rates and Al incorporation were very difficult to control; hence, the thicknesses and group III compositions of the layers varied by a few percent. All samples grown in this study exhibited specular surface morphologies.

A. Prototype Structure

The initial sample was fabricated to determine growth parameters and assess the feasibility of the RPG surface-emitting laser design. The following unintentionally doped epitaxial layers (see Fig. 3) were grown on an n^+-GaAs (100) substrate:

1) a 500 nm GaAs buffer,

2) a short period superlattice consisting of 20 periods of alternating 2.5 nm GaAs/AlAs layers,

3) 32 periods of alternating half-wave (120 nm) $Al_{0.25}Ga_{0.75}As$ barriers and 10 nm GaAs quantum wells,

4) one quarter-wave (60 nm) AlGaAs layer to account for the phase shift of reflected light, and

5) a 5 nm GaAs cap.

The V/III flux ratios for these samples were typically 2.0–2.5.

A 300 nm thick Al film was deposited on the top spacer to enhance the surface reflectivity to $R_1 \approx 75$ percent [37]. The Al-coated side was glued to a glass slide for support, and the GaAs substrate was then removed by standard mechanical polishing and selective chemical etching. The output mirror of the vertical cavity was formed by the uncoated sample/air interface, with Fresnel reflectivity $R_2 \approx 30$ percent. The total thickness of the processed sample (and hence the resonant cavity length) was ~ 4.3 μm, while the total gain length was 320 nm.

B. Structures for Comparative Study

To enable a direct experimental comparison of the RPG laser to conventional DH and MQW surface-emitting

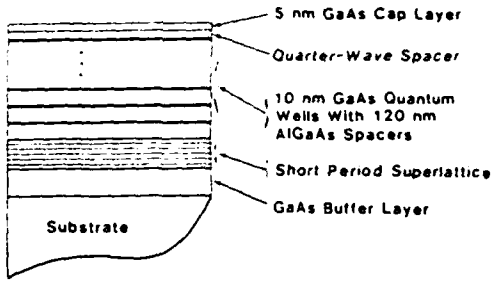

Fig. 3. Schematic diagram of a RPG laser wafer, which was grown on a GaAs substrate by MBE.

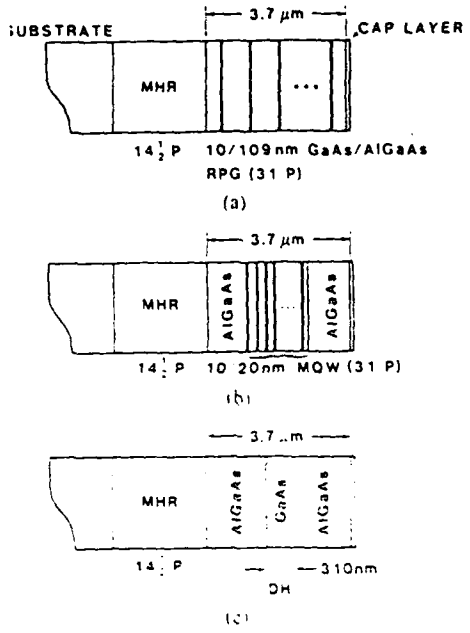

Fig. 4. Schematic diagram of three types of surface-emitting laser structures fabricated for comparative study: (a) RPG, (b) conventional MQW, (c) conventional DH. All three structures have equally long resonators (3.7 μm) and active media (310 nm). An epitaxial AlGaAs/AlAs multilayer high reflector (MHR) with 14½ periods is grown on each GaAs substrate.

structures, a second set of MBE-grown samples, shown schematically in Fig. 4, was prepared. Except for the configuration of the active medium (RPG, conventional MQW, and uniform DH), the samples were otherwise identical. All samples were grown on undoped LEC GaAs (100) substrates. The V/III flux ratios for these samples ranged from 2 to 4. To increase the cavity Q and simplify sample preparation, epitaxial multilayer high reflectors [4], [38] with 14½ periods of alternating quarter-wave layers of $Al_{0.4}Ga_{0.6}As$ (61.4 nm) and AlAs (68.8 nm) were incorporated between the GaAs substrate and each active structure. The RPG (a) and conventional MQW (b) structures each contained 31 GaAs quantum wells indicated by thick lines in Fig. 4. Each quantum well was 10 nm thick, while the half-wave $Al_{0.25}Ga_{0.75}As$ spacers in the RPG structure and the barriers in the MQW structure had thicknesses of 109 and 20 nm, respectively. The RPG active region was clad with a quarter wave (54.6 nm) of $Al_{0.25}Ga_{0.75}As$ on each side, while the conventional MQW was sandwiched between two 1.39 μm layers of $Al_{0.25}Ga_{0.75}As$. The DH sample (c) had a 310 nm bulk

GaAs active region surrounded by two 1.69 μm layers of $Al_{0.25}Ga_{0.75}As$. All three structures had equally long gain media ($\sim$310 nm) and resonant cavities ($\sim$3.7 μm). The top $Al_{0.25}Ga_{0.75}As$ layer in each sample was protected by a 5 nm GaAs cap. No reflective coating was deposited on the top surfaces; hence, the reflectivity of the emitting facet was $\sim$30 percent for each sample.

IV. Cavity Considerations

As in all lasers, proper cavity design is essential for low-threshold operation. This is particularly important for vertical-cavity surface-emitting lasers where the very short cavity length leads to widely spaced cavity resonances ($\sim$20 nm) which are comparable to the spectral width of the gain. The growth of an appropriate resonant structure is, of course, more complex for a quantum-well active medium where the spectral profile of the gain is a sensitive function of the quantum-well width. For an RPG laser, the situation is even more critical since two conditions must now be met simultaneously:

1) the overall cavity resonance must match the quantum-well gain peak, and

2) the half-wave spacers, the reflectors, and the phase shift layers at the ends must ensure that the antinodes of the standing-wave optical field match the position of the quantum wells.

If the phase shift layers are not properly matched to the cavity resonance closest in wavelength to the gain spectral peak, the effective gain will degrade rapidly. It is even possible that the quantum wells might be mistakenly located at the intensity nulls, resulting in nearly zero usable gain!

We start by presenting a simple technique for calculating cavity resonances and reflectivities, applicable to cavities with multilayer reflectors as well as simple metallic or dielectric overlayers. Next, this calculation is applied to the RPG laser with an Al end mirror for which experimental results are given in Section V. Finally, cavity calculations are presented for the three structures (RPG, conventional MQW, and DH, all with multilayer reflectors) compared experimentally in Section VI.

A. Method of Cavity Calculation

Many textbooks on thin-film optical filters present techniques for the calculation of complex reflectivities of multilayer dielectrics [37], [39], [40]. The approach used for the calculations presented here is simply to express the fields at each layer ($j+1$) in terms of the fields at the previous layer (j) and the optical phase shift Φ_j in traversing the jth layer:

$$\begin{pmatrix} E_{j+1}^{+} \\ E_{j+1}^{-} \end{pmatrix} = \frac{1}{2} \begin{pmatrix} \left[1 + \frac{\mu_j}{\mu_{j+1}}\right] e^{i\Phi_j} & \left[1 - \frac{\mu_j}{\mu_{j+1}}\right] e^{-i\Phi_j} \\ \left[1 - \frac{\mu_j}{\mu_{j+1}}\right] e^{i\Phi_j} & \left[1 + \frac{\mu_j}{\mu_{j+1}}\right] e^{-i\Phi_j} \end{pmatrix} \begin{pmatrix} E_j^{+} \\ E_j^{-} \end{pmatrix} \tag{2}$$

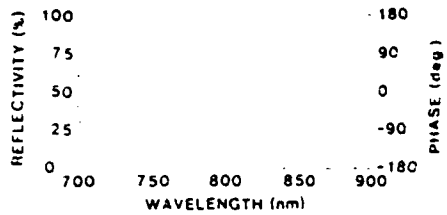

Fig. 5. Calculated power reflectivity and phase for a wave incident onto the short-period superlattice of the RPG structure of Fig. 3.

where μ_{j+1}, μ_j are the respective (complex) refractive indexes, E_{j+1}^{+} and E_j^{+} are the complex electric field amplitudes for waves propagating in the positive z direction (to the right for definiteness), and E_{j+1}^{-}, E_j^{-} are the field amplitudes for waves propagating in the opposite direction. The layers are numbered from the right to the left, with the fields defined at the rightmost edge of each layer. The total cavity reflectivity for waves incident from the left can then be evaluated by taking the boundary condition that there is only an outgoing wave in the medium beyond the right end of the cavity, and carrying out a straightforward series of matrix multiplications to evaluate the incident and reflected fields in terms of this outgoing wave.

A. Prototype RPG Cavity

Fig. 5 shows the result of this procedure for the prototype RPG structure evaluated with the short-period superlattice as the input side (cf. Fig. 3). The complex refractive index for the Al coating was taken as $\mu_{Al} = 2.75 + 8.31i$ [41]. No allowance for wavelength dispersion was made in any of these reflectivity calculations. The refractive index was taken as 3.64 for GaAs, 3.45 for $Al_{0.25}Ga_{0.75}As$, and 3.0 for AlAs. Actual indexes will, of course, vary due to wavelength and material variations, as well as due to the effects of gain and carrier densities in the pumped cavity. Nevertheless, these calculations provide valuable insights into the properties of the RPG structure when placed in a resonant cavity. Note that the calculated resonances are relatively broad. This is due to the poor cavity Q factors: the end reflectivities are 75 percent for the AlGaAs–Al reflector and 30 percent for the short-period superlattice–air interface, yielding a round-trip reflectivity product of only $\sim$23 percent. The variations in depth and width of the resonances are a manifestation of small distributed feedback effects, but these effects are relatively minor and do not strongly modify the cavity Q near the resonant wavelength of 820 nm.

C. Comparison to Conventional Cavities

Fig. 6 shows similar calculations for the three structures used for comparative study as described in Section III. The top trace (a) is for the RPG structure, the middle trace (b) for the conventional MQW, and the bottom trace (c) for the DH structure. The resonances are somewhat sharper than those in Fig. 5, as a result of the higher reflectivity of the multilayer reflector, but the cavity finesse remains low for all three structures. The variation in the two resonances near 825 nm for the RPG cavity is the

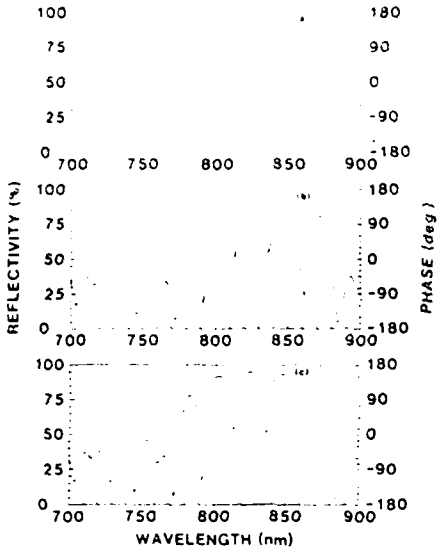

Fig. 6. Calculated power reflectivity and phase for three structures of Fig. 4. The incident wave is on the cap layer side.

result of small residual DFB effects. The RPG structure exhibits a dispersion-like behavior with anti-reflection features at higher frequencies and increased reflectivity below the resonance. Detailed analysis of the cavity and the gain medium under pumped conditions is necessary for optimal design of these complex multilayer devices.

V. Experimental Results

A. Transmission Spectra

Preparation of RPG samples for measurements of transmission spectra using a spectrophotometer required that the GaAs substrate be removed. The bare samples (with no Al reflector) were bonded to supporting glass slides using cyanoacrylate adhesive. Fig. 7 shows a typical room-temperature intensity transmission spectrum between $\lambda = 700$ and 1000 nm. Three strong transitions appear at $\lambda = 858$, 815 and 762 nm, respectively, which we assign to the excitonic absorption (electron–heavy hole) associated with the $n = 1$, 2, and 3 subbands in 10 nm thick GaAs quantum wells [42]. The arrows near the top of Fig. 7 indicate photon energies for electron–heavy hole transitions calculated using the envelope function approximation [43] including nonparabolicity effects. Within the excitonic binding energies (estimated as -8 meV for $n = 1$ [44] and decreasing as $1/n^2$ for higher levels), the excitonic features in the transmission spectra agree well with the calculations. The nonparabolicity is included via the energy-dependent effective masses which for the quantum well are expressed as [45]

$$m_{w\alpha}(E) = m_{w\alpha}(0)(1 + E/E_{gw}) \qquad (3)$$

and which for the spacer material are given by

$$m_{s\alpha}(E) = m_{w\alpha}(0)\left[1 - (\Delta E_\alpha - E)/E_{gs}\right]. \qquad (4)$$

The subscript α represents conduction, heavy hole, or light hole band. $m_{w\alpha}(0)$ and $m_{s\alpha}(0)$ are the bulk effective masses at the corresponding band edges. E_{gw} and E_{gs} are

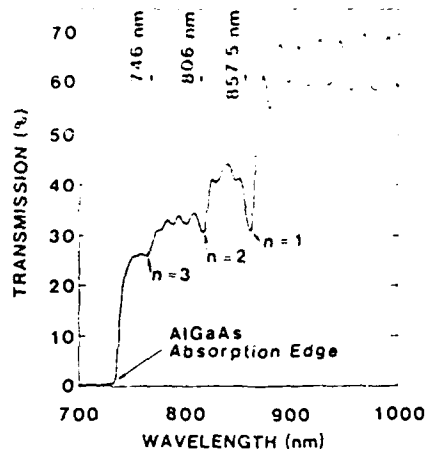

Fig. 7. Room-temperature spectrophotometer scan of the RPG laser structure bonded to a microscope slide, with the GaAs substrate removed. Electron–heavy hole excitonic features corresponding to allowed quantum states are indicated.

the bandgaps of the quantum well and spacer materials, respectively, and ΔE_α is the height of the potential barrier for band α. Various parameters used in the calculations are given in Table I. The total bandgap discontinuity between GaAs and $Al_xGa_{1-x}As$ at room temperature has been determined from the following expression [48]:

$$\Delta E_g = 1.155x - 0.37x^2 \qquad (5)$$

which for $x = 25$ percent gives $\Delta E_g = 312$ meV. The ratio of conduction to valence band offsets was taken as 65:35 [49], [50]; hence, $\Delta E_c = 202$ meV and $\Delta E_v = 110$ meV. For the AlGaAs composition and well width used in the structure, three bound states are allowed for electrons in the conduction band, five states for heavy holes in the valence band, and two states are allowed for light holes (see Table II). It should be noted that it is necessary to account for the nonparabolicity effects in order to predict the existence of the $n = 3$ bound state in the conduction band. For detailed analysis of the experimental data, we have adjusted the quantum-well thickness to obtain the best fit. The result of 10.5 nm agrees well with the crystal growth calibration of 10 nm.

A sharp decrease in transmission near 735 nm in Fig. 7 marks the onset of absorption by $Al_{0.25}Ga_{0.75}As$. Also apparent at long wavelengths are Fabry–Pérot fringes whose separation can be used to estimate the thickness of the entire structure. The observed separation of ~ 18 nm gives a cavity length of ~ 4.3 μm, in agreement with the growth parameters (cf. Section III-A).

B. Photoluminescence Spectra

Optical pumping studies of various coated (Al on one side) and uncoated samples were carried out using a CW Ar^+ laser, an Ar^+-pumped CW dye laser, and a pulsed tunable dye laser (10 Hz repetition rate, 7 ns pulsewidth) pumped by a frequency-doubled Q-switched Nd:YAG laser. The dye lasers (with LDS698 dye dissolved in ethylene glycol) were tunable from ~ 670 to ~ 750 nm. A 1 m double monochromator was used for spectral analysis.

TABLE I
PARAMETERS USED IN CALCULATIONS OF QUANTUM-WELL ENERGY LEVELS

Parameter	Quantum-Well Material (GaAs)	Spacer Material ($Al_{0.25}Ga_{0.75}As$)	Reference
Electron mass	$0.067m_0$	$0.088m_0$	[45]
Heavy hole mass	$0.48m_0$	$0.56m_0$	[45]
Light hole mass	$0.094m_0$	$0.108m_0$	[46]
Bandgap at 300 K	1.45 eV	1.78 eV	

TABLE II
CALCULATED ENERGY LEVELS (IN meV) FOR 10.5 nm THICK $GaAs/Al_{0.25}Ga_{0.75}As$ QUANTUM WELL

Energy Level	Electrons	Heavy Holes	Light Holes
$n = 1$	27	5	17.5
$n = 2$	102	20	68
$n = 3$	196	43.5	—
$n = 4$	—	74.5	—
$n = 5$	—	108.5	—

while a cooled GaAs photomultiplier and a computer-controlled data acquisition system were employed for detection. The experiments were performed using a wide range of excitation intensities both at room temperature and at 77 K. The diameter of the pumped spot (~ 20 μm) was determined by scanning the beam through a narrow slit. All values of pump intensities and pump pulse energies given in this paper are corrected for coupling losses and reflections from the sample surface.

Fig. 8 displays CW photoluminescence (PL) data from the RPG laser structure under low-intensity excitation at room temperature. The PL response to irradiation by the 514.5 nm line of the Ar^+ laser is shown in Fig. 8(a). The absorption coefficient of the spacer material at this wavelength is estimated from GaAs data [51] shifted by ΔE_g as 5 μm^{-1}, giving a penetration depth of 200 nm. Thus, only a few quantum wells near the surface of the sample were excited. The whole structure (all 32 quantum wells) could be excited uniformly with a 710 nm dye laser pump since the absorption coefficient of $Al_{0.25}Ga_{0.75}As$ at this wavelength is ~ 0.9 μm^{-1} (penetration depth of ~ 1.1 μm), as estimated from GaAs data [52]. The corresponding PL spectrum is shown in Fig. 8(b), with the pump intensities indicated in the figure. A prominent feature of each PL spectrum is a strong excitonic peak at 852 nm corresponding to the $n = 1$ electron–heavy hole transition in the 10 nm thick GaAs quantum wells. On the short wavelength side, the spectrum shows emission from light hole excitons as well as small contributions from higher energy levels. The results obtained using CW dye laser excitation at 710 nm [Fig. 8(b)] are almost identical to those shown in Fig. 8(a), without any noticeable broadening of the PL peak. This demonstrates the high quality and remarkable uniformity of the quantum wells, also evidenced by the absence of any structure at the peak, even at 0.1 nm resolution.

We have also used similar low-intensity excitation at 77 K to study excitonic parameters such as the transition

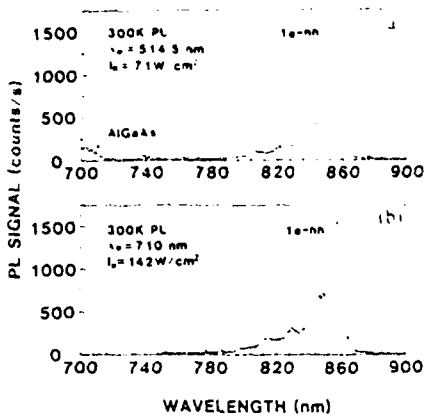

Fig. 8. Room-temperature low-intensity CW PL spectra from the RPG laser structure. (a) 514.5 nm Ar^+ laser excitation. (b) 710 nm dye laser pump. The pump intensities I_p, corrected for coupling losses, are indicated on the plots.

linewidth and the splitting between heavy and light hole excitons [53]. The heavy hole and light hole peaks associated with $n = 1$ subbands were clearly resolved at 77 K. The width of the heavy hole excitonic peak (1.8 meV at 77 K) agrees with recent theoretical calculations [54]. The splitting between the heavy hole and light hole transitions is ~ 9.5 meV (5 nm), close to the predicted value based on the envelope function approximation [43].

Fig. 9 shows representative room-temperature emission data from the RPG structure obtained with a CW dye laser pump operating at ~ 710 nm. The pump intensities in Fig. 9(a), (b) are ~ 10 and ~ 76 kW/cm^2, respectively. Compared to Fig. 8, band filling effects (PL extending further towards the shorter wavelength side) are evident. The modulation of the PL spectra is due to the modes of the Fabry–Pérot cavity formed by the Al-coated surface and the uncoated GaAs/air interface. Due to the short gain length and low cavity Q, the lasing threshold was quite high and these intensities were still considerably below threshold.

C. Lasing Action

Lasing at both room temperature and 77 K was achieved [18] when the device was pumped with 7 ns dye laser pulses at a 10 Hz repetition rate. For uniform pumping of the whole structure, the dye laser was tuned to ~ 680 nm wavelength (penetration depth in $Al_{0.25}Ga_{0.75}As$ estimated as ~ 0.8 μm [51]). Fig. 10 shows a series of emission spectra at 300 K for increasing pump pulse energy, beginning just below the lasing threshold. The pump energies are indicated directly in the figure. The progression from broad-band spontaneous PL to stimulated emission at the $n = 2$ and $n = 3$ subband transitions is evident. The subbands were identified by comparing to the transmission spectrum of Fig. 7. Emission around 820 nm ($n = 2$) corresponds to the resonant wavelength selected in the design of the structure. Emission at ~ 745 nm is attributed to the higher density of states at the $n = 3$ subband transition, resulting in higher material gain at large carrier densities. In fact, in a conventional quantum-well

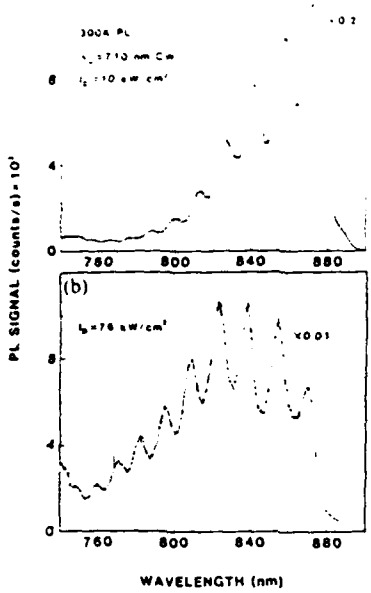

Fig. 9. Room-temperature emission spectra of RPG laser structure optically excited by a CW dye laser at 710 nm using two different pump beam intensities. (a) I_p = 10 kW/cm². (b) I_p = 76 kW/cm².

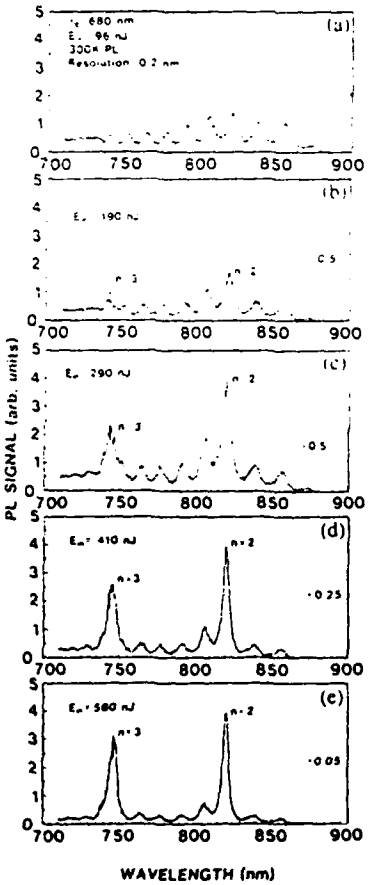

Fig. 10. Room-temperature emission spectra of the RPG laser structure pumped using the 680 nm line of a pulsed dye laser (10 Hz repetition rate, 7 ns pulse duration) at different pulse energies.

medium, the $n = 3$ transition would dominate over $n = 2$. A transition from broad-band spontaneous PL to stimulated emission was observed at ~140 nJ pulse energy. Since the pump pulse was focused into a ~20 μm spot, the room-temperature lasing threshold intensity was ~6 MW/cm². While lasing at 77 K was achieved at a comparable threshold pulse energy, it occurred at 830 nm, corresponding to the transition involving the $n = 1$ subbands [53]. Due to the temperature dependence of the bandgap, the wavelength of the $n = 1$ transition at 77 K more closely matches the periodicity of the gain medium.

Fig. 11 shows the integrated output of the $n = 2$ and $n = 3$ subband transitions in the RPG laser as a function of pump energy. The observed behavior—increased quantum efficiency and narrowed spectral width (cf. Fig. 10)—suggests lasing, albeit marginally in a very poor cavity. The threshold transition is not abrupt because of the short gain length and low cavity Q; the spontaneous emission coupling to the lasing mode(s) is relatively high, and the gain is close to saturating the $n = 2$ subband transition, so that it depends sublinearly on the pump power. Similarly "soft" thresholds and broad spectral linewidths were observed in the vertical-cavity surface-emitting structures developed by Kinoshita and Iga [3] and by Ogura *et al.* [5].

We have thus demonstrated a semiconductor laser with an active medium length of only 320 nm. Previously, the shortest reported gain length was 1.5 μm for a conventional MQW active region and a much higher cavity Q [4]. Significant improvements in the lasing properties of these structures are expected when high-Q cavities are used.

D. RPG Laser Threshold

The threshold optical pump power P_{th} for a vertical-cavity RPG laser can be estimated using the formula given in [8] modified for optical pumping:

$$P_{th} = \frac{\hbar\omega B d}{\eta a^2}\left\{\alpha_a + b + \alpha_s(L-d)/d' + \alpha_d(L/d') + (1/d')\ln\left[(R_1R_2)^{-1/2}\right]\right\}^2 \quad (6)$$

where $\hbar\omega$ is the photon energy at the pump wavelength, B is the effective recombination constant, η is the efficiency of carrier photogeneration, a and b are the linear gain coefficients ($g = aN - b$ where N is the carrier concentration), and L is the cavity length. $d' = G(\lambda)/g$ is the effective gain length; it equals twice the physical length d of the gain medium for an RPG laser ($2ML_z$ with M quantum wells, each of width L_z), but only equals the gain length d for uniform DH or nonresonant MQW structures. R_1 and R_2 are the power reflectivities of the two laser facets, α_a and α_s are the respective free-carrier losses per unit length in the gain regions and spacers, and α_d is the diffraction loss. Note that the effective internal loss in the quantum wells will also be enhanced by a factor of two due to the periodicity of the structure, although this will not be significant in short cavities whose losses are dominated by emission from the ends. Equation (6) applies when the pumped spot diameter is large compared to the electron diffusion length. The cavity parameters appropriate to our initial experiment are d = 320 nm, L =

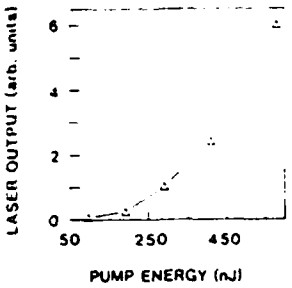

Fig. 11. Total output power versus pump energy for the same conditions as in Fig. 10.

4.32 μm, $R_1 = 0.75$, and $R_2 = 0.3$. The pump wavelength used for threshold evaluation is 680 nm, and η is assumed to be 1. The values of the remaining parameters in (6) relevant for the quantum-well active region are $B = 1.5 \times 10^{-10}$ cm^3/s [55], $a = 9.3 \times 10^{-16}$ cm^2, $b = 1500$ cm^{-1} [56], and $\alpha_a = \alpha_s = \alpha_d = 10$ cm^{-1} [8]. Because of the high carrier densities involved in our experiments, these values should be regarded only as crude order-of-magnitude estimates. In particular, the linear gain coefficient a is not a constant, but rather a decreasing function of pump intensity and carrier concentration for high pumping levels. With this caveat, (6) predicts a threshold of ~ 1 MW/cm^2 for the RPG structure, while the value for a conventional surface-emitting laser with a nonresonant MQW active region is a factor of three or so higher.

Further improvement is possible by incorporating high-reflectivity epitaxial stacks on both sides of the gain medium [4], [38], [57]. This will increase the cavity Q at the desired emission wavelength and will also obviate the necessity for GaAs substrate removal and bonding to a supporting substrate. A large reduction in threshold, down to ~ 10 kW/cm^2, is predicted by (6) when the reflectivities at both ends of the cavity are increased to 95 percent.

E. Linewidth of the RPG Laser

Fig. 10(a)-(e) show noticeable reduction in the spectral widths of the $n = 2$ and $n = 3$ subband transitions as the device is driven above threshold at ~ 200 nJ pulse energy. These widths are still rather broad, from ~ 10 nm in Fig. 10(b) to ~ 3 nm in Fig. 10(e); because of the short gain length and low cavity Q in our prototype samples, the spontaneous emission coupling to the lasing mode(s) is relatively high. Moreover, we estimate that the threshold gain is quite close to the maximum available from the $n = 2$ subband transition, so that this prototype device is operating in a saturated regime, in which the gain varies sublinearly with pump power. Also, the Fresnel number $\mu a^2/L\lambda$ (where a is the active spot size (~ 20 μm), μ is the refractive index, L is the cavity length (~ 4 μm), and λ is the free-space wavelength) is about three orders of magnitude larger than for a conventional edge-emitting laser. This large Fresnel number implies low diffraction losses from the cavity, even for very high-order transverse modes. Hence, the structure can support many transverse modes [58], possibly including some which are of a filamentary nature. All these factors contribute to the broad linewidth and soft threshold (Fig. 11), so that these lasers resemble superluminescent sources when operated close to threshold, especially when pulsed. Similarly broad linewidths and soft thresholds have been reported by Kinoshita and Iga [3] and by Ogura *et al.* [5]. Recent reports by Sakaguchi *et al.* [57], and preliminary results obtained in our laboratories using improved structures with multilayer high reflectors, indicate that increasing the cavity Q, reducing the Fresnel number, and incorporating lateral index steps should reduce the threshold and the spectral width by at least two orders of magnitude.

VI. Comparison to Conventional Surface-Emitting Laser Structures

To assess the efficacy of the RPG medium, we performed experiments similar to those described in Section V, using three sets of structures of equal gain length, as shown in Fig. 4. The refractive index profiles of the structures used in this comparative study are shown in Fig. 12. The peak reflectivity and bandwidth of the multilayer high reflector are estimated [37] as ~ 84 percent and 60 nm, respectively. Such a broad-band reflector can accommodate fluctuations in the designed resonant wavelength. However, the phase of the reflected wave remains crucial for the RPG structure to be effective since we require that the spatial location of the quantum wells be aligned with the peaks of the standing-wave optical field.

Approximately 5×10 mm^2 pieces were cleaved from the wafers of each structure for optical pumping. Because of the multilayer high reflector between the substrate and the active structure, the samples did not require any additional processing for substrate removal. Optical pumping experiments were carried out in a similar way to those described in Section V above.

Fig. 13 shows the low-intensity CW PL data for all three samples pumped with equal intensity ($I_p = 475$ W/cm^2) by 514.5 nm light from an Ar$^+$ laser. Although only a few quantum wells near the surface were sampled, there is evidence of nonuniformity for both the conventional MQW and the RPG structures. The somewhat broader peaks compared to Fig. 8 indicate fluctuations in the quantum well thickness; also, the $n = 1$ peaks in both samples are shifted by ~ 6 nm with respect to each other. The relative PL signal strength under identical pump conditions is small for the conventional MQW and DH structures, mostly because the active region in each case is buried deeper in the AlGaAs than in the RPG structure (cf. Fig. 4). The undulation of the spectra in Fig. 13 is due to the Fabry-Pérot modes of the short cavity (~ 3.7 μm) formed by the multilayer high reflector and the $Al_{0.25}Ga_{0.75}As$/air interface.

Fig. 14 shows relative PL data obtained under intense optical pumping of all three structures using 7 ns pulses at 680 nm pump wavelength. The PL spectrum from the conventional DH structure was obtained with ~ 1020 nJ pulse energy focused by a $5\times$ microscope objective to a spot of ~ 20 μm diameter. To obtain the PL spectrum of the conventional MQW, pump pulses of ~ 1440 nJ were

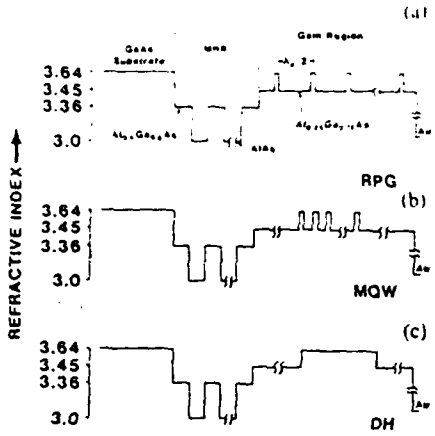

Fig. 12. Refractive index profiles of the three types of surface-emitting laser structures illustrated in Fig. 4: (a) RPG, (b) conventional MQW, (c) conventional DH.

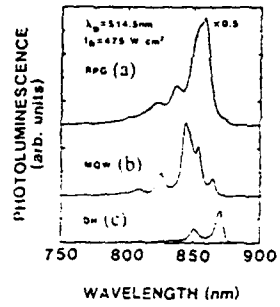

Fig. 13. Comparison of room-temperature low-intensity CW PL spectra from various surface-emitting laser structures (see Fig. 4) excited by a 514.5 nm Ar^+ laser pump at 475 W/cm^2: (a) RPG, (b) conventional MQW, (c) conventional DH.

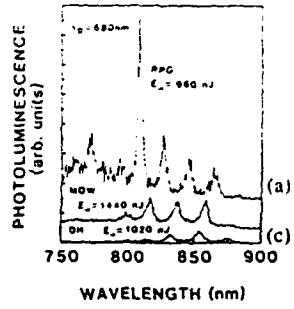

Fig. 14. High-intensity PL spectra from the three structures of Fig. 4: (a) RPG, with a pump energy of 960 nJ/pulse; (b) conventional MQW, with 1440 nJ/pulse; (c) conventional DH, with 1020 nJ/pulse.

used. Despite such intense optical pumping (46–65 MW/cm^2), no lasing action was observed either in DH or conventional MQW structures. These devices did not lase even at pump intensities up to the damage threshold ($\sim$70–100 MW/cm^2).

In contrast to these negative results, the RPG structure did lase on the $n = 2$ transition (805–810 nm) at pump intensities of $\sim$10–15 MW/cm^2 [Fig. 14(a)]. This relatively high threshold can be attributed to the nonuniformity in quantum-well thicknesses and to the structure being far from its optimal condition. Nevertheless, the very demonstration of lasing action in the RPG sample is direct experimental evidence that this structure has a significantly lower threshold than the conventional structures. The absence of lasing at $n = 3$ can easily be explained by the finite bandwidth of the multilayer high reflector which does not extend to the wavelength corresponding to the $n = 3$ subband transitions.

The failure of our conventional structures to lase can be understood using (6). As the parameters used in our calculations for the three structures (DH, conventional MQW, and RPG) involve considerable uncertainties, only rough estimates for their thresholds are obtained. The cavity parameters relevant to structures used in our comparative study are $d = 310$ nm, $L = 3.7$ μm, $R_1 = 0.84$, and $R_2 = 0.3$. The pump wavelength of 680 nm is assumed. For a surface-emitting DH laser with a bulk GaAs active region, (6) yields $\sim$16 MW/cm^2 as the threshold for optical pumping using the parameters of [8] ($B = 3.0 \times 10^{-10}$ cm^3/s, $A_0 = 3.0 \times 10^{-16}$ cm^2, $\alpha_r = 400$ cm^{-1}). For a conventional MQW laser, we obtain 0.9 MW/cm^2, using the material parameters specified in Section V-D. For a vertical-cavity surface-emitting laser with a conventional MQW active region of total length 1.5 μm and with integrated multilayer reflectors ($R \geq 84$ percent), a threshold of 1.6 MW/cm^2 has been reported [4]. The lasing threshold for the RPG structure of Fig. 12(a) is estimated from (6) to be only 0.25 MW/cm^2. These estimates illustrate the large reduction in threshold to be expected when the RPG structure and cavity are optimized.

VII. Conclusions

In summary, we have described a novel resonant periodic gain (or loss) optoelectronic structure which enhances the interaction between a standing-wave optical field and an active medium. The structure features a series of quantum wells separated by half-wave spacers, leading to a high gain and anisotropy. The alignment of the peaks of the optical standing-wave field with the half-wave-spaced quantum-well layers results in an optimal overlap integral between the optical field and the spatial gain/absorption distribution only in the vertical direction and at the desired wavelength. The usual sine-square averaging found in calculating the overlap between a standing wave and a uniform medium is absent, and the effective gain/absorption is increased by a factor of two. We have discussed various potential applications of this structure, with emphasis on surface-emitting lasers. We note again that this general idea will be useful for all devices in which the interaction is with a standing electromagnetic wave.

A number of conditions have to be satisfied in order to obtain lasing action with high efficiency in the RPG laser.

1) A uniform excitation of all quantum wells has to be maintained.

2) Since no external mirror is used, the total optical length of the structure must be an integral multiple of half of the lasing wavelength.

3) The spatial location of the quantum-well active layers in the structure and the phase of the reflected optical wave should be such that the antinodes of the standing wave optical field coincide with the quantum wells.

4) The quantum-well transition should nearly match the resonant wavelength determined by the spatial periodicity of the quantum wells.

Failure to satisfy any of the above conditions can severely impair the operation of the RPG laser. Most probably, such a structure would not enjoy any advantage as a result of the periodic gain medium, and would have a threshold comparable to that of a conventional MQW structure.

We have implemented the RPG design in fabricating a vertical-cavity surface-emitting GaAs/AlGaAs laser and have demonstrated lasing action by optical pumping. Such a novel structure offers several potential advantages over comparable bulk or nonresonant MQW devices, notably lower threshold, higher overall power efficiency, suppression of parasitic amplified spontaneous emission and longitudinal spatial hole burning, and better spectral and power-handling capabilities. The cumulative length of the active medium in the RPG sample incorporating a multilayer high reflector was only 310 nm. To our knowledge, this is the shortest ever gain medium length reported for any laser device. The short gain lengths made possible by the RPG structure may result in very stable, single-mode operation of these devices due to their large longitudinal mode spacings. Various means of reducing the room-temperature threshold of 6 MW/cm^2 for pumping at 680 nm are suggested. We are in the process of fabricating similar structures with integrated epitaxial AlAs/AlGaAs high reflectors grown between the substrate and the active region. We are also investigating electrical pumping schemes for this novel surface-emitting laser.

Acknowledgment

The authors appreciate the assistance of M. A. Mahbobzadeh in some numerical calculations. Stimulating discussions with Dr. W. Streifer of Spectra Diode Laboratories are also acknowledged.

References

[1] H. Soda, K. Iga, C. Kitahara, and Y. Suematsu, "GaInAsP/InP surface emitting injection lasers," *Japan. J. Appl. Phys.*, vol. 18, pp. 2329-2330, Dec. 1979.

[2] M. Ogura, T. Hata, and T. Yao, "Distributed feedback surface emitting laser diode with multilayered heterostructure," *Japan. J. Appl. Phys.*, vol. 23, pp. L512-L514, 1984.

[3] S. Kinoshita and K. Iga, "Circular buried heterostructure (CBH) GaAlAs/GaAs surface emitting lasers," *IEEE J. Quantum Electron.*, vol. QE-23, pp. 882-888, June 1987.

[4] P. L. Gourley and T. J. Drummond, "Visible, room-temperature, surface-emitting laser using an epitaxial Fabry-Perot resonator with AlGaAs/AlAs quarter-wave high reflectors and AlGaAs/GaAs multiple quantum wells," *Appl. Phys. Lett.*, vol. 50, pp. 1225-1227, May 1987.

[5] M. Ogura, W. Hsin, M.-C. Wu, S. Wang, J. R. Whinnery, S. C. Wang, and J. J. Yang, "Surface-emitting laser diode with vertical GaAs/GaAlAs quarter-wavelength multilayers and lateral buried heterostructure," *Appl. Phys. Lett.*, vol. 51, pp. 1655-1657, Nov. 1987.

[6] J. Faist, F. Morier-Genoud, D. Martin, J. D. Ganiere, and F.-K. Reinhart, "Optically pumped GaAs surface-emitting laser with integrated Bragg reflectors," *Electron. Lett.*, vol. 24, pp. 629-630, May 1988.

[7] D. Botez, L. M. Zinkiewicz, L. J. Mawst, and T. J. Roth, "120 mW vertical-cavity surface-emitting diode laser," presented at the 11th IEEE Int. Semiconductor Laser Conf., Boston, MA, Aug. 1988, post deadline paper PD3.

[8] K. Iga, F. Koyama, and S. Kinoshita, "Surface emitting semiconductor lasers," *IEEE J. Quantum Electron.*, vol. QE-24, pp. 1845-1855, Sept. 1988.

[9] H. Matsueda, "AlGaAs OEIC transmitters," *J. Lightwave Technol.*, vol. LT-5, pp. 1382-1390, Oct. 1987.

[10] J. Nitta, Y. Koizumi, and K. Iga, "GaAs, AlGaAs surface-emitting laser-type optical logic and gate device," in *Dig. Tech. Papers, CLEO'86, Conf. Lasers Electro-Opt.*, San Francisco, CA, June 1986, paper FO4, pp. 382-383.

[11] S. Uchiyama and K. Iga, "Two-dimensional array of GaInAsP/InP surface-emitting lasers," *Electron. Lett.*, vol. 21, pp. 162-164, Feb. 1985.

[12] Z. L. Liau and J. N. Walpole, "Surface-emitting GaInAsP/InP laser with low threshold current and high efficiency," *Appl. Phys. Lett.*, vol. 46, pp. 115-117, Jan. 1985.

[13] ——, "Large monolithic two-dimensional arrays of GaInAsP/InP surface-emitting lasers," *Appl. Phys. Lett.*, vol. 50, pp. 528-530, Mar. 1987.

[14] K. Kojima, S. Noda, K. Mitsunaga, K. Kyuma, and K. Hamanaka, "Continuous wave operation of a surface-emitting AlGaAs/GaAs multiquantum well distributed Bragg reflector laser," *Appl. Phys. Lett.*, vol. 50, pp. 1705-1707, June 1987.

[15] N. W. Carlson, G. A. Evans, J. M. Hammer, M. Lurie, L. A. Carr, F. Z. Hawrylo, E. A. James, C. J. Kaiser, J. B. Kirk, W. F. Reichert, D. A. Truxal, J. R. Shealy, S. R. Chinn, and P. S. Zory, "High-power seven-element grating surface emitting diode laser array with 0.012° far-field angle," *Appl. Phys. Lett.*, vol. 52, pp. 939-941, Mar. 1988.

[16] G. A. Evans, N. W. Carlson, J. M. Hammer, M. Lurie, J. K. Butler, L. A. Carr, F. Z. Hawrylo, E. A. James, C. J. Kaiser, J. B. Kirk, W. F. Reichert, S. R. Chinn, J. R. Shealy, and P. S. Zory, "Efficient, high-power (>150 mW) grating surface emitting lasers," *Appl. Phys. Lett.*, vol. 52, pp. 1037-1039, Mar. 1988.

[17] R. Geels, R. H. Yan, J. W. Scott, S. W. Corzine, R. J. Simes, and L. A. Coldren, "Analysis and design of a novel parallel-driven MQW-DBR surface-emitting diode laser," in *Conf. Lasers Electro-Opt. (CLEO '88), Tech. Dig. Ser. 1988*, vol. 7. Washington, DC: Opt. Soc. Amer., paper WM1, p. 206.

[18] M. Y. A. Raja, S. R. J. Brueck, M. Osinski, C. F. Schaus, J. G. McInerney, T. M. Brennan, and B. E. Hammons, "Wavelength-resonant enhanced gain absorption structure for optoelectronic devices," in *Post-Deadline Papers, XVI Int. Conf. Quantum Electron., IQEC'88*, Tokyo, Japan, July 1988, paper PD-23, pp. 52-53.

[19] ——, "Novel wavelength-resonant optoelectronic structure and its application to surface-emitting semiconductor lasers," *Electron. Lett.*, vol. 24, pp. 1140-1142, Sept. 1988.

[20] H. Statz, C. L. Tang, and J. M. Lavine, "Spectral output of semiconductor lasers," *J. Appl. Phys.*, vol. 35, pp. 2581-2585, 1964.

[21] R. Dingle, Ed., *Applications of Multiquantum Wells, Selective Doping, and Superlattices, Semiconductors and Semimetals*, R. K. Willardson and A. C. Beer, Eds., vol. 24. San Diego: Academic, 1987.

[22] T. H. Wood, C. A. Burrus, D. A. B. Miller, D. S. Chemla, T. C. Damen, A. C. Gossard, and W. Wiegmann, "High-speed optical modulation with GaAs/GaAlAs quantum wells in a p-i-n diode structure," *Appl. Phys. Lett.*, vol. 44, pp. 16-18, Jan. 1984.

[23] M. Glick, F. K. Reinhart, G. Weimann, and W. Schlapp, "Quadratic electro-optic light modulation in a GaAs/AlGaAs multiquantum well heterostructure near the excitonic gap," *Appl. Phys. Lett.*, vol. 48, pp. 989-991, Apr. 1986.

[24] G. D. Boyd, D. A. B. Miller, D. S. Chemla, S. L. McCall, A. C. Gossard, and J. H. English, "Multiple quantum well reflection modulator," *Appl. Phys. Lett.*, vol. 50, pp. 1119-1121, Apr. 1987.

[25] K. B. Nichols, B. E. Burke, B. F. Aull, W. D. Goodhue, B. F. Gramstorff, C. D. Hoyt, and A. Vera, "Spatial light modulators using charge-coupled-device addressing and electroabsorption effects in GaAs/AlGaAs multiple quantum wells," *Appl. Phys. Lett.*, vol. 52, pp. 1116-1118, Apr. 1988.

[26] T. H. Wood, C. A. Burrus, A. H. Gnauck, J. M. Wiesenfeld, D. A. B. Miller, D. S. Chemla, and T. C. Damen, "Wavelength-selective voltage-tunable photodetector made from multiple quantum wells," *Appl. Phys. Lett.*, vol. 47, pp. 190-192, Aug. 1985.

[27] H. M. Gibbs, S. S. Tarng, J. L. Jewell, D. A. Weinberger, K. Tai, A. C. Gossard, S. L. McCall, A. Passner, and W. Wiegmann, "Room-temperature excitonic optical bistability in a GaAs GaAlAs

superlattice etalon," *Appl. Phys. Lett.*, vol. 41, pp. 221-222, Aug. 1982.
[28] P. W. Smith, Y. Silberberg, and D. A. B. Miller, "Mode locking of semiconductor diode lasers using saturable excitonic nonlinearities," *J. Opt. Soc. Amer. B*, vol. 2, pp. 1228-1236, July 1985.
[29] D. A. B. Miller, D. S. Chemla, T. C. Damen, A. C. Gossard, W. Wiegmann, T. H. Wood, and C. A. Burrus, *Appl. Phys. Lett.*, vol. 45, pp. 13-15, July 1984.
[30] D. A. B. Miller, D. S. Chemla, D. J. Eilenberger, P. W. Smith, A. C. Gossard, and W. Wiegmann, "Degenerate four-wave mixing in room-temperature GaAs/GaAlAs multiple quantum well structures," *Appl. Phys. Lett.*, vol. 42, pp. 925-927, June 1983.
[31] J. Krause and M. O. Scully, "Theory of the holographic laser: Correlated emission in a ring cavity," *Phys. Rev. A*, vol. 36, pp. 1771-1778, Aug. 1987.
[32] E. Yablonovitch, "Inhibited spontaneous emission in solid-state physics and electronics," *Phys. Rev. Lett.*, vol. 58, pp. 2059-2062, May 1987.
[33] H. Kogelnik and C. V. Shank, "Coupled-wave theory of distributed feedback lasers," *J. Appl. Phys.*, vol. 43, pp. 2327-2335, May 1972.
[34] A. Y. Cho, "Growth of III-V semiconductors by molecular beam epitaxy and their properties," *Thin Solid Films*, vol. 100, pp. 291-317, Feb. 1983.
[35] H. Morkoç, T. J. Drummond, W. Kopp, and R. Fischer, "Influence of substrate temperature on the morphology of $Al_xGa_{1-x}As$ grown by molecular beam epitaxy," *J. Electrochem. Soc.*, vol. 129, pp. 824-826, Apr. 1982.
[36] A. J. SpringThorpe and P. Mandeville, "Mass spectrometry during molecular beam epitaxy: An alternative to a reflection high-energy electron diffraction," *J. Vac. Sci. Technol.*, vol. B6, pp. 754-757, Mar. 1988.
[37] H. A. Macleod, *Thin-Film Optical Filters*, 2nd ed. New York: Macmillan, 1986, pp. 50-52.
[38] M. Ogura, T. Hata, N. J. Kawai, and T. Yao, "GaAs-$Al_xGa_{1-x}As$ multilayer reflector for surface emitting laser diode," *Japan. J. Appl. Phys.*, vol. 22, pp. L112-L114, Feb. 1983.
[39] Z. Knittl, *Optics of Thin Films*. London: Wiley, 1976, pp. 35-51.
[40] M. V. Klein and T. E. Furtak, *Optics*, 2nd ed. New York: Wiley, 1986, pp. 295-300.
[41] *Handbook of Chemistry and Physics*, 67th ed. Boca Raton, FL: CRC Press, 1986, p. E-378.
[42] D. S. Chemla, D. A. B. Miller, P. W. Smith, A. C. Gossard, and W. Wiegmann, "Room temperature excitonic nonlinear absorption and refraction in GaAs/AlGaAs multiple quantum well structures," *IEEE J. Quantum Electron.*, vol. QE-20, pp. 265-275, Mar. 1984.
[43] G. Bastard and J. A. Brum, "Electronic states in semiconductor heterostructures," *IEEE J. Quantum Electron.*, vol. QE-22, pp. 1625-1644, Sept. 1986.
[44] R. L. Greene, K. K. Bajaj, and D. E. Phelps, "Energy levels of Wannier excitons in GaAs-$Ga_{1-x}Al_xAs$ quantum-well structures," *Phys. Rev. B*, vol. 29, pp. 1807-1812, Feb. 1984.
[45] D. F. Nelson, R. C. Miller, and D. A. Kleinman, "Band nonparabolicity effects in semiconductor quantum wells," *Phys. Rev. B*, vol. 35, pp. 7770-7773, May 1987.
[46] B. Saint-Cricq, F. Lozes-Dupuy, and G. Vassilieff, "Well width dependence of gain and threshold current in GaAlAs single quantum well lasers," *IEEE J. Quantum Electron.*, vol. QE-22, pp. 625-630, May 1986.
[47] F. Laruelle and B. Etienne, "Optical investigation of the heavy hole-light hole splitting in thin GaAs/GaAlAs quantum wells," *Solid State Commun.*, vol. 65, pp. 565-569, 1988.
[48] H. J. Lee, L. Y. Juravel, J. C. Wooley, and A. J. SpringThorpe, "Electron transport and band structure of $Ga_{1-x}Al_xAs$ alloys," *Phys. Rev. B*, vol. 21, pp. 659-669, Jan. 1980.
[49] H. Kroemer, W.-Y. Chien, J. S. Harris, and D. D. Edwall, "Measurement of isotype heterojunction barriers by *C-V* profiling," *Appl. Phys. Lett.*, vol. 36, pp. 295-297, Feb. 1980.
[50] H. Kroemer, "Determination of heterojunction band offsets by capacitance-voltage profiling through nonabrupt isotype heterojunctions," *Appl. Phys. Lett.*, vol. 46, pp. 504-505, Mar. 1985.
[51] D. E. Aspnes and A. A. Studna, "Dielectric functions and optical parameters of Si, Ge, GaP, GaAs, GaSb, InP, InAs, and InSb from 1.5 to 6.0 eV," *Phys. Rev. B*, vol. 27, pp. 985-1009, Jan. 1983.
[52] H. C. Casey, D. D. Sell, and K. W. Wecht, "Concentration dependence of the absorption coefficient for n- and p-type GaAs between 1.3 and 1.6 eV," *J. Appl. Phys.*, vol. 46, pp. 250-257, Jan. 1975.
[53] M. Y. A. Raja, S. R. J. Brueck, M. Osinski, C. F. Schaus, J. G. McInerney, T. M. Brennan, and B. E. Hammons, "Surface-emitting, multiple quantum well GaAs/AlGaAs laser with wavelength-resonant periodic gain medium," *Appl. Phys. Lett.*, vol. 53, pp. 1678-1680, Oct. 1988.
[54] D. A. Broido, E. S. Koteles, C. Jagannath, and J. Y. Chi, "Resonance broadening of the light-hole exciton in GaAs/$Al_xGa_{1-x}As$ quantum wells," *Phys. Rev. B*, vol. 37, pp. 2725-2728, Feb. 1988.
[55] E. H. Bottcher, K. Ketterer, D. Bimberg, G. Weimann, and W. Schlapp, "Excitonic and electron-hole contributions to the spontaneous recombination rate of injected charge carriers in GaAs-GaAlAs multiple quantum well lasers at room temperature," *Appl. Phys. Lett.*, vol. 50, pp. 1074-1076, Apr. 1987.
[56] P. L. Derry, A. Yariv, K. Y. Lau, N. Bar-Chaim, K. Lee, and J. Rosenberg, "Ultralow-threshold graded-index separate-confinement single quantum well buried heterostructure (Al, Ga)As lasers with high reflective coatings," *Appl. Phys. Lett.*, vol. 50, pp. 1773-1775, June 1987.
[57] T. Sakaguchi, F. Koyama, and K. Iga, "Vertical cavity surface-emitting laser with an AlGaAs/AlAs Bragg reflector," *Electron. Lett.*, vol. 24, pp. 928-929, July 1988.
[58] A. Yariv, *Quantum Electronics*, 2nd ed. New York: Wiley, 1975, p. 146.

Mohammad Yasin A. Raja was born in Rawalpindi, Pakistan, on May 1, 1953. He received the M.Sc. and M.Phil degrees in physics from Quaid-i-Azam University, Islamabad, Pakistan, in 1976 and 1979, respectively, and the Ph.D. degree, also in physics, from the University of New Mexico, Albuquerque.

He joined PINSTECH where his research involved development and investigation of narrow linewidth CW and pulsed TEA CO_2 lasers. His doctoral research was on wavelength-resonant surface-emitting semiconductor lasers. Currently, he is a Research Associate with the Center for High Technology Materials, University of New Mexico where his research efforts involve investigations on resonant periodic gain surface-emitting lasers, enhanced light-matter interaction, and spectroscopy of optoelectronic devices and materials, e.g., photoluminescence, Raman, and photoacoustic spectroscopy.

Dr. Raja is a member of the Optical Society of America, the Materials Research Society, and a student member of the IEEE Lasers and Electro-Optics Society.

Steven R. J. Brueck (S'63-M'71) received the B.S. degree in electrical engineering from Columbia University, New York, in 1965, and the S.M. and Ph.D. degrees from the Massachusetts Institute of Technology, Cambridge, MA, also in electrical engineering, in 1967 and 1971, respectively. His doctoral research involved the study of spontaneous and stimulated spin-flip Raman scattering in InSb.

After receiving his degree, he joined the staff of the Quantum Electronics Group at the Lincoln Laboratory, Massachusetts Institute of Technology, Lexington, where he carried out experimental studies of a number of material systems. These have included spin-slip Raman scattering, nonlinear optics of simple cryogenic liquids, and vibrational kinetics in simple single and multicomponent liquids. In recent years, his research interests have been in the application of optical techniques to the characterization and development of semiconductor materials, devices, and processing technologies. This has led to work on microstructure electromagnetic effects in a number of optical diagnostic, laser-processing, and electrooptic device applications. In 1985 he joined the faculty of the Electrical and Computer Engineering and Physics Department, University of New Mexico, Albuquerque, where he is now the Director of the Center for High Technology Materials, an interdisciplinary research organization with major thrusts on semiconductor optoelectronics, nonlinear optics, and microelectronics.

Dr. Brueck is a Fellow of the Optical Society of America and a member of the American Physical Society and the Materials Research Society. He has served on various program and administrative committees in addition to a term as an Associate Editor of *Optics Letters*. For three years he served

as an Associate Editor and is currently the Editor of the IEEE JOURNAL OF QUANTUM ELECTRONICS. He was recently elected to a three-year term on the LEOS Administrative Committee.

Marek Osiński (SM'86) was born in Wroclaw, Poland, on May 28, 1948. He received the M.Sc. degree in theoretical physics from Warsaw University, Warsaw, Poland, in 1971 and the Ph.D. degree in physical sciences from the Institute of Physics of the Polish Academy of Sciences (PASc), Warsaw, in 1979.

In 1971 he joined the Institute of Physics of the PASc, where he was engaged in theoretical investigations of waveguiding properties and modal characteristics of semiconductor lasers. From November 1980 until June 1984 he was a Visiting Research Fellow at Southampton University, England, where he conducted theoretical research on long-wavelength injection laser properties relevant to optical fiber communications. From July 1984 until August 1985 he was a British Telecom Senior Research Associate in Coherent Optical Communication at Cambridge University, England, where he was involved in studying picosecond modulation of injection lasers. Currently, he is Research Associate Professor of Electrical and Computer Engineering at the Center for High Technology Materials, University of New Mexico, Albuquerque, on leave at the Research Center for Advanced Science and Technology, University of Tokyo, Meguro-ku, Tokyo, Japan. His main current interests include high-power semiconductor laser arrays coupled waveguide systems, nonlinear dynamics of semiconductor lasers, surface emitting lasers, and material properties of AlGaAs and InGaAsP alloys. He has authored or coauthored over 90 publications.

Dr. Osiński is a member of the IEEE Lasers and Electro-Optics Society, the Optical Society of America, the Polish Physical Society, the European Physical Society, SPIE, and the New Mexico Section of Materials Research Society. He is listed in "American Men and Women of Science."

Christian F. Schaus (M'86) was born in Amsterdam, NY, in 1959. He received the A.A.S. and B.S. degrees in chemistry from the State Universities of New York at Cobleskill and Plattsburgh in 1977 and 1980, respectively, and the M.S. and Ph.D. degrees from Rensselear Polytechnic Institute, Troy, NY, in 1983 and from Cornell University, Ithaca, NY, in 1986, both in electrical engineering.

In 1986 he joined the Center for High Technology Materials, University of New Mexico, as an Assistant Professor of Electrical Engineering, where he is presently. At the University, he has taught graduate courses in semiconductor device physics and developed a course in optoelectronics processing. His research has involved setting up an MOCVD crystal growth facility and device processing laboratories. His primary interests lie in crystal growth and processing of advanced optoelectronic devices and circuits.

Dr. Schaus is a recipient of the 1987 National Science Foundation Presidential Young Investigator Award.

John G. McInerney (M'81) was born in Cork, Ireland, on May 9, 1959. He was a Scholar at the National University of Ireland, University College, Cork, where he received B.Sc. degrees in physics and mathematical science in 1980. In 1985 he received the Ph.D. degree in physics from Trinity College, Dublin, Ireland, for experimental and theoretical investigations of optical bistability and picosecond pulse generation in semiconductor lasers.

During 1981 he was with Standard Telecommunication Laboratories, Harlow, England, doing research on fabrication and characterization of III–V semiconductor lasers. From 1984 to 1986 he was STL Research Fellow in Optoelectronics at the Microelectronics Research Group, Cavendish Laboratory, University of Cambridge, and a Fellow of Robinson College, Cambridge, working on microfabrication of optoelectronic devices using electron-beam lithography. Since 1986 he has been an Assistant Professor of Electrical Engineering at the Center for High Technology Materials, University of New Mexico, Albuquerque. His research interests include complex dynamics of nonlinear optical systems, optical bistability and instabilities, low-dimensionality optoelectronic structures, semiconductor lasers, and integrated optoelectronics. He has authored or coauthored over 50 publications in laser physics and optoelectronics.

Dr. McInerney is a member of IEEE Lasers and Electro-Optics Society, the Optical Society of America, the Institute of Physics (UK), and the Institution of Electrical Engineers (UK).

Thomas M. Brennan, photograph and biography not available at the time of publication.

B. Eugene Hammons, photograph and biography not available at the time of publication.

PROCEEDINGS
SPIE—The International Society for Optical Engineering

Laser Diode Technology and Applications

Luis Figueroa
Chair/Editor

18–20 January 1989
Los Angeles, California

Sponsored by
SPIE—The International Society for Optical Engineering

Cooperating Organizations
Applied Optics Laboratory/New Mexico State University
Center for Applied Optics Studies/Rose-Hulman Institute of Technology
Center for Applied Optics/University of Alabama in Huntsville
Center for Electro-Optics/University of Dayton
Center for Excellence in Optical Data Processing/Carnegie Mellon University
Center for Microwave-Lightwave Engineering/Drexel University
Center for Research in Electro-Optics and Lasers/University of Central Florida
Jet Propulsion Laboratory/California Institute of Technology
Optical Sciences Center/University of Arizona
Optoelectronic Computing Systems Center/University of Colorado, Colorado State University

Published by
SPIE—The International Society for Optical Engineering
P.O. Box 10, Bellingham, Washington 98227-0010 USA
Telephone 206/676-3290 (Pacific Time) • Telex 46-7053

P

Volume 1043

Invited Paper

OPTICAL CAVITY DESIGN FOR WAVELENGTH-RESONANT SURFACE-EMITTING SEMICONDUCTOR LASERS

S. R. J. Brueck, M. Y. A. Raja, M. Osinski, C. F. Schaus, M. Mahbobzadeh, J. G. McInerney, and K. J. Dahlhauser

Center for High Technology Materials
University of New Mexico
Albuquerque, NM 87131

ABSTRACT

Recently, we have demonstrated a novel surface-emitting semiconductor laser with a wavelength-resonant periodic gain medium, which has performed significantly better than conventional double-heterostructure and multiple-quantum-well vertical-cavity devices. The gain medium consists of a series of half-wave-spaced quantum wells which provides enhanced longitudinal gain at a selected wavelength in the vertical direction, reducing transverse amplified spontaneous emission, lowering the threshold and raising the quantum efficiency. However, because the antinodes of the standing-wave optical field must coincide with the quantum wells, considerable attention must be devoted to designing the vertical cavity. Here we examine various cavity configurations in which the wavelength-resonant periodic gain medium has been incorporated. Multilayer epitaxial reflectors are particularly attractive for fabricating monolithic vertical-cavity surface-emitting lasers.

1. INTRODUCTION

Semiconductor lasers which emit from the top (epitaxial) surface [1-8] rather than from the end facets are of considerable interest for a variety of applications such as monolithic optoelectronic integrated circuits [9], optical chip-to-chip interconnects, optical logic devices [10] and high-power, large-area, two-dimensional arrays [11]. Because of their short cavity lengths, these lasers have large Fabry-Pérot mode spacings which favor single longitudinal mode operation. However, development of these systems has been impeded by the limitations of existing surface-

emitting laser designs, particularly the high thresholds and low efficiencies, is those with vertical resonators, which are well suited for forming two-dimensional arrays. These problems are mostly due to short active-region lengths (a few micrometers), very large Fresnel numbers, lack of carrier and optical confinement, and generation of competitive amplified spontaneous emission (ASE) in the transverse plane.

The vertical cavity surface-emitting lasers developed to date have performed poorly compared with conventional edge-emitters, and considerable attention has been paid to alternative geometries whose active regions are configured in the same way as in edge-emitting lasers, but in which radiation is directed towards the surface either by 45° mirrors [12,13] or by second-order distributed Bragg reflectors [14-16]. While some of these designs have performed well, vertical-cavity surface-emitters offer potentially higher packing density, larger emitting areas, better beam quality, unconstrained arrangement of emitters, and planar integration with easier batch processing and on-wafer probe testing.

In this paper, we describe the novel concept of a vertical-cavity, resonant periodic gain surface-emitting semiconductor laser, with particular emphasis on how the gain medium is combined with an optical cavity. In Section 2, the concept of resonant periodic gain (RPG) is described briefly. Section 3 contains calculations of the reflectivity, phase and gain resonances which occur when the RPG medium is placed within an optical cavity, first for the structures used in the initial demonstrations of the RPG principle, then for projected cavity designs utilizing multilayer epitaxial high-reflectors which can be deposited in the same growth process as the gain medium.

2. Resonant Periodic Gain Semiconductor Lasers

The gain experienced by a mode in a semiconductor laser resonator is determined by the interaction of the standing-wave optical field with the material gain distribution in the active region. This interaction is not spatially uniform, but is strongest at the antinodes of the standing-wave optical field and vanishes at the nulls. Hence the material gain in a homogeneous medium is not utilized efficiently by the resonant mode, *i.e.* the effective gain length is shorter than the overall physical length of the gain medium. To overcome this problem, we have developed a new multilayer structure: a resonant periodic gain (RPG) medium which maximizes the modal gain in a semiconductor laser by confining injected carriers, and hence the gain, to the antinode regions [17-21]. This will reduce spontaneous emission due to carriers normally present near the nodes. In addition, competition from amplified spontaneous emission (ASE) in the transverse directions is suppressed due to the poor modal overlap integral. This new design is particularly attractive for vertical-cavity surface-emitting lasers: it has already led to lower thresholds for optical pumping

[17-20], and may well be an important step towards room-temperature cw operation of electrically-pumped devices.

Details of the physics and fabrication of RPG vertical-cavity surface-emitting lasers have already been described elsewhere [17-20]. For completeness, we provide here a brief outline of the basic properties of RPG media, before proceeding to analyze how they are combined with various optical cavity configurations. The most straightforward RPG structure is formed by a series of localized gain regions consisting of single quantum-wells (QWs) or closely spaced groups of QWs, periodically arranged to coincide with the antinodes of the optical standing wave in the vertical cavity at the lasing wavelength. Fig. 1 illustrates the RPG structure schematically: the localized gain regions (GaAs quantum wells) are separated by passive AlGaAs spacers whose thickness determines the resonant wavelength λ_r, at which the interaction of the optical field with the periodic multiple quantum-well gain medium is maximized. This occurs when the gain medium has an optical periodicity of $\lambda_r/2$. For a properly designed structure, the resonant wavelength λ_r should be chosen to correspond to a particular transition in the quantum wells. In addition, it is essential that the RPG medium be placed within the cavity so that the antinodes of the optical standing-wave field coincide with the gain regions, i.e. that the optical thicknesses of the end layers be chosen carefully. In the worst possible case, misplacement of the RPG medium by a quarter-wavelength would result in a total absence of modal gain.

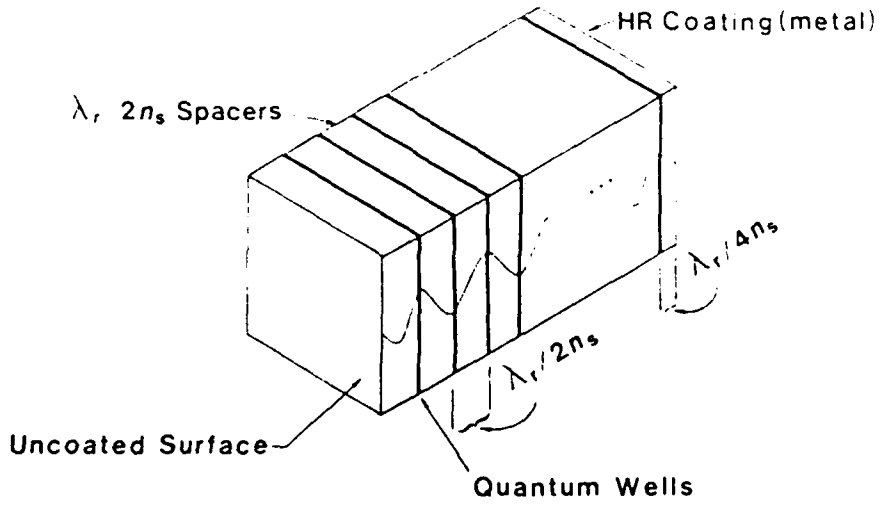

Fig. 1. Schematic diagram of resonant periodic gain (RPG) medium designed to enhance the effective gain length of a vertical-cavity surface-emitting laser. The thick lines represent the quantum wells, λ_r is the resonant wavelength and n_s is the refractive index of the spacer material.

To illustrate the effect of the RPG structure in a vertical-cavity surface-emitting laser, we

calculate the effective gain of a single longitudinal mode propagating along the cavity (z) axis of the laser, for which the integrated gain coefficient $G(\lambda)$ (the product of active medium length and gain per unit length) is given by

$$G(\lambda) = \int_0^L g(z) \sin^2 \left(\frac{2\pi n(z) z}{\lambda} \right) dz, \qquad (1)$$

where λ is the free-space wavelength of the standing-wave optical field, L the cavity length, $g(z)$ and $n(z)$ the material gain and refractive index, respectively. If the medium were uniform, the integral (1) would give $G(\lambda) = gL/2$, *i.e.* only half of the available material gain would be utilized. For the RPG medium illustrated in Fig. 1, with N quantum wells of thickness L_z and separated by $D = \lambda_r/2n_s$, where n_s is the refractive index of the spacer material, we evaluate this integral assuming that each QW has the same constant gain coefficient g_w, to obtain the modal gain spectrum [18-20]

$$G(\lambda) = (Ng_w L_z/2)(1 + \mathrm{sinc}(2\pi L_z n_s/\lambda_r)), \qquad (2)$$

where $\mathrm{sinc}(x) = \sin(x)/x$, and we have ignored the wavelength dependence of the material gain for simplicity. The gain resonance becomes sharper as the number of quantum wells increases, much as the resolution of a diffraction grating is improved by illumination of more grating periods. Away from resonance, the sinc term averages to zero, and $G(\lambda)$ becomes $Ng_w L_z/2$, equal to the integrated gain in a uniform medium of length NL_z and material gain g_w. Hence, the integrated gain coefficient $G(\lambda_r)$ at the resonant wavelength is enhanced by a factor of two over that of a conventional, non-resonant MQW gain medium having equal active length. Because the gain anisotropy reduces ASE in the transverse plane, the RPG laser should have increased power efficiency as well as a lower threshold pump level.

3. Optical Cavity Design for RPG Lasers

The basis for the RPG principle is alignment of the antinodes of the optical standing wave in the laser cavity with a periodic array of localized gain regions (single or multiple quantum wells), so that the effective gain is enhanced as described above. To optimize this arrangement, two conditions must be met simultaneously:

(1) the resonant wavelength, i.e. the period of the RPG medium, must correspond to a strongly amplifying transition in the quantum wells;

(2) the position of the RPG medium within the optical cavity, as determined by the phase shifting layers at the ends, must be such that the antinodes of the standing wave coincide with the quantum wells.

Satisfying these conditions ensures that the resonances of the cavity and gain medium overlap at a design wavelength where there is available gain. In this section we are primarily concerned with the second condition, that is, configuring the cavity with respect to the RPG medium. If the phase shift layers are not properly matched to the cavity resonance closest to the gain peak, the effective gain will degrade rapidly. The worst possible case would have the quantum wells located at the nodes of the optical standing wave, thereby reducing the usable gain to zero. It is therefore not sufficient to optimize the cavity and RPG medium separately; they must also be aligned with respect to each other. Another important consideration is that, because of the short gain length of the structure, the optical cavity must have extremely low losses. Mirror reflectivities must therefore be as close to unity as possible, and this imposes additional constraints on the cavity design.

We start by presenting a simple technique for calculating reflectivity and gain resonances for cavities enclosing RPG media. These calculations are performed for the RPG laser with a deposited aluminum mirror which was first used to demonstrate the principle of resonant periodic gain [19]. For this structure, the importance of correct choice of the thicknesses of the phase shifting end is demonstrated. Next, we consider optimization of the RPG laser by incorporating a high-Q cavity consisting of multilayer epitaxial reflectors, which can be deposited in the same growth run as that used to fabricate the RPG medium itself. The growth tolerances for such an optimized cavity are discussed, and reflectivity and gain resonances for the finished structure are calculated.

A. Method for Calculating Cavity Reflectivity and Gain

Many textbooks on thin film optical filters present techniques for the calculation of complex reflectivities of multilayer dielectric structures [22-24]. The approach used in this work is simply to express the fields E_{j+1} at each layer $(j+1)$ in terms of the fields E_j at the previous layer (j) and the optical phase shift Φ_j in traversing the jth layer, using a transfer matrix of the form

$$\begin{pmatrix} E_{j+1}^{+} \\ E_{j+1}^{-} \end{pmatrix} = \frac{1}{2} \begin{pmatrix} \left[1 + \frac{n_j}{n_{j+1}}\right] e^{i\Phi_j} & \left[1 - \frac{n_j}{n_{j+1}}\right] e^{-i\Phi_j} \\ \left[1 - \frac{n_j}{n_{j+1}}\right] e^{i\Phi_j} & \left[1 + \frac{n_j}{n_{j+1}}\right] e^{-i\Phi_j} \end{pmatrix} \begin{pmatrix} E_j^{+} \\ E_j^{-} \end{pmatrix} \qquad (3)$$

where n_{j+1}, n_j are the respective (complex) refractive indices, E_{j+1}^{+} and E_j^{+} are the complex electric field amplitudes for waves propagating in the positive z-direction (to the right for

definiteness), and E_{j-1}^{+}, E_j^{-} are the field amplitudes for waves propagating in the opposite direction. The layers are numbered from right to left, with the fields defined at the rightmost edge of each layer. The total cavity reflectivity for waves incident from the left can then be evaluated by imposing the boundary condition that there is only an outgoing wave in the medium beyond the right end of the cavity, and carrying out a straightforward series of matrix multiplications to evaluate the incident and reflected fields in terms of this outgoing wave. The effective gain in the structure is calculated by integrating the product of the intensity and gain factor through the layered structure and dividing by the incident intensity. Because we are interested only in matching resonances of the cavity and the RPG medium, we did not include dispersion of the material gain or index in any of these calculations. The additional requirement of placing these resonances close to the gain peak is less critical, and will not be dealt with explicitly in this paper.

B. Prototype RPG Cavity with Al *End Reflector*

The first structure used to demonstrate the resonant periodic gain principle consisted of a series of 32 GaAs quantum wells (L_z = 10 nm) separated by half-wave $Ga_{0.75}Al_{0.25}As$ spacers (D = 109 nm), designed for operation at the n = 2 subband transitions near ~825 nm [17,20]. One end of the structure was uncoated, so that its reflectivity was ~32%, while a layer of Al was deposited onto the other end to obtain a reflectivity of ~75%. The overall reflectivity and effective gain for this device have been calculated as described above, assuming a quarter-wave end spacer on the Al-coated side, and different spacer layer thicknesses on the other end. Figure 2 illustrates the results for a half-wave thick layer on the free (uncoated) end, which is expected to be close to optimum. As anticipated, the effective gain is enhanced by a factor of two at the resonant wavelength of ~825 nm. For comparison, we have performed similar calculations for the same RPG medium with a quarter-wave spacer layer at each end. This structure does not exhibit any enhancement in its effective gain, as shown in Figure 3. The normalized peak gain is given in Figure 4 as a function of the thickness of the final spacer layer on the free (uncoated) end of the resonator. In obtaining Fig. 4, the resonant wavelength was allowed to vary with the total cavity length, hence the observed periodicity in the gain as a function of and spacer thickness differs slightly from the nominal λ_r. The refractive indices used were (2.75 + 8.31i) for Al [25], 3.64 for GaAs and 3.45 for $Al_{0.25}Ga_{0.75}As$ [26,27]. Note that the calculated resonances are relatively broad due to the poor cavity Q-factor; the round trip reflectivity product is only ~0.24. The variations in depth and width of the resonances are a manifestation of small distributed feedback effects due to reflections at the quantum wells. To estimate the magnitude of these distributed Bragg reflection effects, we have modeled the behavior of a structure in which the end reflections have been artificially suppressed by (computationally) attaching thick GaAs films to the ends. The results of these calculations are given in Figure 5. The effects of periodic reflections at the

32 quantum wells lead to effective reflectivity changes of ≤ 20% near the resonant wavelength

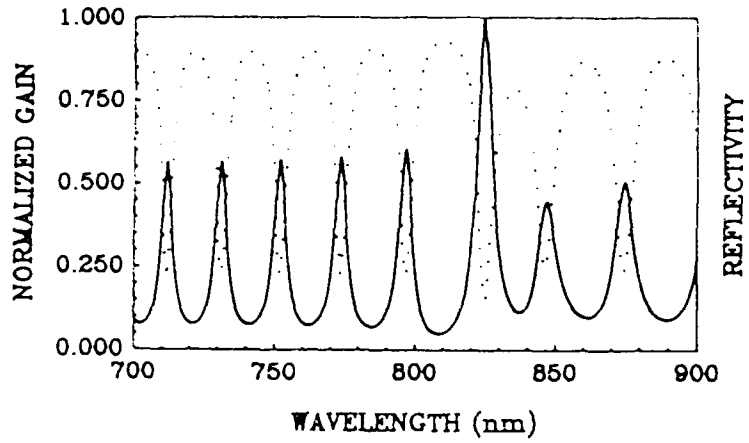

Fig. 2. Calculated normalized gain (solid line) and reflectivity (dotted line) spectra for RPG surface-emitting laser with a quarter-wave end spacer facing a metal reflector, and a half-wave spacer at the opposite end.

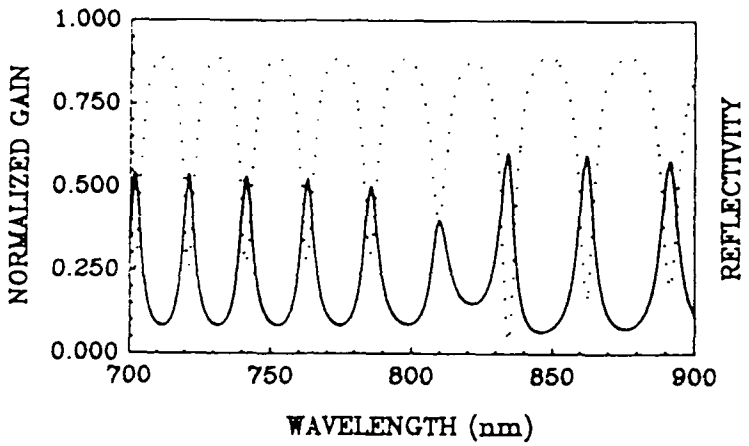

Fig. 3. Calculated normalized gain (solid line) and reflectivity (dotted line) spectra for RPG surface-emitting laser with a quarter-wave end spacer facing a metal reflector, and a quarter-wave spacer at the opposite end.

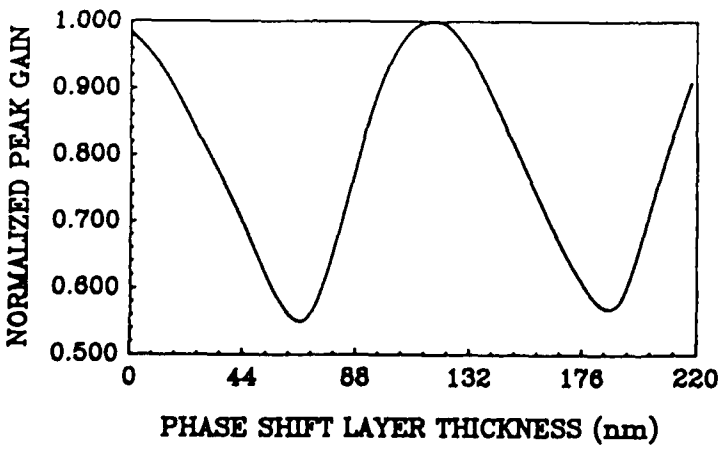

Fig. 4. Calculated variation in peak gain for a RPG surface-emitting laser with a quarter-wave end spacer facing a metal reflector, as a function of the thickness of the spacer at the opposite end.

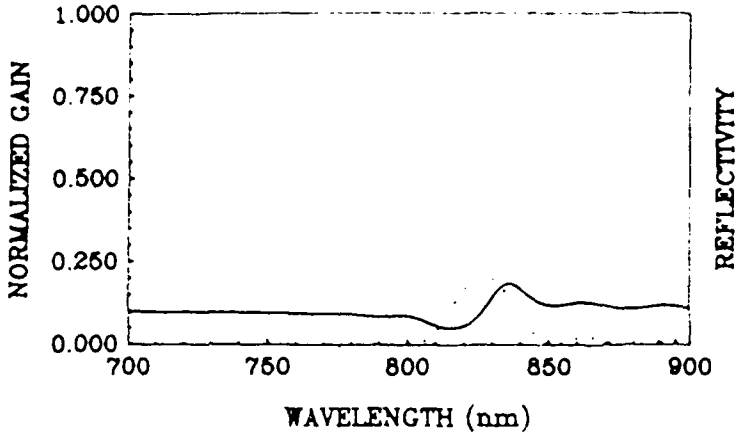

Fig. 5 Calculated normalized gain (solid line) and reflectivity (dotted line) spectra for RPG surface-emitting laser with semi-infinite GaAs layer at each end: this enables evaluation of the effects of distributed reflections at the quantum wells.

C. Improved Cavities Using Multilayer Epitaxial High-Reflectors

Because of its short cavity length, the vertical-cavity surface-emitting laser requires extremely high gain per unit length. The optimal way to configure a vertical-cavity surface-emitting laser is thus to provide a very high-Q cavity, which may be formed by bracketing the gain medium between a pair of epitaxial multilayer high-reflectors (MHRs) consisting of a stack of alternating high-and low-index quarter-wave layers [4,5,28]. The materials for these layers must obviously be chosen to have sufficiently wide bandgaps that excessive absorption losses in the reflectors are avoided. Simple calculations show that for a vertical cavity surface-emitting laser containing a series of ~30 quantum wells of thickness ~10 nm, the threshold gain required is of the order of 4 μm^{-1} when uncoated, 2.5 μm^{-1} when an Al reflector is deposited on one side, but drops to 0.03 μm^{-1} (300 cm^{-1}) when the active medium is bracketed by two MHRs with 99% reflectivity. The reflectivity spectrum for a typical MHR consisting of 20 pairs of alternating quarter-wave layers of indices n_L = 3.20 and n_H = 3.50, is shown in Figure 6.

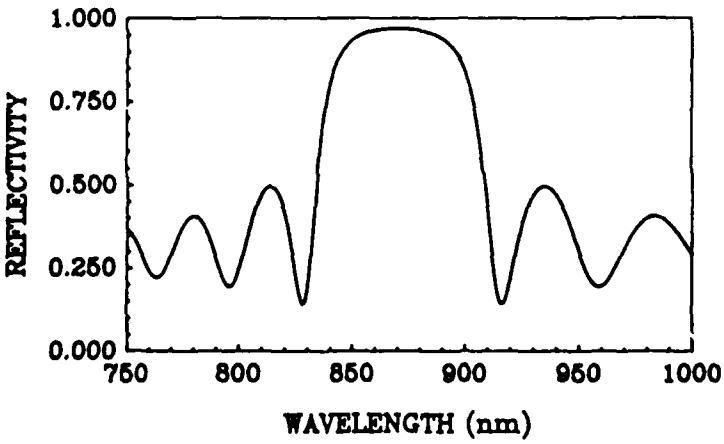

Fig. 6. Calculated reflectivity spectrum of an epitaxial multilayer high-reflector (MHR) consisting of 20 periods of alternating high- and low-index quarter-wave layers with indices n_H = 3.50 and n_L =3.20, respectively.

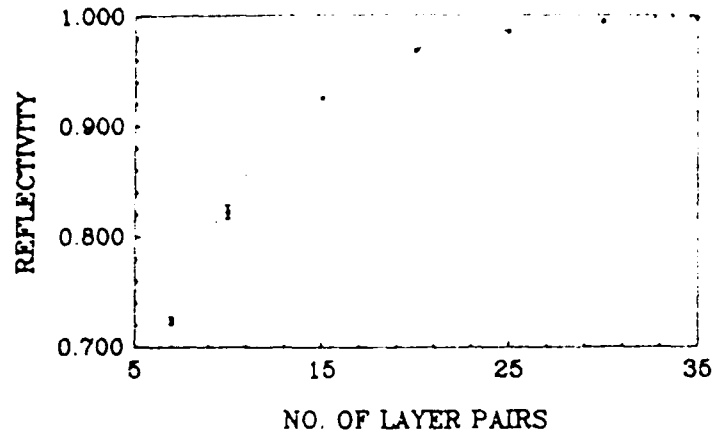

Fig. 7. Spread in reflectivity of a MHR at its design wavelength (825 nm) due to random ± 5% variation in optical thickness of the grown layers.

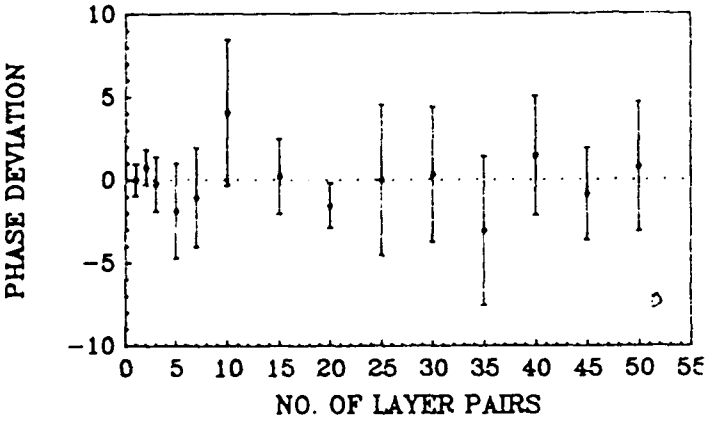

Fig. 8. Fluctuation in the phase shift (in degrees) of a MHR at its design wavelength (825 nm) due to a random ±5% variation in the optical thickness of the grown layers.

Since the inclusion of MHRs in the device dramatically increases the number of layers to be grown, the effects of uncertainties in layer thicknesses and compositions must be considered. In Figure 7 and 8 we plot the spread in the reflectivities (the dotted line is the ideal curve), and variations in the cavity phase shift at the peak, for AlGaAs/AlAs MHRs with different numbers of layer pairs, assuming a random variation of ± 5% in the optical thickness (combined uncertainties in physical thickness and refractive index). The solid curve is the theoretical result for a perfect stack of alternating quarter-wave layers of high-index (61.4 nm of $Al_{0.40}Ga_{0.60}As$, n_H = 3.36) and low-index (68.8 nm of AlAs, n_L = 3.00) materials, while the bars represent the spread in the quantity calculated. These data suggest that, while the spread in reflectivity is minimal when more than ten periods are used, the phase variations are of much greater concern for the RPG laser (refer also to Figure 5). Critical control of the cavity resonance is clearly required if the RPG structure is to be used to its best advantage.

Finally, we have calculated the reflectivity and effective gain for an improved RPG

surface emitting laser using a pair of MHRs. The results of these calculations are shown in Figure 9, and the threshold gain for the structure is estimated to be ~ 0.5 μm^{-1}.

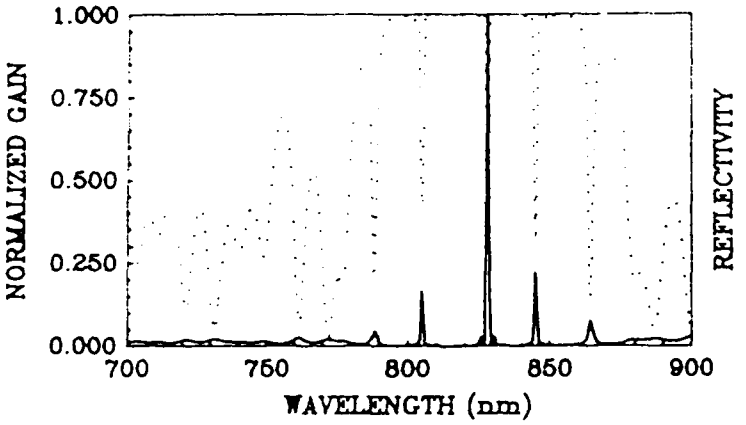

Fig. 9 Calculated reflectivity and gain spectra for improved laser structure using two MHRs.

4. Conclusions

In summary, we have described a novel resonant-periodic-gain (RPG) medium which optimizes the available gain in a vertical-cavity surface-emitting semiconductor laser. The basis for the gain enhancement is alignment of the antinodes of the standing wave optical field in a resonant cavity with periodic localized gain regions such as single or multiple quantum wells. Since the usual sine-square averaging in the overlap integral between the optical field and the spatial gain distribution is absent, the effective gain is increased by a factor of two. One critical condition which must be satisfied to optimize the gain in a RPG medium is that the gain medium must be positioned correctly within the optical cavity. If the RPG medium is misaligned within the cavity, the effective gain degrades rapidly and may actually become less than that of a conventional MQW structure.

Because of the need for very high Q cavities due to the short gain lengths in vertical-cavity surface-emitters, and due to the additional constraints on resonant periodic gain devices, cavity design is of the utmost importance. We have analyzed various cavity configurations for RPG lasers, including an optimized structure with epitaxial multilayer high-reflectors at either end. The tolerances in grown layer thicknesses and compositions required for successful fabrication of such devices are a few percent.

5. Acknowledgements

This work was partially supported by the U. S. Air Force Office of Scientific Research

and by the National Science Foundation. Stimulating discussions with Dr. William Streifer of Spectra Diode Laboratories are also acknowledged.

6. REFERENCES

[1] H. Soda, K. Iga, C. Kitahara, and Y. Suematsu, "GaInAsP/InP surface emitting injection lasers", Japan. J. Appl. Phys. vol. 18, pp. 2329-2330, Dec. 1979.

[2] M. Ogura, T. Hata, and T. Yao, "Distributed feedback surface emitting laser diode with multilayered heterostructure", Japan. J. Appl. Phys., vol. 23, pp. L512-L514, 1984.

[3] S. Kinoshita and K. Iga, "Circular buried heterostructure (CBH) GaAlAs/GaAs surface emitting lasers", IEEE J. Quantum Electron., vol. QE-23, pp. 882-888, June 1987.

[4] P. L. Gourley and T. J. Drummond, "Visible, room-temperature, surface-emitting laser using an epitaxial Fabry-Perot resonator with AlGaAs/AlAs quarter-wave high reflectors and AlGaAs/GaAs multiple quantum wells", Appl. Phys. Lett., vol. 50, pp. 1225-1227, May 1987.

[5] M. Ogura, W. Hsin, M.-C. Wu, S. Wang, J. R. Whinnery, S. C. Wang, and J. J. Yang, "Surface-emitting laser diode with vertical GaAs/GaAlAs quarter-wavelength multilayers and lateral buried heterostructure", Appl. Phys. Lett., vol. 51, pp. 1655-1657, Nov. 1987.

[6] J. Faist, F. Morier-Genoud, D. Martin, J. D. Ganiere, and F.-K. Reinhart, "Optically pumped GaAs surface-emitting laser with integrated Bragg reflectors", Electron. Lett., vol. 24, pp. 629-630, May 1988.

[7] D. Botez, L. M. Zinkiewicz, L. J. Mawst, and T. J. Roth, "120 mW vertical-cavity surface-emitting diode laser", 11th IEEE International Semiconductor Laser Conf., Boston, MA, Aug. 29 - Sept. 1, 1988, Post-deadline paper PD3.

[8] K. Iga, F. Koyama, and S. Kinoshita, "Surface emitting semiconductor lasers", IEEE J. Quantum Electron., vol. QE-24, pp. 1845-1855, Sept. 1988.

[9] H. Matsueda, "AlGaAs OEIC transmitters", J. Lightwave Technol., vol. LT-5, pp. 1382-1390, Oct. 1987.

[10] J. Nitta, Y. Koizumi, and K. Iga, "GaAs/AlGaAs surface-emitting-laser-type optical logic and gate device", Digest of Technical Papers, CLEO'86 Conference on Lasers and Electro-Optics, San Francisco, 9-13 June 1986, paper FO4, pp. 382-383.

[11] S. Uchiyama and K. Iga, "Two-dimensional array of GaInAsP/InP surface-emitting lasers", Electron. Lett., vol. 21, pp. 162-164, Feb. 1985.

[12] Z. L. Liau and J. N. Walpole, "Surface-emitting GaInAsP/InP laser with low threshold current and high efficiency", Appl. Phys. Lett., vol. 46, pp. 115-117, Jan. 1985.

[13] Z. L. Liau and J. N. Walpole, "Large monolithic two-dimensional arrays of GaInAsP/InP surface-emitting lasers", Appl. Phys. Lett., vol. 50, pp. 528-530, March 1987.

[14] K. Kojima, S. Noda, K. Mitsunaga, K. Kyuma, and K. Hamanaka, "Continuous wave operation of a surface-emitting AlGaAs/GaAs multiquantum well distributed Bragg reflector laser", Appl. Phys. Lett., vol. 50, pp. 1705-1707, June 1987.

[15] N. W. Carlson, G. A. Evans, J. M. Hammer, M. Lurie, L. A. Carr, F. Z. Hawrylo, E. A. James, C. J. Kaiser, J. P. Kirk, W. F. Reichert, L. A. Truxal, J. R. Shealy, S. R. Chinn, and P. S. Zory, "High power seven element grating surface emitting diode laser array with 0.012° far-field angle", Appl. Phys. Lett., vol. 52, pp. 939-941, March 1988.

[16] G. A. Evans, N. W. Carlson, J. M. Hammer, M. Lurie, J. K. Butler, L. A. Carr, F. Z. Hawrylo, E. A. James, C. J. Kaiser, J. B. Kirk, W. F. Reichert, S. R. Chinn, J. R. Shealy, and P. S. Zory, "Efficient, high-power (>150 mW) grating surface emitting lasers", Appl. Phys. Lett., vol. 52, pp. 1037-1039, March 1988.

[17] M. Y. A. Raja, S. R. J. Brueck, M. Osinski, C. F. Schaus, J. G. McInerney, T. M. Brennan, and B. E. Hammons, "Wavelength resonant enhanced gain/absorption structure for optoelectronic devices", in Post Deadline Papers, XV International Conference on Quantum Electronics IQEC'88, Tokyo, Japan, July 18-21, 1988. Paper PD-23, pp. 52-53.

[18] M. Y. A. Raja, S. R. J. Brueck, M. Osinski, C. F. Schaus, J. G. McInerney, T. M. Brennan, and B. E. Hammons, "Novel wavelength-resonant optoelectronic structure and its application to surface-emitting semiconductor lasers", Electron. Lett., vol. 24, pp. 1140-1142, Sept. 1988.

[19] M. Y. A. Raja, S. R. J. Brueck, M. Osinski, C. F. Schaus, J. G. McInerney, T. M. Brennan, and B. E. Hammons, "Surface emitting, multiple quantum well GaAs/AlGaAs laser with wavelength-resonant periodic gain medium", Appl. Phys. Lett., Vol. 53, pp. 1678-1680, October 1988.

[20] M. Y. A. Raja, S. R. J. Brueck, M. Osinski, C. F. Schaus, J. G. McInerney, T. M. Brennan, and B. E. Hammons, "Wavelength-Resonant, Surface-Emitting Semiconductor Laser: A Novel Quantum Optical Structure," 1988 IEEE-LEOS Annual Meeting, Nov. 2-4, 1988, Santa Clara, CA.

[21] R. Geels, R. H. Yan, J. W. Scott, S. W. Corzine, R. J. Simes and L. A. Coldren, "Analysis and design of a novel parallel-driven MQW-DBR surface-emitting diode laser", in Conf. on Lasers and Electro-Optics, Tech. Digest Ser. 1988, Vol. 7 (Optical Society of America, Washington DC, 1988), paper WM1, p. 206.

[22] H. A. Macleod "Thin-Film Optical Filters", 2nd Ed., pp. 50-52, New York: Macmillan 1986.

[23] Z. Knittl, "Optics of Thin Films", pp. 35-51, London: Wiley 1976.

[24] M. V. Klein and T. E. Furtak, "Optics", 2nd Ed., pp. 295-300, New York: Wiley 1986.

[25] "Handbook of Chemistry and Physics", 67th Ed., p. E-378, Boca Raton, FA: CRC Press 1986.

[26] D. E. Aspnes and A. A. Studna, "Dielectric functions and optical parameters of Si, Ge, GaP, GaAs, GaSb, InP, InAs, and InSb from 1.5 to 6.0 eV", Phys. Rev. B, vol. 27, pp. 985-1009, Jan. 1983.

[27] H. C. Casey, D. D. Sell, and K. W. Wecht, "Concentration dependence of the absorption coefficient for n- and p-type GaAs between 1.3 and 1.6 eV", J. Appl. Phys., vol. 46, pp. 250-257, January 1975.

[28] M. Ogura, T. Hata, N. J. Kawai, and T. Yao, "GaAs/$Al_xGa_{1-x}As$ multilayer reflector for surface emitting laser diode", Japan. J. Appl. Phys., vol. 22, pp. L112-L114, Feb. 1983.

CONFERENCE ON LASERS AND ELECTRO-OPTICS

1989 Technical Digest Series
Volume 11

Conference Edition

Summaries of papers presented at the
Conference on
Lasers and Electro-Optics
24–28 April 1989
Baltimore, Maryland

Sponsored by
Lasers and Electro-Optics Society of the
Institute of Electrical and Electronics Engineers
and Optical Society of America
in cooperation with
Quantum Electronics Division of the European Physical Society
and Japanese Quantum Electronics Joint Group

Optical Society of America
1816 Jefferson Place, N.W.
Washington, D.C. 20036
(202) 223-8130

not demonstrated here. The active region consists of 600-Å GaAs wells spaced by integral numbers of halfwaves with intervening barriers of $Al_{0.3}Ga_{0.8}As$ alternately doped p and n type.[4] A different structure BI061 was grown with quantum wells of GaAs/$Al_{0.3}Ga_{0.7}As$ (100 Å/200 Å) uniformly distributed throughout the active region. The quantum wells are not commensurate with the standing wave. Another structure BI071 was grown in sequence with BI061. It had nominally identical mirrors and active region thickness. However, the active region comprised quantum wells positioned at the standing-wave maxima.

A photograph of a low divergence beam emitted from sample BI071 in cw lasing conditions at room temperature is shown in Fig. 1. The small bright spot (~7 μm) on the left side of the photo is the photopumped sample. The laser emits ~20 mW in a concentrated circular beam which strikes an IR sensing card ~30 cm away. Intensity contours of the beam cross section are very circular. Measured profiles of the beam cross section indicate that the laser operates in the fundamental TEM_{00} mode in the diffraction limit. The measured beam divergence was as low as 2.5°. Measured lasing linewidths were as narrow as 2 Å for all structures. A lasing spectrum for UCSB-1 is shown in Fig. 2.

All structures lased cw at room temperature with substantial output power. Total output powers up to ~50 mW were observed for both BI071 and BI061. Up to ~30-mW output was observed for UCSB-1. The overall forward output efficiency for these ESELs is as high as 36%. The differential quantum efficiency is as high as 80%. Compared to BI071, the absorbed power at threshold was ~60% lower than for sample BI061.

This result is consistent with calculations of the absorbed power threshold which predict 75% lower threshold for BI071. The threshold condition is $G_2 = A_2 + (1/N_{eff}) \ln(1/r_1 r_2)$, where G_2 and A_2 are the gain and loss per quantum well, r_1 and r_2 are amplitude reflectivities, and N_{eff} is the effective number of quantum wells participating in the gain process. For N quantum wells with halfwave periodicity, all quantum wells participating imply that low threshold single quantum well ESELs should be possible with present semiconductor mirror technology. **(12 min)**

1. S. Kinoshita, K. Morito, F. Koyama, and K. Iga, Electron. Lett. **24**, 699 (1988) and references therein.
2. M. Ogura, W. Hsin, M. Wu, S. Wang, J. R. Whinnery, S. C. Wang, and J. J. Yang, Appl. Phys. Lett. **51**, 1655 (1987).
3. P. L. Gourley and T. J. Drummond, Appl. Phys. Lett. **50**, 1225 (1987).
4. R. Geels, R. H. Yan, J. W. Scott, S. W. Corzine, R. J. Simes, and L. A. Coldren, in *Technical Digest, Conference on Lasers and Electro-Optics* (Optical Society of America, Washington, DC, 1988), paper WM1.
5. M. Y. A. Raja, S. R. J. Brueck, M. Osinski, C. F. Schaus, J. G. McInerney, T. M. Brennan, and B. E. Hammons, Electron. Lett. **24**, 1140 (1988).

FC4 Surface-emitting lasers: a comparison of resonant periodic gain and conventional structures

M. Y. A. RAJA, STEVE R. J. BRUECK, M. OSINSKI, C. F. SCHAUS, J. G. MCINERNEY, U. New Mexico, Center for High Technology Materials, Albuquerque, NM 87131. T. M. BRENNAN, B. E. HAMMONS, Sandia National Laboratories, P.O. Box 5800, Albuquerque, NM 87185

Recently, we proposed a novel resonant periodic gain (RPG) structure for surface-emitting (SE) lasers consisting of quantum well (QW) layers spaced at one-half of the lasing wavelength and have demonstrated lasing action with the shortest gain medium length ever reported, we believe.[1,2] Here we report a systematic comparison between the new structure and conventional vertical-cavity designs of equivalent active medium length.

Due to the vanishing interaction of the optical field with the carriers in the vicinity of the standing-wave nulls, conventional SE lasers[3-5] do not fully utilize the gain of the medium. The light–carrier interaction and hence the effective gain can be maximized when the gain medium is confined to the antinode regions. This is accomplished in the new structure, incorporating a series of single or multiple QWs separated by relatively thick spacers. To optimize the light–carrier interaction in the QW region, the spacer thickness has to match one half of the wavelength in the medium corresponding to a particular QW transition.

Theoretical estimates[1,2] for this structure predict that the integrated gain in the vertical direction at the resonant wavelength should be twice that away from the resonance or that in a uniform medium of equal gain length. Apart from enhanced integrated gain and wavelength selectivity, this structure has the additional advantage of reduced amplified spontaneous emission, since no free carriers can accumulate in the spacers. Likewise, longitudinal spatial hole burning is eliminated.

Figure 1 shows the three structures used in this study with (a) the RPG active medium, (b) conventional multiple QW, and (c) bulk active region. All three structures were MBE grown with identical AlAs/$Al_{0.4}Ga_{0.6}As$ multilayer high reflectors[4] on the substrate side and with the uncoated top AlGaAs surfaces serving as the front reflectors. Each sample had a total cavity length of ~3.7 μm and a total active medium length of only 310 nm. Figure 2 shows photoluminescence (PL) spectra obtained under low intensity (0.5–0.9-kW/cm²) cw optical pumping using the 514.5-nm lime of an Ar-ion laser. Wide Fabry-Perot resonances are evident. Under high intensity dye laser pumping (7-ns pulses, 680-nm wavelength), no lasing action was observed in the PL spectra of structures (b) and (c) with a pump intensity of 46–65 MW/cm² [Fig. 3(b) and (c)] and even up to the damage limit of ~100 MW/cm². In contrast, the RPG structure lased on the $n = 2$ transition (805–810 nm) at threshold pump intensities of 10–15 MW/cm². Figure 3(a) shows the lasing spectrum at 44 MW/cm². We have thus demonstrated that the new structure represents a superior design for vertical-cavity SE lasers offering significantly lower thresholds and higher efficiencies. The active-medium length of 310 nm is the shortest ever realized in any laser device. The lasing threshold can still be considerably reduced with a properly optimized structure and high Q cavity. Cavity mode calculations and additional experimental results on lasing behavior are presented. **(12 min)**

1. M. Y. A. Raja, S. R. J. Brueck, M. Osinski, C. F. Schaus, J. G. McInerney, T. M. Brennan, and B. E. Hammons, in *Postdeadline Papers, Sixteenth International Conference on Quantum Electronics*, (1988), paper 23.
2. M. Y. A. Raja, S. R. J. Brueck, M. Osinski, C. F. Schaus, J. G. McInerney, T. M. Brennan, and B. E. Hammons, Electron. Lett. **24**, 1140 (1988).
3. S. Kinoshita and K. Iga, IEEE J. Quantum Electron. **QE-23**, 882 (1987).
4. P. L. Gourley and T. J. Drummond, Appl. Phys. Lett. **50**, 1225 (1987).
5. M. Ogura, W. Hsin, M.-C. Wu, S. Wang, J. R. Whinnery, S. C. Wang, and J. J. Yang, Appl. Phys. Lett. **51**, 1655 (1987).

FC5 Lasing at ~1 μm from $In_{0.2}Ga_{0.8}As$/GaAs quantum well surface-emitting resonators with GaAs/AlAs mirrors

K. TAI, K. F. HUANG, J. L. JEWELL, R. J. FISCHER, S. L. MCCALL, A. Y. CHO, AT&T Bell Laboratories, Murray Hill, NJ 07974

Ultralow threshold surface emitting lasers[1] may be useful for long range and chip to chip optical communications. The focus of many efforts is to use quantum well structures and minimize the active material volume[2] while maximizing the mirror reflectivities.[3] All epitaxially grown Fabry-Perot resonators are suited for both of these purposes. Additionally it is desirable to have the substrate be transparent at the lasing wavelength. Here we demonstrate optically pumped surface-emitting lasing from MBE grown resonators containing $In_{0.2}Ga_{0.8}As$/GaAs strained quantum wells active layers and GaAs/AlAs mirrors. The emission wavelength ranged from ~0.98 to 1.0 μm in the two samples grown and varied with position on the samples. The lasing threshold was 50 pJ on an estimated area of 30 μm². Nonlinear optical switching at 1.06 μm with a 5:1 contrast was also achieved with a 20-pJ, 0.9-μm pump.

The resonator structures were grown by MBE on Si doped GaAs substrates. 12.5 periods of AlAs/GaAs (834/707 Å) were followed by seventy $In_{0.2}Ga_{0.8}As$/GaAs wells/barriers (80/150 Å). The second mirror grown on top of these achieved the same reflectivity as the first (~95%) with eight periods of the same thickness GaAs/AlAs structures due to the air–GaAs interface. Similar InGaAs quantum wells grown with the same conditions but without mirrors exhibited distinct exciton resonances at 300 K. A cw mode-locked dye laser provided 0.875-μm, 10-ps pulses at a 80-MHz rate to pump the structures. Figure 1 shows the output vs input characteristic with a sharp lasing threshold at 50-pJ incident pump energy. The single-mode emission linewidth just above threshold was 1 nm. At high pump energies the observed spectrum (time-integrated) was broadened toward short wavelengths mainly due to dynamic tuning of the cavity. The threshold carrier density was estimated to be 5×10^{12} cm^{-2}/well using a 30-μm² spot area and 25-pJ absorbed energy. We estimate a threshold current density for these structures if they would be pumped electrically to be 20 μA/μm². In the calculation, the estimated carrier lifetime of 0.4 ns at the threshold was obtained by using a bimolecular recombination rate of 4×10^{-10} cm³/s. This result suggests the possibility of an ultralow threshold current surface-emitting diode laser in InGaAs/GaAs quantum well microresonator structures. Since the output can transmit through the substrate, we can use a thick gold top contact layer which with only a small number of mirror layers yields high reflectivity (>99%). Such a top contact structure is not possible in GaAs/AlGaAs systems. Threshold densities can be further reduced by using higher reflectivity mirrors and fewer quantum wells. For optical gating/switching it is advantageous to have transparent substrates and operate at the wavelength of high power lasers such as Nd:YAG. The present structure gated 1.06-μm wavelength pulses from the Nd:YAG laser which was used to pump the dye laser; 20-pJ incident pump energy shifted the transmission peak of the Fabry-Perot by one FWHM. **(12 min)**

1. M. Ogura, W. Hsin, M-C. Wu, S. Wang, J. R. Whinnery, S. C. Wang, and J. Yang, Appl. Phys. Lett. **51**, 1655 (1987).
2. J. L. Jewell, A. Scherer, S. L. McCall, A. C. Gossard, and J. H. English, Appl. Phys. Lett. **51**, 94 (1987).

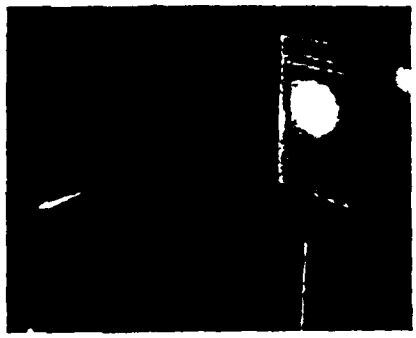

FC3 Fig. 1. Infrared laser beam emitted from sample BI071 with periodic gain.

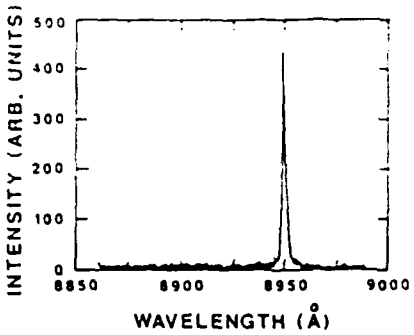

FC3 Fig. 2. Lasing spectrum of sample UCSB-1.

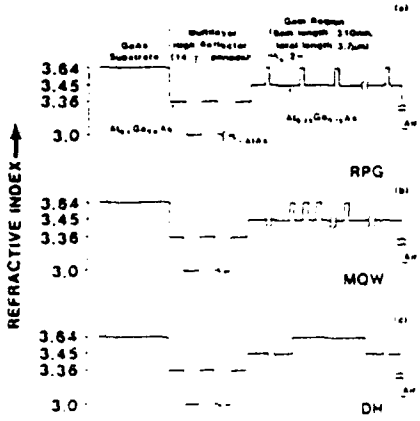

FC4 Fig. 1. Refractive index profiles for three MBE grown samples: (a) resonant periodic gain structure with 10-nm wells and 110-nm spacers; (b) conventional multiquantum well with 10-nm wells and 20-nm spacers, and (c) double heterostructure. Each sample has a multilayer reflector situated between the substrate and gain region.

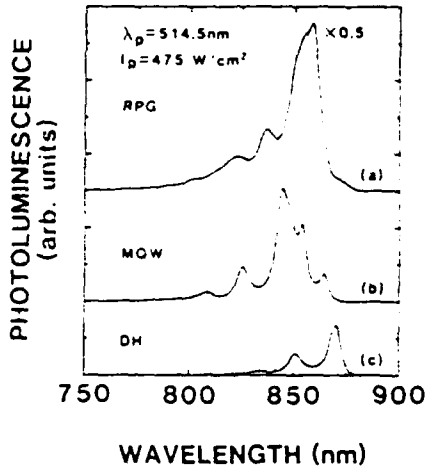

FC4 Fig. 2. Photoluminescence spectra for low intensity cw pumping of the three samples at 514.5 nm. Curves are offset for clarity, and the intensities are directly comparable. Note the cavity Fabry-Perot fringes.

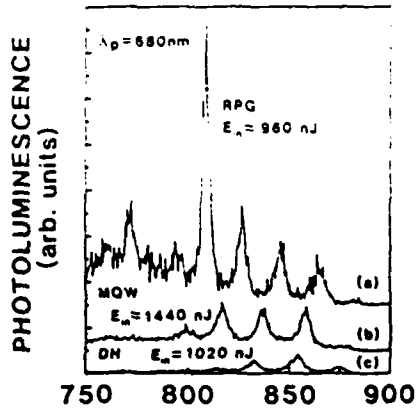

FC4 Fig. 3. Photoluminescence spectra for high intensity pulsed pumping at 680 nm (7-ns pulses, 20-μm diam spot). Note the lasing at 805 nm for the RPG structure at fluences below those for the other two structures.

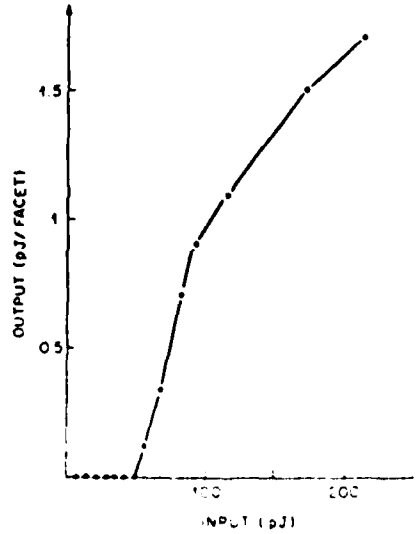

FC5 Fig. 1. Lasing output vs input characteristic in an optically pumped surface-emitting InGaAs/GaAs resonator with GaAs/AlAs mirrors.

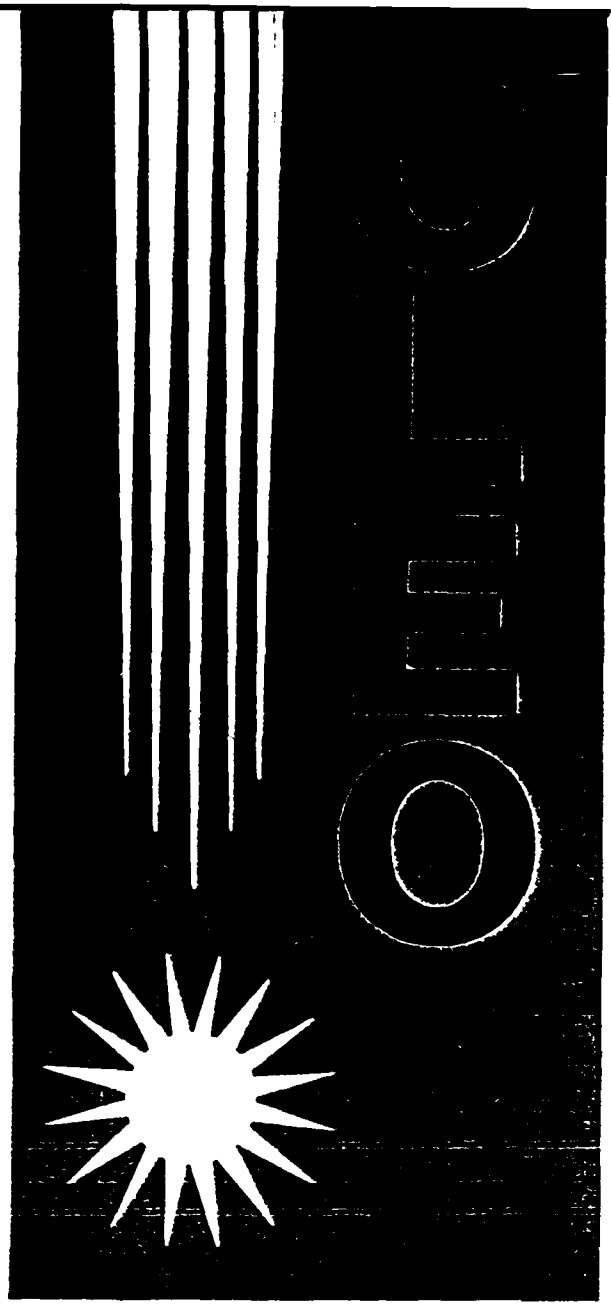

1 9 8 9

APRIL 24-28

BALTIMORE, MARYLAND

POSTDEADLINE PAPERS

300K CW OPERATION OF MOCVD GROWN OPTICALLY PUMPED GaAs/AlGaAs RESONANT PERIODIC GAIN VERTICAL CAVITY LASERS WITH 45% EFFICIENCY

C. F. Schaus, S. Sun, H.E. Schaus, M.Y.A. Raja, J G McInerney, S.R.J. Brueck
Center for High Technology Materials
University of New Mexico
Albuquerque, NM 87131

The fabrication of vertical cavity surface-emitting semiconductor lasers incorporating half-wave periodic gain, or resonant periodic gain (RPG), have recently been demonstrated using molecular beam epitaxy (MBE) [1-5]. Here we describe structures grown entirely by MOCVD which exhibit the highest efficiency in a vertical cavity laser reported to date.

The RPG medium allows the half-wave-spaced localized gain regions (single quantum wells in this case) to become aligned with the antinodes of the standing-wave optical field in the laser cavity. The effective gain along the cavity axis is twice that in the transverse direction and parasitic amplified spontaneous emission in the transverse direction is suppressed. However, there are several important design considerations for optimizing this structure. First, the periodicity of the RPG must match one-half the lasing wavelength. This wavelength must simultaneously match the n=1 quantum well transition, and the entire RPG medium must be placed in the cavity so that the antinodes align with the quantum wells. This requires a high degree of accuracy in the optical thickness control of the many MOCVD grown layers.

The RPG laser structure grown for this study is shown in Fig. 1. Epitaxial layers were grown in a low pressure horizontal MOCVD reactor at 725°C. The resulting layer thicknesses were uniform to within ± 2% over 90% of a 50 mm diameter GaAs substrate. Thickness reproducibility was measured at ± 0.25% from run to run. The multilayer epitaxial reflectors (MLRs) on either side of the RPG medium are designed to provide reflectivities of 99.70% (30.5-periods grown on GaAs) and 99.95% (20-periods ending in air) for the output coupler (right) and reflector (left), respectively. The device incorporates an RPG active region consisting of 20 10-nm GaAs quantum wells separated by $Al_{0.20}Ga_{0.80}As$ spacers. The structure was optically pumped using a CW dye laser focused with a microscope objective lens (5x or 20x), which also served as collection optics for the RPG laser output. The threshold energy for the structure was measured as a function of wavelength, showing a minimum near 739 nm. The device operated in a single longitudinal mode (Fig. 2) with spectral widths as narrow as ~0.27 Å FWHM. Fig. 3 shows the output *vs* input powers for the device at 739 nm pump wavelength. The overall power conversion efficiency is over 45% at 18 mW output power.

In conclusion,high efficiency $GaAs/Al_xGa_{1-x}As$ vertical cavity surface-emitting lasers with resonant periodic gain have been fabricated and demonstrated. The threshold was 15 mW at 300K CW using 739 nm excitation. The device exhibits stable single longitudinal mode output at ~860 nm with 0.27 Å FWHM, and power conversion efficiencies over ~45%.

REFERENCES:

[1] S. W. Corizine, R. S. Geels, J. W. Scott, L. A. Coldren, and P. L. Gourley, in *IEEE Lasers and Electro-Optics Society Annual Meeting Proceedings*, Paper OE1.2 (1988).

[2] M. Y. A. Raja, S. R. J. Brueck, M. Osinski, C. F. Schaus, and J. G. McInerney, in *IEEE Lasers and Electro-Optics Society Annual Meeting Proceedings*, Paper OE1.3 (1988).

[3] M. Y. A. Raja, S. R. J. Brueck, M. Osinski, C. F. Schaus, J. G. McInerney, T. M. Brennan, and B. E. Hammons, *Electron. Lett.* 24, 1140 (1988).

[4] M. Y. A. Raja, S. R. J. Brueck, M. Osinski, C. F. Schaus, J. G. McInerney, T. M. Brennan, and B. E. Hammons, *Appl. Phys. Lett.*, 53, 1678, (1988).

[5] P. L. Gourley, T. M. Brennan, B. E. Hammons, S. W. Corizine, R. S. Geels, R. H. Yan, J. W. Scott, and L. A. Coldren, *Appl. Phys. Lett.*, 54, 1209, (1989).

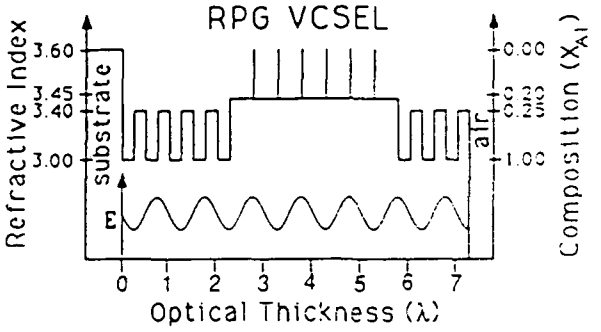

Figure 1. A schematic illustration of the RPG laser structure in which the number of periodic layers has been reduced in order to simplify interpretation. Also shown is the standing wave electric field corresponding to the resonant mode of the cavity.

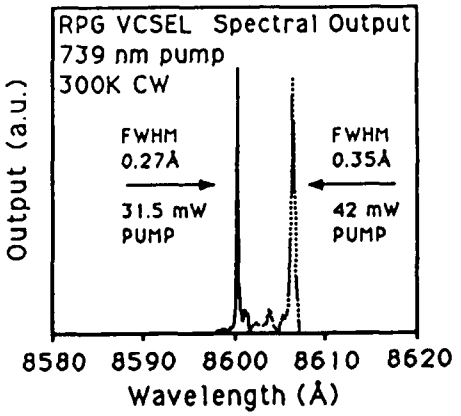

Figure 2. Spectral output above threshold (5x objective).

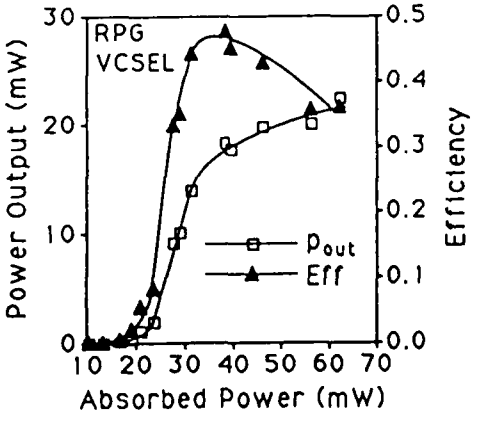

Figure 3. Optical power output *vs* input curve at 739-nm excitation (20x objective).

DYNAMICS OF RESONANT PERIODIC GAIN GaAs/AlGaAs SURFACE-EMITTING LASERS UNDER PICOSECOND OPTICAL EXCITATION

by

M. Y. A. Raja, A. Mukherjee, M. A. Mahbobzadeh, C. F. Schaus, and S. R. J. Brueck
Center for High Technology Materials, University of New Mexico
Albuquerque, New Mexico 87131

ABSTRACT

The output of a resonant periodic gain surface-emitting GaAs/AlGaAs laser was modulated by changing the phase and reflectivity of a monolithic cavity mirror by the absorption of picosecond optical pulses. Dynamical processes, studied as function of cw pump power, picosecond laser wavelength and pulse energy, are reported.

Corresponding Author:

Dr. Anadi Mukherjee
Center for High Technology Materials
EECE Building #125
University of New Mexico
Albuquerque, New Mexico 87131

Ph# (505) 277-6033
Fax:(505) 277-6433

DYNAMICS OF RESONANT PERIODIC GAIN GaAs/AlGaAs SURFACE-EMITTING LASERS UNDER PICOSECOND OPTICAL EXCITATION

M. Y. A. Raja, A. Mukherjee, M. A. Mahbobzadeh, C. F. Schaus, and S. R. J. Brueck, Center for High Technology Materials, University of New Mexico, Albuquerque, NM 87131

Resonant periodic gain (RPG) vertical cavity, surface-emitting semiconductor lasers [1] are promising for various optoelectronic applications. RPG structures utilize spatially periodic quantum well gain regions to provide an enhanced light-matter interaction [1] leading to higher gain, frequency discrimination and reduction in transverse amplified spontaneous emission [1]. Recent optical pumping results [2-3] have shown that when such RPG structures are integrated with epitaxially grown multilayer high-reflectors, low thresholds (~ kW/cm^2), high efficiencies (> 45%) and narrow linewidths (< 0.25Å) are obtained. Here, we present recent results on the investigation of the dynamics of RPG surface-emitting lasers.

In our experiments, MOCVD-grown 20-period GaAs/AlGaAs RPG structures with integrated multilayer high-reflectors [3] are used. In such laser structures phase of the optical standing wave plays an important role in optimizing the interaction with the active sections (quantum wells). The top mirror (19 1/2 period $Al_{0.25}Ga_{0.75}As$/AlAs quarterwave stack) was modulated optically with cavity-dumped dye laser pulses (λ = 620 nm, 10 psec., 80 kHz) while the RPG structure was continously pumped by a cw dye laser operating at 740 nm.

Fig. 1 shows a typical output pulse from this structure as well as the 10-picosecond dye-laser pulse. The temporal resolution was limited by the electronics. The delay between the picosecond pump pulse and the RPG lasing pulse depends on the cw dye laser pump power. Secondary pumping of the gain region by photoluminescence from the mirror potentially plays a role in these results. Evolution of the RPG output pulse was studied as a function of various parameters including: picosecond pulse energy, wavelength, and cw dye laser power. These dynamical measurements not only give an insight to the physics of RPG laser structure but also show its potential for an active modulator. Basic mechanisms leading to this output pulse evolution and modulation properties will be presented along with details of the results.

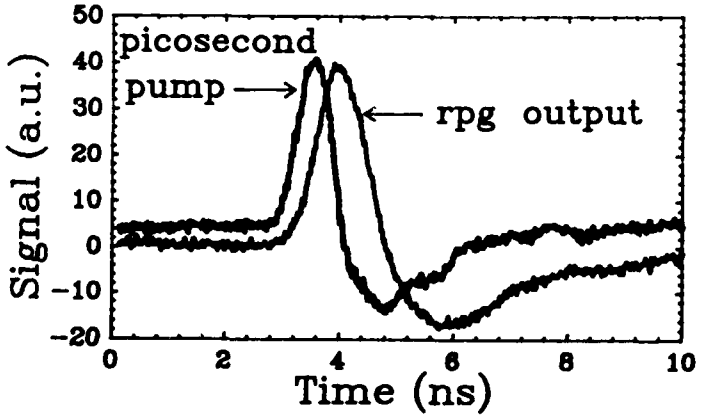

Fig 1. Output of RPG pumped with 30 mW cw and ~ 0.5 nJ10 psec. dye laser pulse. (electronics limited).

References:

1. M. Y. A. Raja, S. R. J. Brueck, M. Osinski, C. F. Schaus, J. G. McInerney, T. M. Brennan, and B. E. Hammons, *IEEE J. Quantum Electron*, QE-25, No 6 (1989).
2. P. L. Gourley, T. M. Brennan, B. E. Hammons, S. W. Corzine, R. S. Geels, R. H. Yan, J. W. Scott, and L. A. Coldren, *Appl. Phys. Lett.* 54, 1209 (1989).
3. C. F. Schaus, M. Y. A. Raja, J. G. McInerney, H. E. Schaus, S. Sun, M. Mahbobzadeh, and S. R. J. Brueck, *Electron. Lett.* 25, 637 (1989).

Partial funding for this work was provided by the US Air Force Office of Scientific Research.

TRANSVERSE MODE STRUCTURE OF OPTICALLY PUMPED RESONANT PERIODIC GAIN SEMICONDUCTOR LASERS

by

M. Y. A. Raja, J. G. McInerney, C. F. Schaus, S. R. J. Brueck, H. E. Schaus, and S. Sun
Center for High Technology Materials, University of New Mexico
Albuquerque, New Mexico 87131 USA

ABSTRACT

The transverse mode behavior and spectral properties of vertical cavity, high efficiency surface-emitting GaAs/AlGaAs resonant periodic gain lasers, are described and analyzed.

Corresponding Author:

Dr. M. Yasin Akhtar Raja
Center for High Technology Materials
EECE Building, Room #125
University of New Mexico
Albuquerque, NM 87131

Ph# (505) 277-6033
Fax: (505) 277-6433

TRANSVERSE MODE STRUCTURE OF OPTICALLY PUMPED RESONANT PERIODIC GAIN SEMICONDUCTOR LASERS

M. Y. A. Raja, J. G. McInerney, C. F. Schaus, S. R. J. Brueck, H. E. Schaus, and S. Sun
Center for High Technology Materials, University of New Mexico, Albuquerque, NM 87131

Recently, CW lasing has been demonstrated at room temperature [1-2] in resonant periodic gain (RPG) GaAs/AlGaAs vertical-cavity surface-emitting lasers [3]. Optically pumped RPG structures grown by MBE [1] and MOCVD [2] have shown very low thresholds (~ kW/cm^2), high conversion efficiencies ($\geq$ 45%) and narrow linewidths (~ 0.25Å) [2]. RPG laser structures make use of an enhanced interaction of the optical standing wave with a spatially periodic gain medium ($\lambda/2$ - spaced quantum wells) which not only doubles the effective gain coefficient and reduces the amplified spontaneous emission, but also offers high wavelength selectivity [3]. Such laser structures inherently operate in a single longitudinal mode because of their short cavity-lengths (few μm).

Here, we describe the transverse mode characteristics of RPG laser structures [2] with integrated multilayer high-reflectors for various optical pumping conditions. Both pulsed and CW experiments were carried out at 300 K. The experimental setup allowed simultaneous measurements of transverse mode structure, wavelength and output power. The transverse modes depend strongly on the pump spot diameter. For a small pump spot (~ 5 μm) the laser output is TEM_{00} for up to 4 x the threshold pump power. For higher pump power, the output switches to a higher order mode (c.f. Fig. 1 (a),(b)). With a slight decrease (~ 0.2%) in pump power the higher order mode switches back to TEM_{00} mode. (c.f. Fig. 1(c)). This variation of the output mode is accompanied by a dramatic increase in the output power (~ 5 x) for the higher order mode, as well as a wavelength shift.

In the absence of any transverse guiding structure such mode switching can be attributed to the carrier-induced antiguiding and gain guiding. The pump spot dependence may be explained by considering the large Fresnel numbers associated with the short cavity-lengths and large pump spot. The frequency selectivity of the RPG structure as well as the large Fresnel numbers, also permit several degenerate higher order transverse modes at the same wavelength. Higher order transverse modes which satisfy the resonance condition for the RPG structure and micro cavity (Fabry-Perot), are supported by carrier diffusion from the pumped region. It was also observed that the mode of the pump laser also influences the RPG laser mode. Beam quality of these RPG lasers and the study of near- and far-field mode-patterns will be discussed. Analysis and possible use of such modal and spectral properties as a switch will also be presented.

Fig 1.

(a) (b) (c)

References:

1. P. L. Gourley, T. M. Brennan, B. E. Hammons, S. W. Corzine, R. S. Geels, R. H. Yan, J. W. Scott, and L. A. Coldren, *Appl. Phys. Lett.* 54, 1209 (1989).
2. C. F. Schaus, M. Y. A. Raja, J. G. McInerney, H. E. Schaus, S. Sun, M. Mahbobzadeh, and S. R. J. Brueck, *Electron. Lett.* 25, 637 (1989).
3. M. Y. A. Raja, S. R. J. Brueck, M. Osinski, C. F. Schaus, J. G. McInerney, T. M. Brennan, and B. E. Hammons, *IEEE J. Quantum Electron.* (Special Issue) QE-25, No. 6 (1989).

Partial funding for this work was provided by the US Air Force Office of Scientific Research.